Universidade Estadual de Campinas
Faculdade de Engenharia Elétrica e de Computação

Iury Bertollo Gomes Pôrto

On the Phase of the κ-μ Fading Process

Sobre a Fase do Processo de Desvanecimento κ-μ

Campinas
2017

Universidade Estadual de Campinas
Faculdade de Engenharia Elétrica e de Computação

Iury Bertollo Gomes Pôrto

On the Phase of the κ-μ Fading Process

Sobre a Fase do Processo de Desvanecimento κ-μ

PhD's thesis presented to the School of Electrical and Computer Engineering in partial fulfillment of the requirements for the degree of PhD in Electrical Engineering. Concentration area: Telecomunications and Telematics.

Tese de doutorado apresentada à Faculdade de Engenharia Elétrica e de Computação como parte dos requisitos exigidos para a obtenção do título de Doutor em Engenharia Elétrica. Área de concentração: Telecomunicações e Telemática.

Advisor: Michel Daoud Yacoub

Orientador: Michel Daoud Yacoub

Este exemplar corresponde à versão final da tese defendida pelo aluno, e orientada pelo Professor Michel Daoud Yacoub.

Campinas
2017

Agência(s) de fomento e nº(s) de processo(s): Não se aplica.
ORCID: http://orcid.org/0000-0002-9274-7675

Ficha catalográfica
Universidade Estadual de Campinas
Biblioteca da Área de Engenharia e Arquitetura
Luciana Pietrosanto Milla - CRB 8/8129

P838p

Pôrto, Iury Bertollo Gomes, 1986-
On the phase of the kappa-mu fading process / Iury Bertollo Gomes Pôrto. – Campinas, SP : [s.n.], 2017.

Orientador: Michel Daoud Yacoub.
Tese (doutorado) – Universidade Estadual de Campinas, Faculdade de Engenharia Elétrica e de Computação.

1. Canal em desvanecimento. 2. Variáveis aleatórias. 3. Métodos de simulação. 4. Distribuição (Probabilidades). I. Yacoub, Michel Daoud,1955-. II. Universidade Estadual de Campinas. Faculdade de Engenharia Elétrica e de Computação. III. Título.

Informações para Biblioteca Digital

Título em outro idioma: Sobre a fase do processo de desvanecimento kappa-mu
Palavras-chave em inglês:
Fading channels
Random variables
Simulation methods
Distribution (Probabilities)
Área de concentração: Telecomunicações e Telemática
Titulação: Doutor em Engenharia Elétrica
Banca examinadora:
Michel Daoud Yacoub [Orientador]
Adriano Almeida Goes
Cláudio Ferreira Dias
Diana Cristina González González
Paulo Cardieri
Data de defesa: 14-07-2017
Programa de Pós-Graduação: Engenharia Elétrica

COMISSÃO JULGADORA - TESE DE DOUTORADO

Candidato: Iury Bertollo Gomes Pôrto
Data da Defesa: 14 de Julho de 2017

Título da Tese: On the Phase of the κ-μ Fading Process

Dr. Michel Daoud Yacoub (Presidente, FEEC/UNICAMP)
Dr. Adriano Almeida Goes (Universidade São Francisco)
Dr. Cláudio Ferreira Dias (Consultor)
Dra. Diana Cristina González González (FEEC/UNICAMP)
Dr. Paulor Cardieri (FEEC/UNICAMP)

A ata de defesa, com as respectivas assinaturas dos membros da Comissão Julgadora, encontra-se no processo de vida acadêmica do aluno.

Acknowledgments

I would like to thank everyone who helped making this work possible, in special to

my advisor Professor Michel Yacoub, for the precious guidance;

my family, my mother Dilva, my father Natal, my brother Victor and my sister Larissa, for the unconditional support and general positive influence that I can always rely on;

my friend Tiago Ricciardi, for the motivation;

my friend Fernando Lira, for the gorgeous graphics;

my love Sarah, for staying with me through hard times and inspiring me to be better;

my close friends, for giving me the strength I needed to complete this work;

the School of Electrical and Computer Engineering/University of Campinas (FEEC/UNICAMP), for the essential support provided over the years;

all the professors whose classes I had the pleasure to attend to, for the great courses that were offered;

the members of the examining committee, Dr. Adriano Almeida Goes, Dr. Cláudio Ferreira Dias, Dr. Diana Cristina González González, and Dr. Paulo Cardieri, for the suggestions and contributions to the final version of this thesis;

all the people that contributed with my personal growth and were not mentioned. This thesis would not exist without you.

Abstract

This thesis presents a study on the κ-μ and the generalized Nakagami-m phase statistics. The exact formula of the phase Cumulative Distribution Function (CDF) and its inverse of the generalized Nakagami-m model are found and described. An approximation for both the Phase Crossing Rate (PCR) and Phase Probability Density Function (PDF) of the κ-μ model are found, as analytic closed-form expressions. These approximations yield results almost indistinguishable from the exact integral formulation but require significantly less computational resources. In particular, the approximation of the Phase PDF is itself a new general distribution, bounded in the interval $[0, 2\pi)$ and inheriting both the generality and physical meaning of the κ-μ model, which makes it suitable to be used as a standalone random variable to study phase processes. This new distribution encompasses both the *exact* Nakagami-m phase as well as the *exact* Von Mises (Tikhonov) densities as special cases. Joint statistics involving combinations of the envelope, phase, and their time derivatives are defined in an exact manner. Furthermore, the error between the approximation and the exact solution is computed for a wide range of the parameters κ, μ and ϕ, delineating the regions where the approximation follows more closely the exact solution. The shortcomings of the existing simulation models for the phase of the κ-μ fading model are discussed and a new simulator is described. The new simulator generates correlated κ-μ samples that are distributed according to the exact κ-μ first and second order statistics. The formulations and the simulator presented here drastically facilitate the use of the κ-μ model to study fading channels.

Key-words: Fading channels, kappa-mu fading, Nakagami-m fading, phase statistics, simulation, random variable.

Resumo

Esta tese apresenta um estudo sobre as estatísticas de fase dos modelos κ-μ e Nakagami-m generalizado. São encontradas e descritas as fórmulas exatas da Função Distribuição Acumulada da Probabilidade (FDA) de Fase e sua inversa, do modelo Nakagami-m generalizado. Foram também encontradas aproximações analíticas para a Taxa de Cruzamento de Fase (TCF) e para a Função Densidade de Probabilidade (FDP) de Fase do modelo κ-μ, em fórmulas fechadas. Estas aproximações tem valores quase indistinguíveis das fórmulas exatas, mas requerem consideravelmente menos recursos computacionais para o seu cálculo. Em particular, a aproximação da FDP de Fase é uma nova distribuição de probabilidade, restrita ao intervalo $[0, 2\pi)$, e que herda tanto a generalidade quanto o significado físico do modelo κ-μ, o que a torna adequada para o estudo da fase de sinais propagados em canais com desvanecimento. Esta distribuição tem como casos particulares tanto a distribuição *exata* de fase de Nakagami-m como a FDP *exata* de Von Mises (Tikhonov). Diversas fórmulas exatas de estatísticas conjuntas da distribuição κ-μ envolvendo combinações do envelope, fase e suas respectivas derivadas no tempo são apresentadas. Adicionalmente, o erro entre as aproximações encontradas e a solução exata é calculado para uma grande faixa dos parâmetros κ, μ e ϕ, delimitando as regiões onde a aproximação e a solução exata são mais próximas. Os problemas com os modelos de simulação da fase do modelo κ-μ são discutidos e um novo simulador foi desenvolvido. O novo simulador gera amostras correlacionadas que são distribuídas de acordo com as estatísticas exatas de primeira e segunda ordem do modelo κ-μ. As estatísticas derivadas aqui e o simulador apresentado facilitam drasticamente o uso do modelo κ-μ para estudo de canais com desvanecimento.

Palavras-chave: Canal em desvanecimento, desvanecimento kappa-mu, desvanecimento Nakagami-m, estatísticas de fase, simulação, variável aleatória.

List of Figures

List of Acronyms

CPU	Central Processing Unit
FM	Frequency Modulation
IID	Independent and Identically Distributed (Random Variables)
LoS	Line-of-Sight
NLoS	Non-Line-of-Sight
PCR	Phase Crossing Rate
PDF	Probability Density Function
CDF	Cumulative Density Function
RMS	Root Mean Square
RV	Random Variable

Contents

Chapter 1

Introduction

1.1 Modeling the Mobile Radio Channel

Modeling the mobile radio channel is a very hard task. Unlike wired and other forms of electronic communication propagated via a solid medium, the wireless propagation environment is chaotic. Once the signal leaves the transmitter station it has to go through an unknown environment, potentially filled with obstacles and many sources of corruption, before reaching the receiving station. The transmitting and receiving stations are often in movement in regard to one another, adding a Doppler shift to the problem. The signal will usually travel through multiple paths of different lengths before reaching its destination, interfering with time-shifted copies of itself. Furthermore, each transmission has to compete with the interference from all the other transmissions using the same frequency band, which can add up to a substantial noise in places such as office spaces where WiFi stations contend with bluetooth devices and microwave ovens over the usage of the same 2.4 GHz band. All things considered, it might come as a surprise to the uninitiated that any wireless communication is possible at all. A very good understanding of the mobile radio channel is the working basis for all the techniques that make that kind of communication a reality.

The study of signal fading is an important part of understanding the wireless communication channel. Signal fading is a phenomenon that causes the signal to randomly drop below detectable levels at the receiver and it can have many causes. Movement between the transmitter and receiver may cause obstacles to come amidst the propagation path, multiple reflectors may cause the signal to destructively interfere with copies of itself and the Doppler shift complicates everything. In general, the many sources of signal fading can be broadly divide into two distinct groups: fast fading and slow fading [1, 2]. The terms slow and fast refers to the duration of the fade in relation to the coherence time of the channel, which is a measure of the time taken by the signal to become uncorrelated with itself. Obstacles moving into and out of the propagation path would cause slow fading, whereas multipath interference is one source of fast fading [3]. Due to the random nature of the changes in the propagation channel, both types of fading are modeled as random variables. Slow fading is well modeled by the lognormal distribution [4, 5], for which a physical model was proposed in [1], linking the lognormal distribution to the attenuation caused by random obstacles with different attenuation coefficients. On the other hand, it is harder to pin down a single mathematical model to fast fading. Channel characteristics such as line-of-sight (LOS), or lack thereof, the tendency to form multipath clusters and the number of clusters formed, and the

Doppler effect, among others, change the nature of fast-fading. Thus, many different fading models have been proposed to represent the many different fast fading conditions.

One of the first and most influential investigations of the statistical properties of fading was conducted by S. O. Rice in his seminal work "Statistical properties of sine wave plus random noise" [6]. His paper introduces the Ricean distribution, one of the most used fading distributions for LOS propagation, and lays the foundation for the study of higher order statistics, introducing the Level Crossing Rate (LCR) and Phase Crossing Rate (PCR) among other statistics.

The first work to tackle fading in terms of the interaction between multiple reflected waves was proposed by J. F. Ossanna in [7]. It modeled a mobile receiver moving through a field of vertical reflectors randomly distributed, representing buildings around a street, so that a stationary wave results from the multiple reflections. The model was rather brittle and, whereas it modeled well the received signal within 2 miles from the transmitter, lacked the flexibility to adjust for different street directions. Moreover, it didn't allow for different ratios of the power of the direct waves to the reflected waves, assuming it to be fixed [8]. Nevertheless it was an important work which allowed the development of more general models.

R. H. Clarke proposed a more flexible model in [8]. The Clarke model assumes that the received signal is composed by the sum of a great number of scattered waves, that reach the receiver at random angles and with independent and uniformly distributed phases. Clarke shows that his model predicts an envelope distributed according to the Rayleigh distribution, thus establishing the theoretical groundwork to explain previous studies that had found that, for certain propagation conditions, field data had a good fit to the Rayleigh distribution, such as [9]. Based on Clarke's model, Jakes proposed an isotropic channel simulator in [10].

In [11], M. Nakagami describes the m-distribution, widely known as Nakagami-m, which generalizes the Rayleigh distribution. Nakagami derived his distribution directly from field data by finding a mathematical function that provided a good fit to the observed fading, in contrast to the physical-modeling approach of Rice, Ossana and Clarke. Then, in [12], M. D. Yacoub proposed an underlying physical model that leads to the Nakagami-m statistics, similarly to what Clarke did to the Rayleigh distribution. This model allowed the derivation of higher order statistics of the Nakagami-m model. In [13], the Nakagami-m model was generalized by the addition of a phase parameter, which gave the model more flexibility and allowed its use to the study of phase.

More general distributions to describe the mobile radio channel have been recently proposed. [14] introduces the $\alpha - \mu$ model, which presents a physical propagation model that leads to the Stacy distribution, describing a non-linear channel. The $\kappa - \mu$ and $\eta - \mu$ models, introduced in [15], describe environments that cause the transmitted signal to arrive at the receiver station as multiple clusters, with the former describing LOS conditions and the latter non-LOS channels. These general models are suited to fit data from many different real situations, due to their greater flexibility.

The $\kappa - \mu$ model is of special interest for this thesis, as most of the following work is based on it. It assumes that the received signal is composed of μ different clusters, with a distinction between the direct wave arriving by the LOS path and the scattered waves. The ratio between the power of the dominant component to the scattered components is κ. It contains several of the previously cited model as special cases: (i) the model reduces to the Rice distribution when $\mu = 1$ and $\kappa = k$, whereas k is the Rice parameter; (ii) Nakagami-m

is obtained by setting $\kappa \to 0$ and $\mu = m$, in which m is the Nakagami parameter; and (iii) Rayleigh, being itself a special case of the Nakagami-m model when $m = 1$. The model was expanded in [16] [17] to include a phase parameter, ϕ, that describe the ratio of the power of the in-phase components to the quadrature components, and higher order statistics of the envelope were described in [18].

In addition to the field data in previous literature that corroborates the special case distributions, it was found that the general $\kappa-\mu$ distribution is well suited to describe a range of real world propagation conditions, including its first- [15] and second-order statistics [18]. The $\kappa - \mu$ fading distribution is being used in recent research to study system performance under this type of fading. These investigations encompass subjects such as cognitive radio systems [19,20], retransmission systems [21,22], transmission systems with diversity [23–26], symbol error rates [27] and outage probability and channel capacity [28]. Numerous other investigations concerning the envelope statistics have been appearing in the literature (e.g. [29–37]). Additionally, the phase behavior can be used in the synchronization process of coherent receivers for which carrier recovery schemes are necessary [38]. Phase statistics also affect the performance of modulation systems using both non-ideal coherent detection or incoherent detection [39]. It influences the performance of modulation schemes in OFDM signals [40], and impacts on the capacity of MIMO channels [41, 42]. Moreover, the Phase Crossing Rate is central to the study of the error rate performance of FM receivers using a limiter-discriminator based detection, where random FM spikes are generated by phase jumps [43].

1.2 Contributions

The main contribution of this thesis is to further the study of the phase process in channels subjected to both generalized Nakagami-m and κ-μ fading. It accomplishes the following contributions:

- Provides the Cumulative Density Function of the Generalized Nakagami-m fading model as an analytic expression;
- Completes the work started in [44], by finding an analytic approximation to the $\kappa - \mu$ Phase Crossing Rate;
- Introduces the $\mathbb{O}$ random variable with its corresponding analytic PDF, which is a new distribution based on the $\kappa - \mu$ fading that is fit to describe phase processes;
- Provides the formulas for a number of joint statistics of the phase, envelope and their derivatives of the $\kappa - \mu$ channel;
- Derives the PDF of the time derivative of the phase of the $\kappa - \mu$ channel;
- Describes a new integral identity of the confluent hypergeometric function of the first kind;
- Proposes a simulator to the $\kappa - \mu$ fading channel that produces correlated phase samples.

1.3 Structure

The research for this work lead to the publication of two papers, [45] and [46]. Those papers are presented in this thesis, alongside additional unpublished research, as follows:

Chapter 2 is an introductory chapter presenting the basic expressions that constitutes the mathematical basis for the thesis. This chapter gives an overview of the Rayleigh, Generalized Nakagami-m, Rice and κ-μ fading channels, including their physical models, exactly how each model is related to the others and the formulas of their first and second order statistics. It also presents the definition of the Phase Crossing Rate statistic and discusses the basis of the simulation techniques that are used to generate the appropriately correlated samples needed to simulate a fading channel. The chapter is intended as a foundation upon which the rest of the thesis is built.

Chapters 3 and 4 are the extended versions of papers [45] and [46] respectively. Chapter 3 concerns the Generalized Nakagami-m fading channel, presenting the derivation of the formulas of its phase CDF and inverse CDF. It also presents evidence of real world occurrence of this type of fading, in form of field data fitted to the Generalized Nakagami-m phase statistics.

Chapter 4 is about the first and second order statistics of the κ-μ model. It defines various joint statistics for the distributions of phase, envelope and its first time derivatives. It also presents analytic approximations of both the phase PDF and the PCR of the κ-μ model, which are compared to their respective exact counterparts through various plots and through a distance measure based on the Kullback-Leibler divergence.

Chapter 5 introduces the simulation technique developed. It starts with the discussion of the shortcomings of the previous simulation techniques and the intrinsic difficulties to simulate the κ-μ fading channel. The chapter then presents a series of different simulators, building up to the definitive simulation developed, which is shown to generate samples that are distributed according to the exact κ-μ theoretical statistics.

Finally, Chapter 6 concludes the thesis.

Chapter 2

Fading Models Revisited

This chapter revisits the foundations of the statistical modeling of fading channels. It is an introductory chapter that aims to give the reader the means to follow the rest of the thesis. A summary of the relevant theory regarding the Rayleigh, Nakagami-m, Rice and $\kappa-\mu$ models are given, along with the corresponding physical model and the most important mathematical expressions.

2.1 The Phase Crossing Rate

The PCR is a second order statistics that measures the average number of upward (or downward) crossings per second of a given phase θ. The PCR of a continuous process is given as

$$N_{\Theta}(\theta) = \int_0^{\infty} \dot{\theta} f_{\Theta,\dot{\Theta}}(\theta, \dot{\theta}) d\dot{\theta}. \tag{2.1}$$

2.2 The Rayleigh Fading

In the Rayleigh Fading channel, the phase and the envelope are independent. The Probability Density Function (PDF) of the envelope is the Rayleigh distribution,

$$f_R(r) = \frac{r}{\sigma^2} \exp(\frac{-r^2}{2\sigma^2}), \tag{2.2}$$

for $r \geq 0$, and the phase PDF is the uniform RV defined by

$$f_{\Theta}(\theta) = \frac{1}{2\pi}, \tag{2.3}$$

for $-\pi < \theta \leq \pi$.

This distribution arises from the physical model of the complex envelope given by

$$\mathbb{Z} = X + jY, \tag{2.4}$$

in which X and Y are Gaussian RVs with zero mean and variance σ^2. In turn, these Gaussian RVs model a isotropic scattering propagation channel, in which the received signal is comprised of many reflected clusters of random phase and a Doppler shift that is dependent on the angle of reflection [8, 10]. X and Y are given by

$$X = \frac{1}{\sqrt{N}} \sum_{j=1}^{N} \cos(\cos(\alpha_j)\omega_d t + \phi_j) \tag{2.5}$$

and

$$Y = \frac{1}{\sqrt{N}} \sum_{j=1}^{N} \sin(\cos(\alpha_j)\omega_d t + \phi_j), \tag{2.6}$$

in which N is the number of different paths leading to the receiver, α_j is the angle of arrival at the receiver in relation to the direction of movement of the station, ω_d is the maximum radial Doppler shift and ϕ_j is the phase shift associated with the N^{th} path [8]. Both α_j and ϕ_j are RVs uniformly distributed over the interval $[-\pi, \pi)$. When N is large enough, both X and Y become Gaussian distributions (as a result of the Central Limit Theorem).

The theoretical power spectrum of the signal arriving at a moving station is

$$S(f) = \begin{cases} \frac{1}{\pi f_d \sqrt{1-((f-f_c)/f_d)^2}} & \text{if } |f - f_c| < f_d \\ 0 & \text{elsewise,} \end{cases} \tag{2.7}$$

in which f is the frequency in Hertz, f_c is the carrier frequency and $f_d = V/\lambda_c$ is the frequency of the maximum Doppler shift, with V being the speed of the receiving station and λ_c being the carrier wavelength [8, 10].

The auto-correlation between two samples of this process taken at a time difference of τ is

$$\mathbb{R}(\tau) = J_0(2\pi f_d \tau), \tag{2.8}$$

in which $J_0(x)$ is the zeroth-order Bessel function of the first kind [47, Eq.(9.1.18)].

The PCR of Rayleigh is

$$N_\Theta(\theta) = \frac{f_d}{2\sqrt{2}}. \tag{2.9}$$

The PCR is simply a constant because the phase is uniformly distributed.

2.3 The Generalized Nakagami-m Model

The Generalized Nakagami-m model is a modified version of the original Nakagami-m model that allows for an imbalance between the phase and the quadrature components [48]. The physical model of the complex envelope is given as

$$R^2 = \sum_{i=1}^{m_X} X_i^2 + \sum_{i=1}^{m_Y} Y_i^2, \tag{2.10}$$

in which each pair (X_i, Y_i) are Gaussian random variables with the same variance and zero mean, and m_X and m_Y are the number of multipath clusters in the in-phase and quadrature components. The phase parameter $-1 < p < 1$ measures the phase imbalance and is given as

$$p \triangleq \frac{m_X - m_Y}{m_X + m_Y}, \tag{2.11}$$

in which m_X and m_Y relates to the m parameter of the original Nakagami-m model by

$$2m = m_X + m_Y. \tag{2.12}$$

The phase-envelope PDF is

$$f_{R,\Theta}(r,\theta) = \frac{m^m |\sin\theta\cos\theta|^{m-1} r^{2m-1}}{\Omega^m \Gamma\left(\frac{1+p}{2}m\right)\Gamma\left(\frac{1-p}{2}m\right)|\tan\theta|^{pm}} \exp\left(-\frac{mr^2}{\Omega}\right), \tag{2.13}$$

$r \geq 0$, $-\pi < \theta \leq \pi$, in which $\Gamma(x)$ is the gamma function [47, Eq. (6.1.1)] and Ω is the mean value of the square of the envelope,

$$\Omega = E[R^2]. \tag{2.14}$$

The marginal PDFs of the envelope and phase are found to be

$$f_R(r) = \frac{2m^m r^{2m-1}}{\Omega^m \Gamma(m)} \exp\left(-\frac{mr^2}{\Omega}\right). \tag{2.15}$$

and

$$f_\Theta(\theta) = \frac{\Gamma(m)}{2^m \Gamma\left(\frac{1+p}{2}m\right)\Gamma\left(\frac{1-p}{2}m\right)} \frac{|\sin 2\theta|^{m-1}}{|\tan\theta|^{pm}}. \tag{2.16}$$

The PCR of the generalized Nakagami-m model is [49]

$$N_\Theta(\theta) = \frac{\sqrt{\pi} f_d |\sin 2\theta|^{m-1} |\tan\theta|^{-pm} \Gamma\left(m - \frac{1}{2}\right)}{2^{m+\frac{1}{2}} \Gamma\left(\frac{1+p}{2}m\right)\Gamma\left(\frac{1-p}{2}m\right)}. \tag{2.17}$$

2.3.1 Special Cases

When $p = 0$, the fading channel is balanced and the Generalized Nakagami-m reverts to its classical formulations. With this condition, the PDFs and PCR of the classical Nakagami-m fading channel can be easily found from the equations above.

From Equations (2.4) and (2.10) it is clear that Rayleigh fading is a special case of the Generalized Nakagami-m fading when $m_X = m_Y = 1$.

2.4 Rice Fading

The complex envelope of the Ricean process is

$$\mathbb{Z} = (X + p) + j(Y + q), \tag{2.18}$$

in which X and Y are Gaussian random variables with zero mean and variance σ^2 and p and q represent the power of the LOS components. The Ricean phase-envelope joint distribution is

$$f_{P,\Theta}(\rho,\theta) = \frac{1+k}{\pi}\rho \exp\left(-(1+k)\rho^2 + 2\sqrt{k(1+k)}\rho\cos(\theta-\phi) - k\right), \tag{2.19}$$

$\rho \geq 0$, $-\pi < \theta \leq \pi$, in which $k = (p^2+q^2)/(2\sigma^2)$ is the ratio of the power of the LOS components to the power of the scattered waves. The variable ρ is defined as $\rho = r/\hat{r}$, with $\hat{r}$ being the RMS value of r.

The marginal PDF of the normalized envelope is

$$f_P(\rho) = 2(1+k)\rho \exp\left[-(1+k)\rho^2 - k\right] I_0\left[2\sqrt{k(1+k)}\rho\right], \tag{2.20}$$

$\rho \geq 0$, and the marginal PDF of the phase is

$$f_\Theta(\theta) = \frac{\exp(-k)}{2\pi}(1 + \sqrt{k\pi}\exp(k\cos^2(\theta-\phi))\cos(\theta-\phi)[1+\mathrm{erf}(\sqrt{k}\cos(\theta-\phi))]), \quad (2.21)$$

$-\pi < \theta \leq \pi$, in which $\mathrm{erf}(\cdot)$ denotes the error function [47, Eq.(7.1.1)].

The PCR of the Rice fading model is [50]

$$N(\theta) = \frac{f_d}{2\sqrt{2}}\exp\left(-\frac{d^2\sin^2(\theta-\phi)}{2\sigma^2}\right)\left[1+\mathrm{erf}\left(\frac{d\cos(\theta-\phi)}{\sqrt{2}\sigma}\right)\right], \quad (2.22)$$

in which d is defined as

$$d^2 \triangleq p^2 + q^2. \quad (2.23)$$

2.4.1 Special Cases

Rayleigh fading is a special case of the Ricean fading when $p = q = 0$. This can be verified from comparing the definitions of the complex envelopes of those models, described in Equations (2.4) and (2.18), and likewise, all the equations for Rayleigh fading can be found by making this substitution to the Ricean equations.

2.5 The κ-μ Fading Model

The κ-μ envelope is defined as [15]

$$R^2 = \sum_{i=1}^{\mu}(X_i + p_i)^2 + \sum_{i=1}^{\mu}(Y_i + q_i)^2, \quad (2.24)$$

in which X_i and Y_i are independent Gaussian random variables with zero mean and variance σ^2, with each pair (X_i, Y_i) being a realization of the stochastic process defined in Equations (2.5) and (2.6). The parameter μ is the number of multipath clusters formed in the communication channel.

The in-phase and quadrature parts of the signal are given, respectively, as

$$X^2 = \sum_{i=1}^{\mu}(X_i + p_i)^2 \quad (2.25)$$

and

$$Y^2 = \sum_{i=1}^{\mu}(Y_i + q_i)^2. \quad (2.26)$$

in which the terms p_i and q_i are the mean values of the in-phase and quadrature components of the multipath cluster i.

Throughout the text, whenever X and Y can be used interchangeably they are often referred to as the variable Z, in which case p or q are denoted by λ. More specifically, let Z be

$$Z^2 = \sum_{i=1}^{\mu}(Z_i + \lambda_i)^2, \quad (2.27)$$

in which: (i) Z may denote either X or Y, defined in Equations (2.25) and (2.26); (ii) Z_i are independent Gaussian RVs with zero mean and variance σ^2; (iii) λ_i^2 is the power

of the dominant component of the multipath cluster i, denoting either p or q expressed in Equation (2.28); and (iv) μ is the number of multipath clusters.

The power of the in-phase and quadrature components are given as

$$p^2 = \sum_{i=1}^{\mu} p_i^2 \qquad \text{and} \qquad q^2 = \sum_{i=1}^{\mu} q_i^2, \tag{2.28}$$

and the total power of the dominant components is

$$d^2 = \sum_{i=0}^{\mu} \left(p_i^2 + q_i^2\right). \tag{2.29}$$

The parameter κ is the ratio of the total power of the dominant components and the power of the scattered waves,

$$\kappa = d^2/2\mu\sigma^2. \tag{2.30}$$

The variance of the Gaussian processes can be written as a function of the parameters κ and μ and the root mean square (RMS) value of the envelope $\hat{r} = \sqrt{E[R^2]}$,

$$\sigma^2 = \frac{\hat{r}^2}{2\mu(1+\kappa)}. \tag{2.31}$$

In [16], a phase parameter $\phi \triangleq \arg(p + jq)$ was introduced. It allows the terms p and q to be written as a function of κ, μ and ϕ,

$$p = \sqrt{\frac{\kappa}{1+\kappa}}\hat{r}\cos(\phi) \tag{2.32}$$

and

$$q = \sqrt{\frac{\kappa}{1+\kappa}}\hat{r}\sin(\phi). \tag{2.33}$$

The PDF of $|Z|$ and Z are given as [16]

$$f_{|Z|}(z) = \frac{z^{\frac{\mu}{2}}}{\sigma^2|\lambda|^{\frac{\mu}{2}-1}} \exp\left(-\frac{z^2+\lambda^2}{2\sigma^2}\right) I_{\frac{\mu}{2}-1}\left(\frac{|\lambda|z}{\sigma^2}\right), \tag{2.34}$$

$z \geq 0$, and

$$f_Z(z) = \frac{|z|^{\frac{\mu}{2}}}{2\sigma^2|\lambda|^{\frac{\mu}{2}-1}} \exp\left(-\frac{(z-\lambda)^2}{2\sigma^2}\right) I_{\frac{\mu}{2}-1}\left(\frac{|\lambda z|}{\sigma^2}\right) \operatorname{sech}\left(\frac{\lambda z}{\sigma^2}\right), \tag{2.35}$$

in which $I_\nu(z)$ denotes the modified Bessel function of the first kind [47, Eq. (9.6.3)] and $\operatorname{sech}(\cdot)$ denotes the hyperbolic secant [47, Eq. (4.5.5)].

Observe that although the probability distribution of the in-phase or quadrature components is known, the complex envelope is not. Equation (2.35) was achieved by combining the PDF of $|Z|$, the absolute value of the RV Z, with the knowledge of the PDF of Z at a particular case. More details on this derivation are found in [16]. The absence of a well defined complex envelope complicates the simulation of the phase, as will be discussed in later parts.

The joint PDF of the normalized envelope P and the phase Θ of the κ-μ model is given as [16]

$$\begin{aligned} f_{P,\Theta}(\rho,\theta) &= \frac{1}{2}\mu^2\kappa^{1-\frac{\mu}{2}}(1+\kappa)^{\frac{\mu+2}{2}}\rho^{\mu+1}|\sin 2\theta|^{\frac{\mu}{2}}|\sin 2\phi|^{1-\frac{\mu}{2}} \\ &\times \exp\left(-\mu(1+\kappa)\rho^2 - \kappa\mu + 2\mu\sqrt{\kappa(1+\kappa)}\rho\cos(\theta-\phi)\right) \\ &\times I_{\frac{\mu}{2}-1}\left(2\mu\sqrt{\kappa(1+\kappa)}\rho|\cos\theta\cos\phi|\right)\operatorname{sech}\left(2\mu\sqrt{\kappa(1+\kappa)}\rho\cos\theta\cos\phi\right) \\ &\times I_{\frac{\mu}{2}-1}\left(2\mu\sqrt{\kappa(1+\kappa)}\rho|\sin\theta\sin\phi|\right)\operatorname{sech}\left(2\mu\sqrt{\kappa(1+\kappa)}\rho\sin\theta\sin\phi\right), \end{aligned} \tag{2.36}$$

$\rho \geq 0$, $-\pi < \theta \leq \pi$.

In this thesis P denotes the envelope normalized by its RMS value, rather than the scaled version found in [16]. Two particular cases of the joint envelope were also presented in [16], for $\phi = \pm n\pi$ and for $\phi = \pm\frac{(2n+1)\pi}{2}$. They are

$$\begin{aligned} f_{P,\Theta}(\rho,\theta)|_{\phi=\pm n\pi} &= \frac{1}{\Gamma\left(\frac{\mu}{2}\right)}\mu^{1+\frac{\mu}{2}}\kappa^{\frac{1}{2}-\frac{\mu}{4}}(1+\kappa)^{\frac{1}{2}+\frac{3\mu}{4}}\rho^{\frac{3\mu}{2}}|\sin\theta|^{\mu-1}|\cos\theta|^{\frac{\mu}{2}} \\ &\times \exp\left(-\mu(1+\kappa)\rho^2 - \kappa\mu + 2\mu\sqrt{\kappa(1+\kappa)}\rho\cos\theta\cos\phi\right) \\ &\times I_{\frac{\mu}{2}-1}\left(2\mu\sqrt{\kappa(1+\kappa)}\rho|\cos\theta|\right)\operatorname{sech}\left(2\mu\sqrt{\kappa(1+\kappa)}\rho\cos\theta\right) \end{aligned} \tag{2.37}$$

and

$$\begin{aligned} f_{P,\Theta}(\rho,\theta)|_{\phi=\pm\frac{(2n+1)\pi}{2}} &= \frac{1}{\Gamma\left(\frac{\mu}{2}\right)}\mu^{1+\frac{\mu}{2}}\kappa^{\frac{1}{2}-\frac{\mu}{4}}(1+\kappa)^{\frac{1}{2}+\frac{3\mu}{4}}\rho^{\frac{3\mu}{2}}|\cos\theta|^{\mu-1}|\sin\theta|^{\frac{\mu}{2}} \\ &\times \exp\left(-\mu(1+\kappa)\rho^2 - \kappa\mu + 2\mu\sqrt{\kappa(1+\kappa)}\rho\sin\theta\sin\phi\right) \\ &\times I_{\frac{\mu}{2}-1}\left(2\mu\sqrt{\kappa(1+\kappa)}\rho|\sin\theta|\right)\operatorname{sech}\left(2\mu\sqrt{\kappa(1+\kappa)}\rho\sin\theta\right), \end{aligned} \tag{2.38}$$

in which $\Gamma(\cdot)$ is the complete gamma function [47, Eq.(6.1.1)]. The PDF of the normalized envelope P can be found by integrating Equation (2.36) with respect to Θ from $-\pi$ to π or it can be derived in a straightforward fashion as shown in [15]. It is given as

$$f_P(\rho) = \frac{2\mu(1+\kappa)^{\frac{\mu+1}{2}}}{\kappa^{\frac{\mu-1}{2}}\exp(\mu\kappa)}\rho^{\mu}\exp\left[-\mu(1+\kappa)\rho^2\right] I_{\mu-1}\left[2\mu\sqrt{\kappa(1+\kappa)}\rho\right], \tag{2.39}$$

$\rho \geq 0$.

The phase PDF is found by integrating either one of Equations (2.36) to (2.38)) with respect to ρ from 0 to ∞,

$$f_\Theta(\theta) = \int_0^\infty f_{P,\Theta}(\rho,\theta)d\rho. \tag{2.40}$$

No closed-form expression was found for this integral and it can only be calculated numerically.

The PCR of the $\kappa-\mu$ fading channel was found as an integral form in [44]. Let $N_\Theta(\theta)$ denote the κ-μ PCR and let the function $N_\Theta(\rho,\theta)$ be defined in such a way that

$$N_\Theta(\theta) = \int_0^\infty N_\Theta(\rho,\theta)d\rho. \tag{2.41}$$

$N_\Theta(\rho,\theta)$ was found to be [44, 46]

$$\begin{aligned} N_\Theta(\rho,\theta) &= \frac{\sqrt{\pi}f_d}{2\sqrt{2}}\mu^{3/2}\kappa^{1-\frac{\mu}{2}}(1+\kappa)^{\frac{\mu+1}{2}}\rho^{\mu} \\ &\times \exp(-\kappa\mu)|\sin 2\theta|^{\frac{\mu}{2}}|\sin 2\phi|^{1-\frac{\mu}{2}} \\ &\times \exp\left(-\mu(1+\kappa)\rho^2 + 2\mu\sqrt{\kappa(1+\kappa)}\rho\cos(\theta-\phi)\right) \\ &\times I_{\frac{\mu}{2}-1}\left(2\mu\sqrt{\kappa(1+\kappa)}\rho|\cos\theta\cos\phi|\right) \\ &\times I_{\frac{\mu}{2}-1}\left(2\mu\sqrt{\kappa(1+\kappa)}\rho|\sin\theta\sin\phi|\right) \\ &\times \operatorname{sech}\left(2\mu\sqrt{\kappa(1+\kappa)}\rho\cos\theta\cos\phi\right) \\ &\times \operatorname{sech}\left(2\mu\sqrt{\kappa(1+\kappa)}\rho\sin\theta\sin\phi\right), \end{aligned} \tag{2.42}$$

and the exact PCR can be found by perform the integration described in Equation (2.41).

2.5.1 Special Cases

The original formulation of the Nakagami-m fading model, obtained by setting $p = 0$ in Equation (2.11), is a special case of the $\kappa - \mu$ fading channel when $\kappa \to 0$.

The Ricean channel is also a particular case of the κ-μ process when $\mu = 1$ and $\kappa = k$.

The Rayleigh fading channel, being a special case of both Rice and Nakagami-m models, is also a special case of the $\kappa - \mu$ model, obtained when $\mu = 1$ and $\kappa \to 0$.

2.6 Simulation Techniques

As showed in the previous sections, the Complex Envelopes of various fading channels are described in terms of algebraic operations over Gaussian RVs. In turn, these RVs model the signal resulted from multiple reflections, causing the signal to arrive at a moving receiving station from multiple angles, with a random phase and frequency shift due to the Doppler effect. Each different reflection is then, in itself, a random variable, and the Central Limit Theorem assures that, given enough random variables, their sum can be adequately approximated by a Gaussian RV. The fact that a station is in continuous movement makes each Gaussian RV resulting from the process above have a particular power spectrum, described by Equation (2.7), and to be correlated according to Equation (2.8).

With this theory established, the path to a simulator becomes clear. First it is necessary to generate properly correlated, Gaussian distributed, random samples and then combine the samples in the adequate way according to which model is being simulated. The latter is only a matter of applying the suitable operations of the relevant model. For instance, starting from two correlated sequences X_n and Y_n, one can simulate a Rayleigh channel sequence Z_n by simply substituting each X_n and Y_n in Equation (2.4). As for the former, a few strategies have been derived.

The most straightforward simulator that generates Gaussian-distributed samples with the desired auto-correlation and power spectrum is perhaps the Jakes' simulator [10]. The simulator discretizes the angles of arrival and uses a series of oscillators to simulate each reflected component. It outputs a continuous signal that approximates well the power spectrum and auto-correlation, becoming better with a greater number of oscillators. The power spectrum becomes a discrete version of Equation (2.7).

An efficient discrete simulator can be achieved with the aid of the Inverse Discrete Fourier Transform (IDFT) [51–53]. First a sequence of uncorrelated Gaussian distributed samples is generated. Then, each sample is multiplied by a filter sequence and then the IDFT is performed over the sequence. The result is a Gaussian distributed complex sequence, with auto-correlation defined by the filter sequence. By choosing an appropriate filter, it is possible to obtain a sequence correlated according to Equation (2.8). The result is a complex valued, Gaussian distributed, auto-correlated, discrete sequence. Since the real and imaginary parts are correlated to each other, the imaginary part is usually discarded, resulting in a real valued sequence. This process can be repeated with as many sequences of uncorrelated Gaussian samples as needed in order to generate the number of RVs used by a particular model. For instance, to simulate the complex envelope of a Rayleigh channel described in Equation (2.4), the process would be repeated two times to generate the X and Y sequences. The same can be done to simulate the Ricean fading. The Generalized Nakagami-m channel requires $m_X + m_Y$ Gaussian sequences, whereas the κ-μ channel requires 2μ.

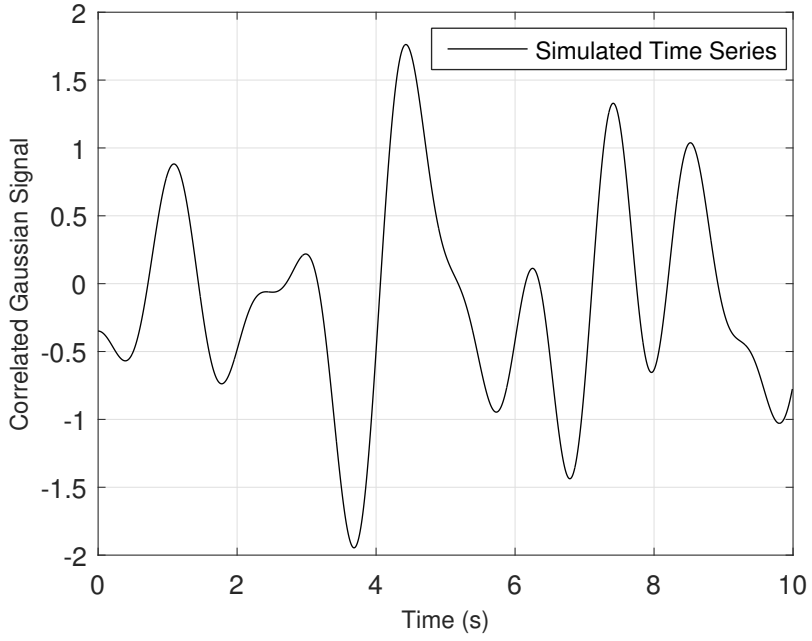

Figure 2.1: Simulated correlated Gaussian time series, with normalized maximum Doppler shift $f_D = 1$ and sample frequency $F_s = 100F_D$. The Gaussian distribution used to generate the time series has zero mean and unitary variance.

In the simulations presented in this thesis, the following filter sequence described in [51,52] was used,

$$F[k] = \begin{cases} 0, & k = 0, \\ \sqrt{\dfrac{1}{1\sqrt{1-\left(\frac{k}{Nf_d}\right)^2}}}, & k = 1, 2, \ldots, k_m - 1, \\ \sqrt{\frac{k}{2}\left[\frac{\pi}{2} - \arctan\left(\frac{k-1}{\sqrt{2k-1}}\right)\right]}, & k = k_m, \end{cases} \tag{2.43}$$

in which $k_m = \lfloor f_d N \rfloor$. Each term of the filter sequence is multiplied by a sample of the N-long Gaussian sequence prior to the application of the IDFT. Since the IDFT itself is a weighted sum of the Gaussian samples, the output of the IDFT will have a Gaussian distribution. The overarching idea of this process is to shape the power spectrum of the output sequence so that it agrees with Equation (2.7). Note that the filter sequence is the discretized version of the continuous auto-correlation, from $f = 0$ to $f = f_D$, with the last term being an approximation to the weight of the area under the last bin of the discretized frequency, to avoid the infinity at f_D that would arise if the exact formula was used.

Figures 2.1 and 2.2 show the time series and auto-correlation of a simulated Gaussian sequence, normalized for unitary variance. In Figure 2.2, the exact auto-correlation is compared with the simulated samples auto-correlation, showing a remarkable agreement. Figure 2.3 portrays the distribution of the samples superimposed with a zero mean, unitary variance Gaussian distribution, illustrating that the process of multiplying a Gaussian sequence by the filter sequence and then performing an IDFT over the sequence preserves the Gaussian nature of the original samples, as expected.

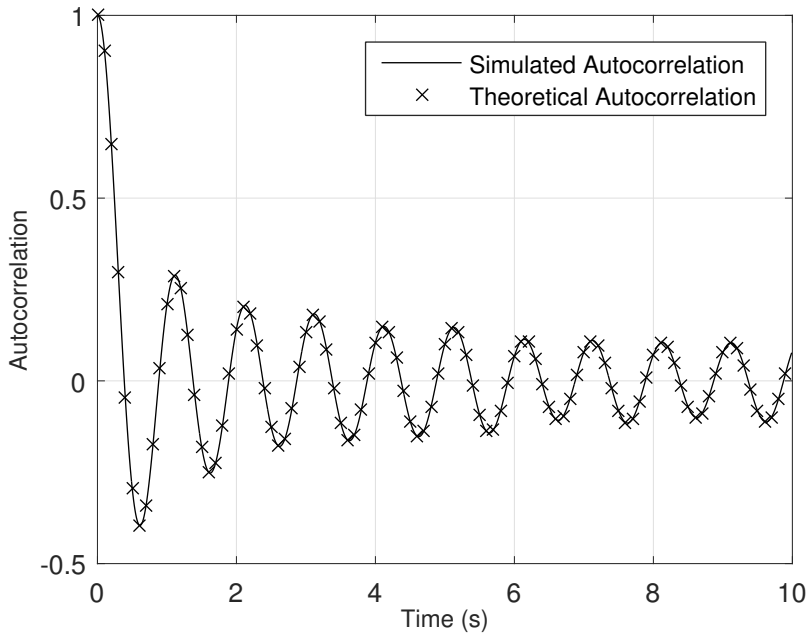

Figure 2.2: Simulated and theoretical auto-correlation, with normalized maximum Doppler shift $f_D = 1$ and sample frequency $F_s = 100F_D$. The theoretical auto-correlation function depicted here is $J_0(2\pi t)$.

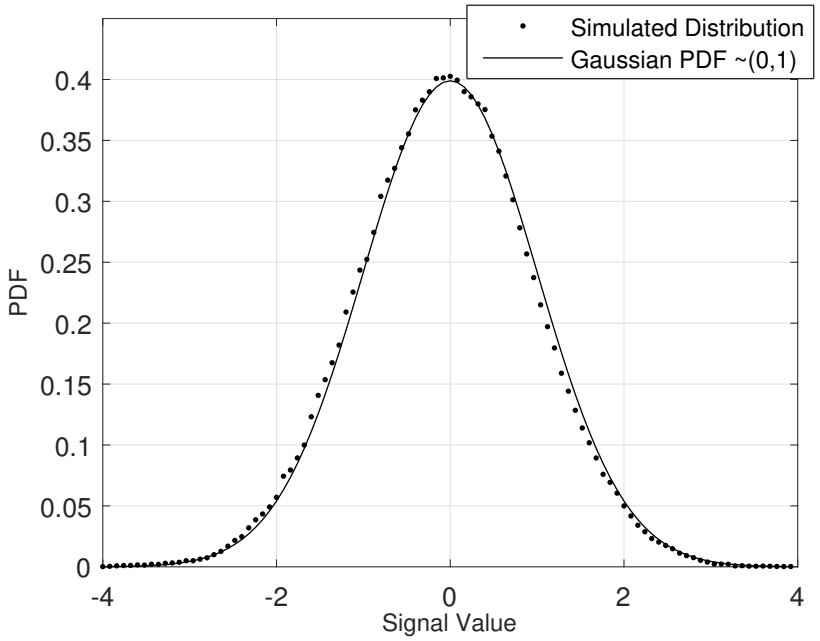

Figure 2.3: Simulated and theoretical sample distribution, showing the Gaussian nature of the correlated samples.

2.6.1 The simulation of the absolute value of the κ-μ components

The absolute value of the components of the κ-μ fading model can be simulated in a straightforward way with the aid of the physical model in Equation (2.24), for integer μ. The variables X_i and Y_i can be modeled in time as the discrete samples $X_i[k]$ and $Y_i[k]$ of a stochastic process, with the auto-correlation in Equation (2.8). Let Z be X or Y and λ be p or q as required. The series $|Z[k]|$ of the κ-μ model can be obtained with the aid of the inverse Fourier transform, according to the block diagram in Figure 2.4 [53]. The filter sequence in the diagram is the one defined in Equation (2.43), and the output sequence will be distributed according to the statistics of $|Z|$.

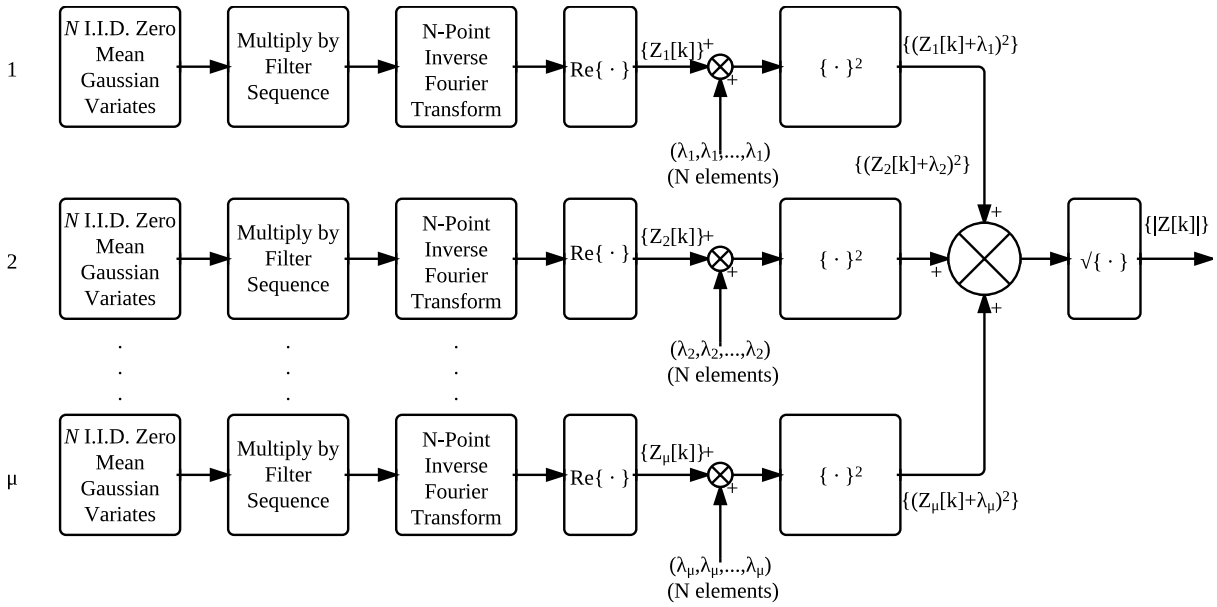

Figure 2.4: Block diagram of the simulation of Z.

On an ending note, only the envelope of the κ-μ process is defined. There is no physical model for the complex envelope, $\mathbb{Z} = X + jY$, which complicates the simulation. This will be further discussed in Chapter 5, in which a simulation model is developed.

Chapter 3

The Phase CDF and The Inverse Phase CDF of the Generalized Nakagami-m Fading Process

3.1 Introduction

This chapter contains an expanded version of the original paper published in [45]. It presents the derivations of the exact, closed-form formulations for the CDF of the phase Θ of the Generalized Nakagami-m fading process and its inverse, denoted respectively by $F_{\Theta}(\theta)$ and $F_{\Theta}^{-1}(y)$. The formulations found are then fitted to field measurements. The original paper presented for the first time such practical validation of the phase statistics of the generalized Nakagami-m fading channel.

3.2 Phase CDF

The straightforward way to find the phase CDF is to integrate the phase PDF, presented in Equation (2.16), with regards to θ. The direct integration is, however, hindered by the absolute valued functions that are part of the phase PDF expression. One way to tackle the integration is to first divide the domain of the function in smaller parts in which the signal of the absolute valued functions is invariant, evaluate the integral in one of these smaller domains and then expand the expression to the whole domain by using the symmetries and periodicity of the phase PDF.

From Equation (2.16) it can be seen that the phase PDF is periodic with period π, and has even symmetry. Define the auxiliary functions $a_1(\theta)$ and $a_2(\theta)$ over the interval $[0, \pi/2)$ as

$$a_1(\theta) = \begin{cases} f_{\Theta}(\theta) & \text{if } 0 \leq \theta < \pi/2, \\ 0 & \text{elsewhere,} \end{cases} \tag{3.1}$$

and

$$a_2(\theta) = \begin{cases} f_{\Theta}(-\theta + \pi/2) & \text{if } 0 \leq \theta < \pi/2, \\ 0 & \text{elsewhere.} \end{cases} \tag{3.2}$$

Note that in the interval $[0, \pi/2)$ considered, both $\sin(2\theta)$ and $\tan(\theta)$ are always non negative. Thus, in this interval, the phase PDF becomes

$$f_\Theta(\theta) = a_1(\theta) = \frac{\Gamma(m)}{2^m \Gamma\left(\frac{1+p}{2}m\right)\Gamma\left(\frac{1-p}{2}m\right)} \frac{(\sin 2\theta)^{m-1}}{(\tan\theta)^{pm}}, \text{ for } 0 \leq \theta < \pi/2. \tag{3.3}$$

The auxiliary functions $a_1(\theta)$ and $a_2(\theta)$ are related to each other as

$$a_2(\theta) = a_1(\pi/2 - \theta). \tag{3.4}$$

Figure 3.1 shows the auxiliary functions in comparison to the phase PDF. The $a1$ function is congruous to the phase PDF in the $[0, \pi/2)$ interval, whereas the $a2$ function is a mirrored version of $a1$ in that interval.

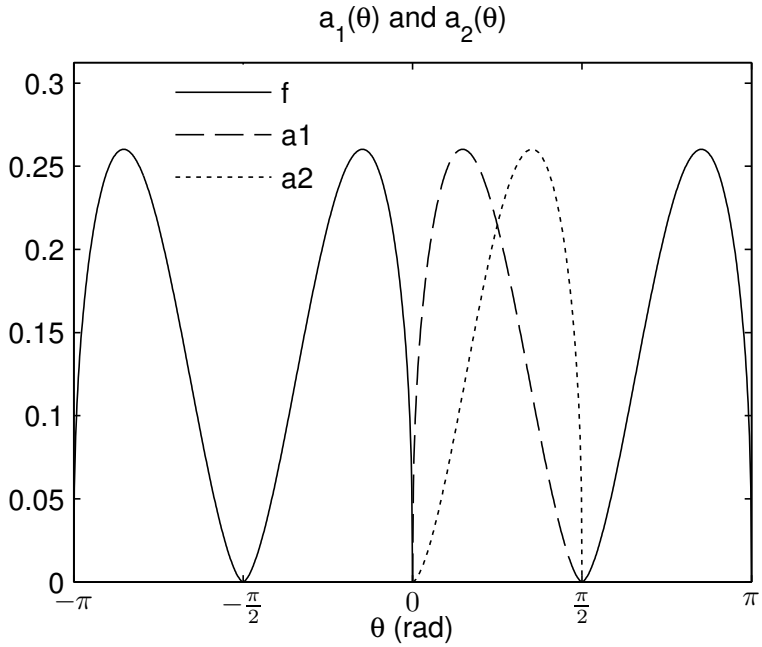

Figure 3.1: Comparison between the phase PDF and auxiliary functions $a1$ and $a2$.

The phase PDF $f_\Theta(\theta)$ can be expressed in a piecewise fashion as

$$f_\Theta(\theta) = \begin{cases} a_1(\theta + \pi) & \text{if } -\pi \leq \theta < -\pi/2 \\ a_2(\theta + \pi/2) & \text{if } -\pi/2 \leq \theta < 0 \\ a_1(\theta) & \text{if } 0 \leq \theta < \pi/2 \\ a_2(\theta - \pi/2) & \text{if } \pi/2 \leq \theta < \pi. \end{cases} \tag{3.5}$$

The advantage of this representation lies in the fact that the integral of $a_1(\theta)$ as well as that of $a_2(\theta)$ may be found in closed form, as discussed next. From Equations (3.4) and (3.5), it can be inferred that $\int_0^{\pi/2} a_1(\theta)d\theta = \int_0^{\pi/2} a_2(\theta)d\theta = 1/4$, since the area below $f_\Theta(\theta)$ is equal to 1. By defining $A_1(\theta) = \int_0^\theta a_1(x)dx$ and $A_2(\theta) = \int_0^\theta a_2(x)dx$, we can write the phase CDF as

$$F_\Theta(\theta) = \begin{cases} 0 & \text{if } \theta < -\pi \\ A_1(\theta+\pi) & \text{if } -\pi \le \theta < -\pi/2 \\ 1/4 + A_2(\theta+\pi/2) & \text{if } -\pi/2 \le \theta < 0 \\ 1/2 + A_1(\theta) & \text{if } 0 \le \theta < \pi/2 \\ 3/4 + A_2(\theta-\pi/2) & \text{if } \pi/2 \le \theta < \pi \\ 1 & \text{if } \theta \ge \pi. \end{cases} \tag{3.6}$$

The integration of $a_1(\theta)$ results in

$$A_1(\theta) = 1/4 - \frac{1}{4} I_{\cos^2(\theta)}\left(\frac{1}{2}m(p+1), \frac{1}{2}m(1-p)\right), \tag{3.7}$$

in which $I_v(a,b)$ denotes the regularized beta function [47, Eq. (6.6.2)].

By defining the auxiliary function $U(\theta)$ as

$$U(\theta) = \frac{1}{4} I_{\cos^2(\theta)}\left(\frac{1}{2}m(p+1), \frac{1}{2}m(1-p)\right) \tag{3.8}$$

the functions $A_1(\theta)$ and $A_2(\theta)$ can be succinctly written as

$$A_1(\theta) = 1/4 - U(\theta) \text{ and} \tag{3.9}$$

$$A_2(\theta) = U(\pi/2 - \theta), \tag{3.10}$$

$0 \le \theta < \pi/2$.

Replacing Equations (3.9) and (3.10) into Equation (3.6), $F_\Theta(\theta)$ is found as

$$F_\Theta(\theta) = \begin{cases} 0 & \text{if } \theta < -\pi \\ 1/4 - U(\theta+\pi) & \text{if } -\pi \le \theta < -\pi/2 \\ 1/4 + U(-\theta) & \text{if } -\pi/2 \le \theta < 0 \\ 3/4 - U(\theta) & \text{if } 0 \le \theta < \pi/2 \\ 3/4 + U(\pi-\theta) & \text{if } \pi/2 \le \theta < \pi \\ 1 & \text{if } \theta \ge \pi. \end{cases} \tag{3.11}$$

In Equation (3.11), $U(\theta)$ is defined for $\theta \in [0, \pi/2)$. By allowing θ to assume any value within $[-\pi, \pi)$, the following properties of $U(\theta)$ can be derived as

$$U(\theta) = U(-\theta), \tag{3.12}$$

$$U(\theta+\pi) = U(\theta) \text{ and} \tag{3.13}$$

$$U(\pi-\theta) = U(\theta). \tag{3.14}$$

Combining the previous identities with Equation (3.11), $F_\Theta(\theta)$ can be further simplified to

$$F_\Theta(\theta) = \begin{cases} 0 & \text{if } \theta < -\pi \\ 1/4 - U(\theta) & \text{if } -\pi \le \theta < -\pi/2 \\ 1/4 + U(\theta) & \text{if } -\pi/2 \le \theta < 0 \\ 3/4 - U(\theta) & \text{if } 0 \le \theta < \pi/2 \\ 3/4 + U(\theta) & \text{if } \pi/2 \le \theta < \pi \\ 1 & \text{if } \theta \ge \pi. \end{cases} \tag{3.15}$$

This piecewise formula can be grouped into a single equation with the aid of the sign and square wave functions as

$$F_\Theta(\theta) = \frac{2 + \text{sign}(\theta)}{4} - \text{S}\left(\frac{\theta}{\pi}\right) U(\theta), \quad -\pi \leq \theta < \pi, \tag{3.16}$$

in which the sign function $\text{sign}(x)$ is defined as being valued -1 for $x < 0$, 0 for $x = 0$ and 1 for $x > 0$, and the square wave function $\text{S}(x)$ is defined as $\text{S}(x) \triangleq \text{sign}(\sin(2\pi x))$.

3.3 Inverse Phase CDF

The same piecewise approach used to find the phase CDF can be used to find its inverse. This allows the inverse CDF to be expressed in terms of $U^{-1}(y)$, $0 \leq y < 1/4$, with $U^{-1}(y)$ meaning the inverse of $U(\theta)$ for $0 \leq \theta < \pi/2$. The restriction to the domain of $U(\theta)$ is needed to guarantee that the function is a bijection, which is a necessary condition for it to have an inverse function. From inspection of Equation (3.11), the inverse CDF can be written as

$$F_\Theta^{-1}(y) = \begin{cases} U^{-1}(1/4 - y) - \pi & \text{if } 0 \leq y < 1/4 \\ -U^{-1}(y - 1/4) & \text{if } 1/4 \leq y < 1/2 \\ U^{-1}(3/4 - y) & \text{if } 1/2 \leq y < 3/4 \\ \pi - U^{-1}(y - 3/4) & \text{if } 3/4 \leq y < 1, \end{cases} \tag{3.17}$$

$0 \leq y < 1$. The function $U^{-1}(y)$ is found from Equation (3.8) as

$$U^{-1}(y) = \arccos\left(\sqrt{I_{4y}^{-1}\left(\frac{1}{2}m(p+1), \frac{1}{2}m(1-p)\right)}\right), \tag{3.18}$$

$0 \leq y < 1/4$. Finally, we combine Equations (3.17) and (3.18)) in a single equation,

$$F_\Theta^{-1}(y) = \text{S}(2y) \times U^{-1}\left(\frac{\text{T}(2y + 1/4) + 1}{8}\right) + \pi\lfloor 2y - 1/2 \rfloor, \tag{3.19}$$

with the aid of the square wave function $\text{S}(x)$ defined above and the triangular wave function defined as $\text{T}(x) \triangleq \frac{2}{\pi}\sin^{-1}(\sin(2\pi x))$. This concludes the derivation of the inverse phase CDF of the Nakagami-m signal.

3.4 Some Plots

Figure 3.2 shows two families of the CDF for the general case, for the fading parameters $m = 1.5$ and $m = 0.75$, and varying phase parameter p, described in Equation (2.11). As can be seen, for any p, the phase is equally likely to be found in any one of the four quadrants. However, as p departs from zero toward one or minus one, the distribution becomes more impulsive. This happens because when $p = 1$ there are no quadrature component, and when $p = -1$ there are no in-phase component, so, for these values of p, the phase concentrate respectively at the specific values 0 and π, or $\pi/2$ and $-\pi/2$.

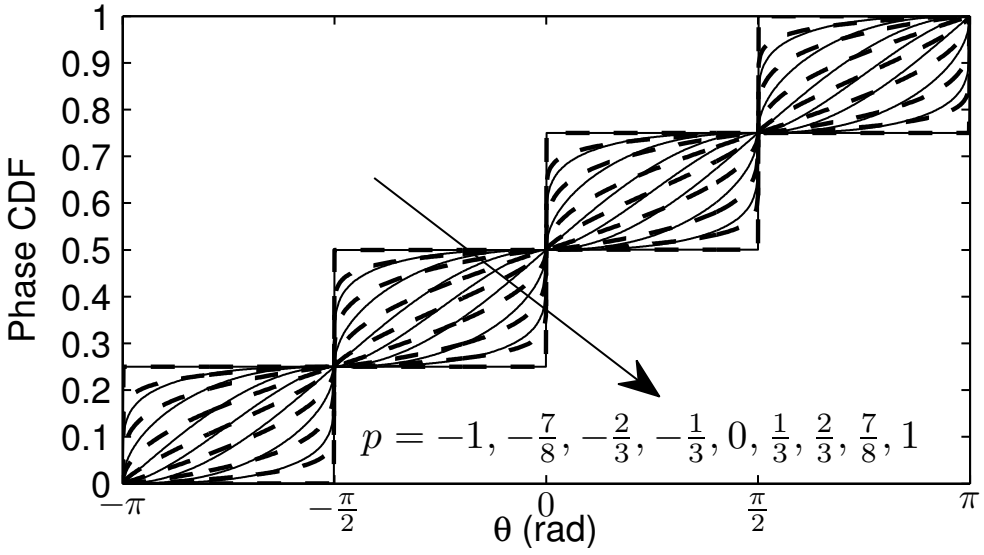

Figure 3.2: Two families of curves of the phase CDF, for a varying phase parameter and fading parameters $m = 1.5$ (solid line) and $m = 0.75$ (dashed line). The arrow indicates the direction of growing p.

3.5 Fitted Field Data

In this section, field data from experiments conducted by Cotton et al. [54] is fitted to the Generalized Nakagami-m channel PDF and CDF. In these experiments, a transmitter located at the user's left waist transmitted at 2.45 GHz and the signal was received by 5 mm higher mode microstrip patch antennas [55] arranged in a body area network setup throughout the body of the subject. The receivers were placed on the right side of the head, front chest, waist, knee, ankle, wrist, and elbow of the subject, and recorded by a vector network analyzer (Rhode & Schwarz ZVB-8 VNA) that was configured to take measurements at 5 ms intervals for 30 seconds. During the experiment, the subject simulated a walking motion. From the data acquired, the phase PDF, CDF and PCR were calculated and then fitted to the theoretical expressions.

To fit the data, a parametric search method to find good estimations for the parameters m and p was performed. First a non-linear optimization algorithm set to minimize the mean square error between the theoretical expression and the field measurements was used to find a starting point for p and m. From those parameters, a manual search was performed to refine the fit. The goal of this optimization was to find theoretical curves that yielded a good representation of the features of the phase PDF of the experimental data while maintaining a low error.

Figures 3.3 to 3.6 show the data for two sensors in the anechoic chamber, the ones on the ankle and wrist of the subject. This kind of chamber is engineered to minimize any environmental reflections, which means that any multipath clusters will be primarily caused by diffracted creeping waves and on-body surface waves. The signal captured by the sensor in the ankle is well modeled by a parameter $m < 1$, suggesting a partial cluster leading to a severe fading, whereas the estimated m parameter greater than one on the ankle sensor implies the occurrence of some type of clustering. Note how these odd phase shapes are

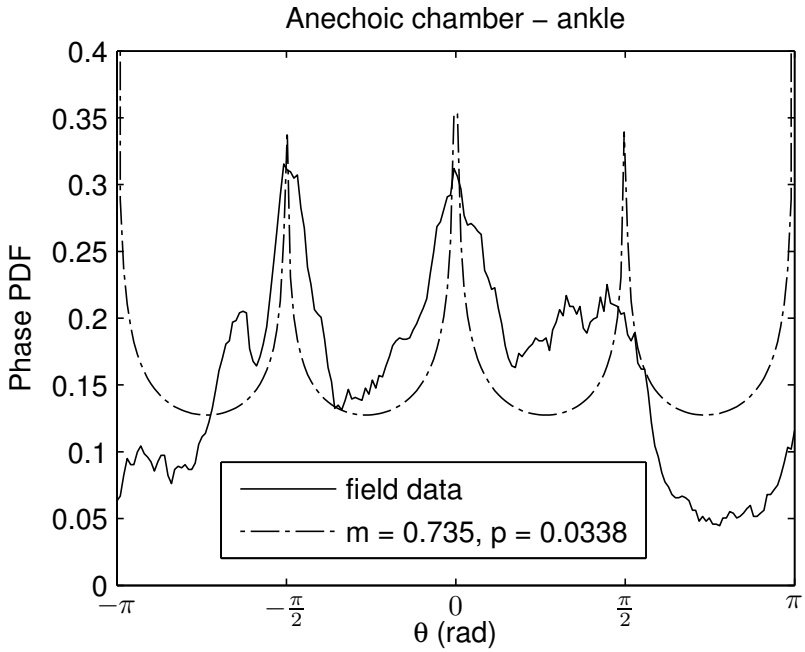

Figure 3.3: Phase PDF for $m < 1$ adjusted to field measurements.

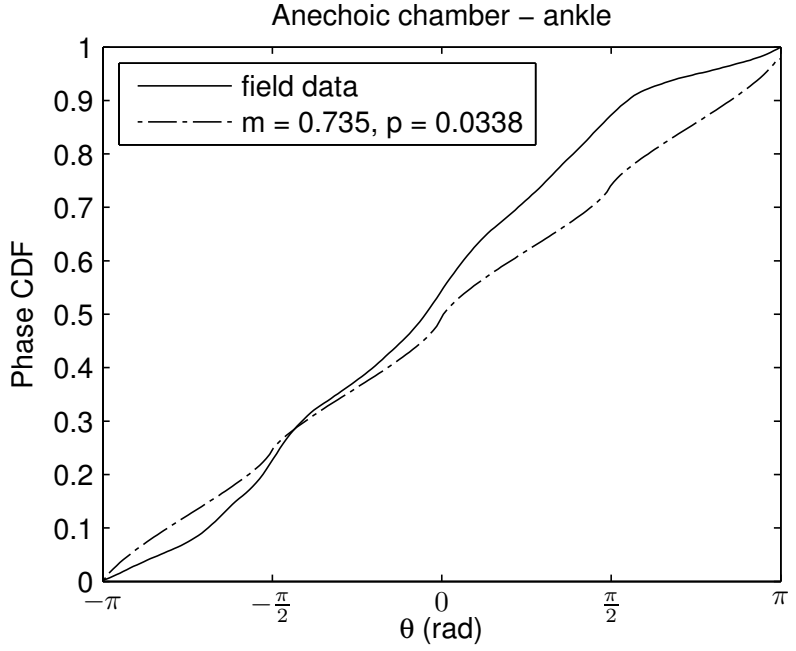

Figure 3.4: Phase CDF for $m < 1$ adjusted to field measurements.

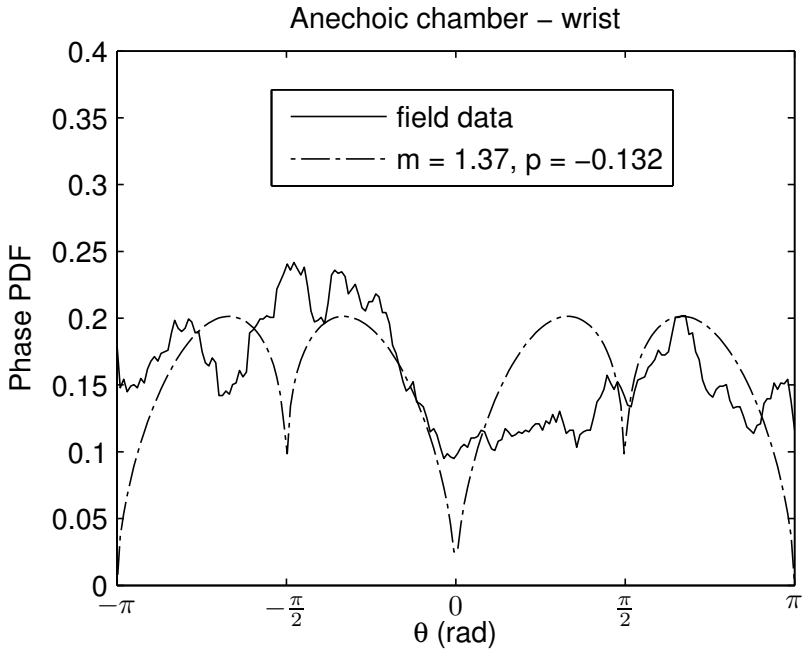

Figure 3.5: Phase PDF for $m > 1$ adjusted to field measurements.

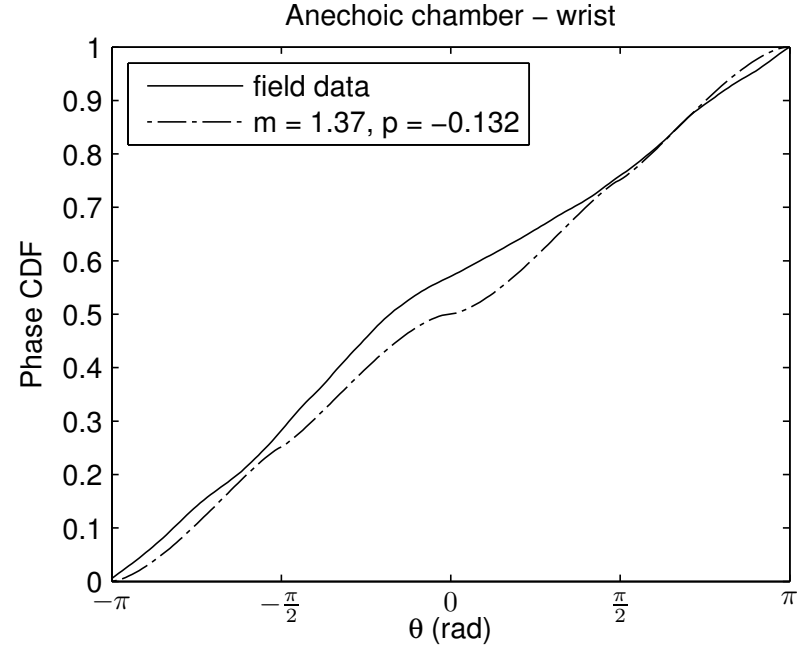

Figure 3.6: PCR for $m > 1$ adjusted to field measurements.

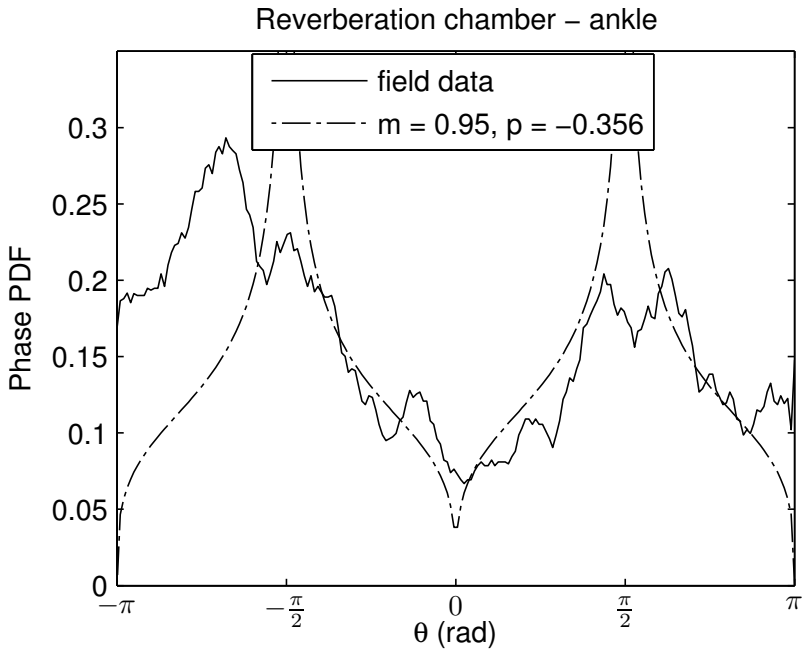

Figure 3.7: Phase PDF for $m < 1$ adjusted to field measurements.

reasonably followed by the theoretical curves. Figures 3.3 and 3.4 show a very low power imbalance p parameter, meaning that the received signal's power is shared almost equally between the in-phase and quadrature components. In both the ankle and wrist sensors, the signal reception will be strongest when the respective limb moves from its position alongside the body to the front of the body. In terms of phase, the paths linking the two antennas will be constantly changing. However, the phase repeats as the arm or leg moves from behind to the front of the body and back again.

Figures 3.7 to 3.10 show the phase PDF and CDF of the signal captured by two sensors in the reverberation chamber experiment. In contrast with the anechoic chamber, the reverberation chamber is built in order to increase the reflections of the waves, generating a great number of multipath clusters. The data obtained from this chamber fits better the Generalized Nakagami-m model, which is expected since this fading channel assumes non-LOS conditions.

Finally, Figures 3.11 and 3.12 show the Phase Crossing Rate of the ankle sensor in both the anechoic and reverberation chambers. As can be inferred through their respective theoretical formulations, the shapes of the phase PDF and PCR are akin to each other, bearing the same overall shape for the same set of parameters. Interestingly, for the majority of the curves, the same set of parameters used to fit the phase PDF (or CDF) also yielded a very good fit to the PCR, which is well illustrated by the two examples here. This suggests that the underlying physical processes involved in the modeling of the Nakagami-m complex signal are plausible, since the second order statistics predicted by the model find validation in the field data. Another interesting observation is that although the propagation conditions estimated are found to be rather close to that of Rayleigh (m approaching one), the measured PCR departs from the classical Rayleigh PCR, which is supposed to be constant. Indeed, as predicted by Equations (2.16) and (2.17), even the Rayleigh condition ($m = 1$) may be associated to a non-uniform phase PDF or a non-constant PCR, depending on the

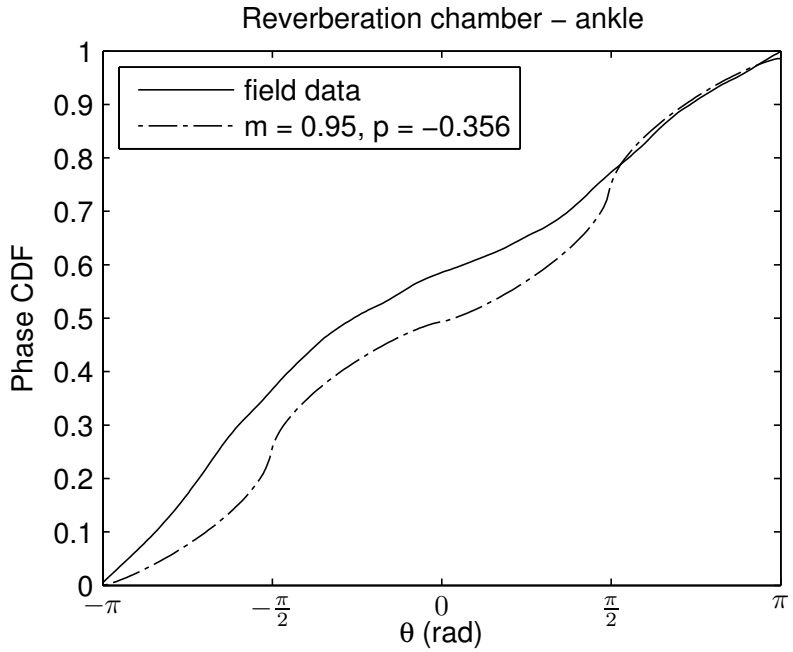

Figure 3.8: Phase CDF for $m < 1$ adjusted to field measurements.

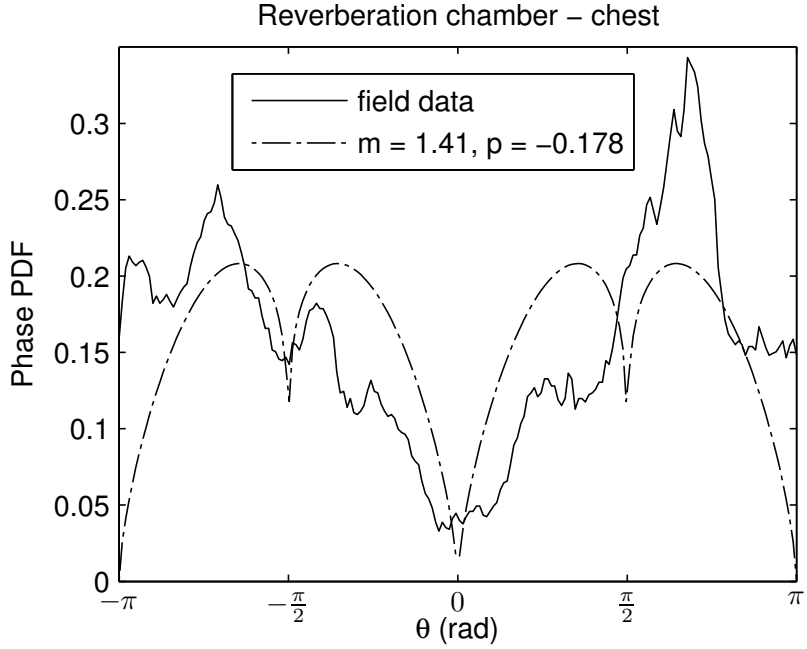

Figure 3.9: Phase PDF for $m > 1$ adjusted to field measurements.

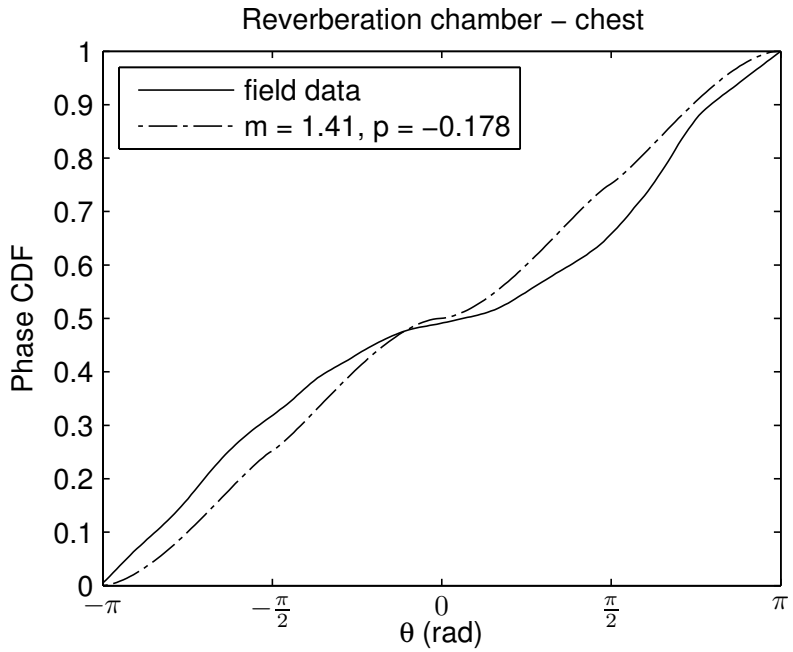

Figure 3.10: Phase CDF for $m > 1$ adjusted to field measurements.

phase parameter p. Figures 3.11 and 3.12 are thus an example of conditions for which the Generalized Nakagami-m model is more suited than the Rayleigh channel.

As can be seen in all plots, although some distance between theoretical and practical plots exists, the shapes of the curves are very similar to each other.

3.6 Conclusion

In this Chapter, exact, closed-form expressions for both the CDF and the inverse CDF of the phase of the Nakagami-m fading model have been derived. Validation of the phase statistics derived here and in [48] has been achieved through careful comparison with field measurements. It has been shown that the intriguing shapes of the phase statistics as predicted in the Nakagami-m complex model are actually found in practice. Notwithstanding the contributions made here, the authors recognize that other phase models may be associated to Nakagami-m fading (e.g., [56]) that lead to different shapes of the statistics. This topic will be the direction of future investigations.

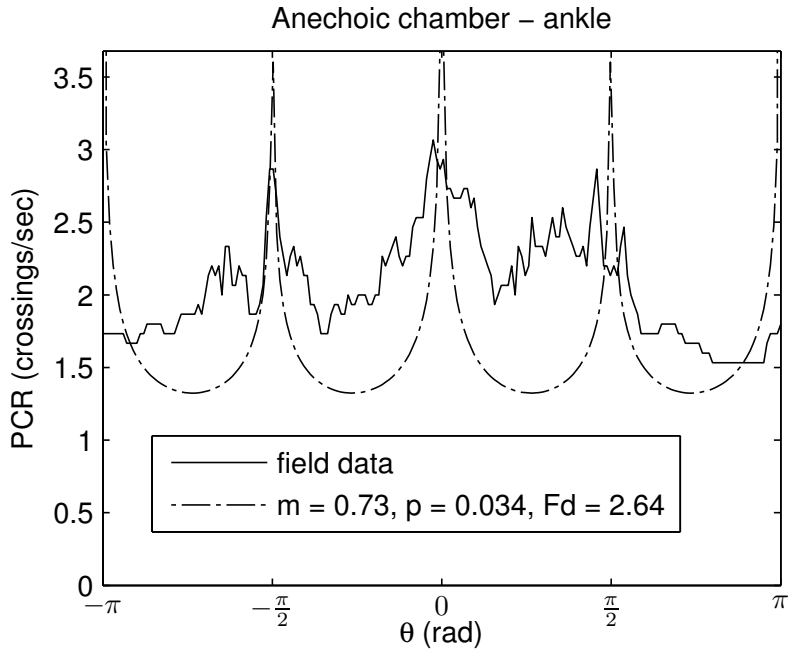

Figure 3.11: PCR for $m < 1$ adjusted to field measurements.

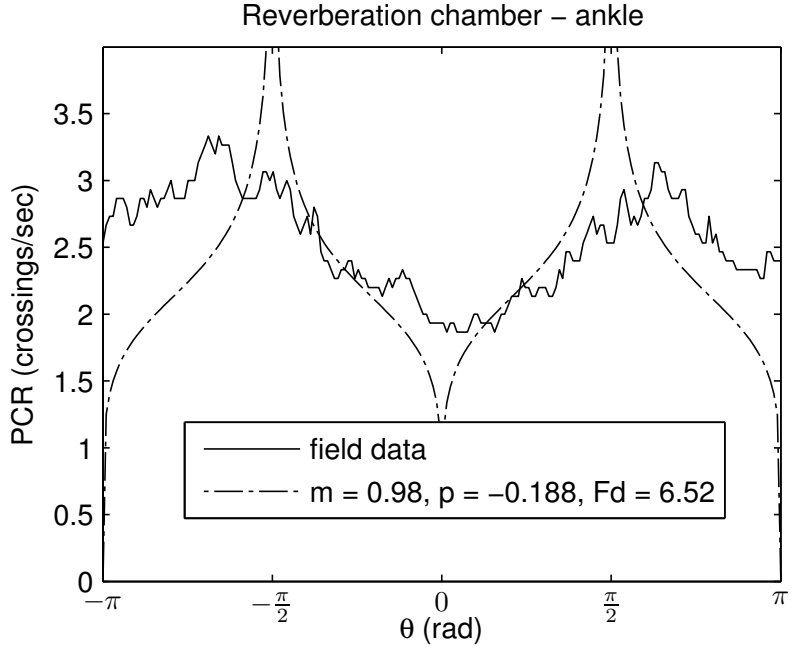

Figure 3.12: PCR for $m < 1$ adjusted to field measurements.

Chapter 4

Exact and Approximate Higher Order Statistics of the κ-μ Fading Process

4.1 Introduction

This chapter contains an adapted version of the paper published in [46]. The aim of this chapter is to further the study of the phase of the κ-μ fading model. It presents the continuation of the work in [44], by finding the analytic formula to both the PCR and phase PDF approximations found in that work, removing the need of any integrations to evaluate those statistics. The approximate phase PDF described here is a closed form description of a new random variable, that is extremely flexible, relatively simple and can be used on its own to model phase processes. During the derivation of these statistics, a new integral identity of the confluent hypergeometric function of the first kind was discovered and is also included. Most interestingly, and strikingly, whereas the *exact* κ-μ phase PDF, given in integral-form, contains as special cases the *exact* Nakagami-m phase PDF and the *exact* Rice phase PDF, the *approximate* κ-μ phase PDF, given in closed-form, though *approximate*, contains as special cases the *exact* Nakagami-m phase PDF and the *exact* Von Mises (Tikhonov) phase PDF. In the same way, the *approximate* κ-μ PCR, given in closed-form, though *approximate*, contains as a special case the *exact* Nakagami-m PCR. A comparison between the approximations and the exact solutions show the excellent fit between them, making the approximate solutions directly applicable to the study of the phase. The PDF of the time derivative of the phase of the κ-μ channel is also derived in an exact manner and in closed-form. A number of other joint distributions comprising envelope, phase, and their time derivatives are presented in closed-form. Finally, a numerical comparison between exact and approximate solutions is presented.

The chapter is structured in seven sections. Section 4.2 proposes a tight closed-form approximation for the phase Probability Density Function. Section 4.3 derives the exact second order statistics of the κ-μ model, presenting several joint statistics of the envelope, phase, the time derivative of the envelope and the time derivative of the phase. Section 4.4 proposes a closed-form approximation for the Phase Crossing Rate. Section 4.5 presents sample plots for the new formulations. Section 4.6 compares the exact and approximate solutions. Section 4.7 concludes the chapter.

Mathematical Functions. Throughout the text: $\Gamma(a)$ denotes the gamma function [47, Eq. (6.1.1)]; $I_v(a)$ denotes the modified Bessel function of the first kind [47, Eq. (9.6.18)];

${}_1F_1(a;b;c)$ denotes the confluent hypergeometric function of the first kind, also known as Kummer's function [47, Eq. (13.1.2)].

4.2 First Order Statistics - A Tight Closed-Form Approximation

The phase-envelope joint distribution of the κ-μ channel was found in [16]. Whereas the phase-envelope joint PDF was described as an analytical expression, the marginal phase PDF was left in integral form. The exact solution of the phase PDF is the integration of Equation (2.36) shown in Equation (2.40).

An exact result given in integral-form is certainly useful but restricts its applicability, chiefly if its computation is to be performed repeatedly. For instance, finding an optimal set of parameters to fit experimental data implies a non-linear optimization problem that requires multiple evaluations of the statistics being considered. The lack of a closed-form expression for the phase PDF of the κ-μ model hinders the practicality of its use to study phase related phenomena. A tight approximation with an analytic expression can make the model more readily usable.

As will be shown later in the chapter, the function $f_{\mathbb{O}}(\theta) \approx f_{\Theta}(\theta)$, given in Equation (4.1), is a tight closed-form approximation to the κ-μ phase PDF.

$$
\begin{aligned}
f_{\mathbb{O}}(\theta) = {} & \frac{\mu\sqrt{\kappa(1+\kappa)}}{4I_{\mu-1}\left(2\mu\sqrt{\kappa(1+\kappa)}\right)} |\sin 2\theta|^{\frac{\mu}{2}} |\sin 2\phi|^{1-\frac{\mu}{2}} \\
& \times \exp\left(2\mu\sqrt{\kappa(1+\kappa)}\cos(\theta-\phi)\right) \\
& \times I_{\frac{\mu}{2}-1}\left(2\mu\sqrt{\kappa(1+\kappa)}|\cos\theta\cos\phi|\right) \\
& \times I_{\frac{\mu}{2}-1}\left(2\mu\sqrt{\kappa(1+\kappa)}|\sin\theta\sin\phi|\right) \\
& \times \operatorname{sech}\left(2\mu\sqrt{\kappa(1+\kappa)}\cos\theta\cos\phi\right) \\
& \times \operatorname{sech}\left(2\mu\sqrt{\kappa(1+\kappa)}\sin\theta\sin\phi\right),
\end{aligned}
\tag{4.1}
$$

for $-\pi \leq \theta < \pi$.

This formula is derived in Section 4.2.1 and captures all of the properties of the exact phase PDF, including maxima and minima occurring at values of θ very close to those of the original function. It has the following symmetry properties also found in the exact phase PDF: when ϕ is an integer multiple of $\pi/2$ or when $\mu = 1$, both functions are symmetric around ϕ; when $\mu \neq 1$, the PDF is quadrimode, reaching zero ($\mu > 1$) or infinity ($\mu < 1$) when θ is an integer multiple of $\pi/2$. Although approximate, by construction, this is a true PDF, since it is non-negative and integrates to 1 over its domain.

Equation (4.1) leads to indeterminacy for certain values of μ when ϕ is an integer multiple of $\pi/2$. However, the limits $\lim_{\phi\to n\pi} f_{\mathbb{O}}(\theta)$ and $\lim_{\phi\to(2n+1)\pi/2} f_{\mathbb{O}}(\theta)$, $n \in \mathbb{Z}$, exist and are given by Equations (4.2) and (4.3),

$$
\begin{aligned}
f_{\mathbb{O}}(\theta)_{\phi\to n\pi} &= \frac{(\mu\sqrt{\kappa(1+\kappa)})^{\frac{\mu}{2}}}{2\Gamma(\mu/2)I_{\mu-1}\left(2\mu\sqrt{\kappa(1+\kappa)}\right)} \\
&\times|\sin\theta|^{\mu-1}|\cos\theta|^{\frac{\mu}{2}}\operatorname{sech}\left(2\mu\sqrt{\kappa(1+\kappa)}\cos\theta\right) \\
&\times\exp\left(2\mu\sqrt{\kappa(1+\kappa)}\cos(\theta)\cos(\phi)\right) \\
&\times I_{\frac{\mu}{2}-1}\left(2\mu\sqrt{\kappa(1+\kappa)}|\cos\theta|\right)
\end{aligned}
\tag{4.2}
$$

and

$$
\begin{aligned}
f_{\mathbb{O}}(\theta)_{\phi\to\frac{(2n+1)\pi}{2}} &= \frac{(\mu\sqrt{\kappa(1+\kappa)})^{\frac{\mu}{2}}}{2\Gamma(\mu/2)I_{\mu-1}\left(2\mu\sqrt{\kappa(1+\kappa)}\right)} \\
&\times|\cos\theta|^{\mu-1}|\sin\theta|^{\frac{\mu}{2}}\operatorname{sech}\left(2\mu\sqrt{\kappa(1+\kappa)}\sin\theta\right) \\
&\times\exp\left(2\mu\sqrt{\kappa(1+\kappa)}\sin(\theta)\sin(\phi)\right) \\
&\times I_{\frac{\mu}{2}-1}\left(2\mu\sqrt{\kappa(1+\kappa)}|\sin\theta|\right).
\end{aligned}
\tag{4.3}
$$

The derivation of the proposed approximation for the general case is carried out in two steps, as detailed next: first, a function bearing the same behavior of the exact phase PDF is obtained; then, this function is normalized to have unitary area.

4.2.1 Derivation of the Tight Approximate Solution

Initially, a Taylor expansion of Equation (2.36) with respect to θ for a fixed ρ was considered. [1] The idea was to truncate the series in order to achieve a first order approximation of the function. This strategy failed, however, because each term of the Taylor expansion is itself expressed as an integral over ρ, for which no analytic solution was found, increasing the complexity of the problem instead of reducing it. An alternative and definitive approach was then pursued. Instead of Taylor expanding $f_{P,\Theta}(\rho,\theta)$ with respect to θ for a fixed ρ, the integrand of Equation (2.36) was expanded in terms of ρ for a fixed θ. The series thus obtained was truncated before the integration was performed. Note that, strictly speaking, this is not a first order approximation, since the function is truncated prior to the integration. Nonetheless, the function found this way, and normalized to guarantee unitary area, had the desired behavior, allowing it to be used as an approximate PDF. However, there is an inherent problem with the proposed Taylor expansion solution.The Taylor series is obviously a polynomial function on ρ and, since the range of ρ is infinite, the integral will diverge for all truncated versions of the expansion. The integral only converges if the number of terms remains infinite. A workaround to address this problem is achieved by manipulating the integration. First, the interval of integration is divided in two ranges, namely from 0 to 1 and from 1 to ∞, as

$$
f_{\Theta}(\theta) = \int_0^1 f_{P,\Theta}(x,\theta)dx + \int_1^{\infty} f_{x,\Theta}(x,\theta)dx. \tag{4.4}
$$

Next, the variable x of the second integral is changed to $y = 1/x$, so that $y = 0$ when $x = \infty$, $y = 1$ when $x = 1$, and $dx = -\frac{dy}{y^2}$. Then, the dummy variable y is changed back to x and

[1] The first part of this derivation was presented in [44]. However, in that work, although the formula was almost analytic, there still remained an integral term to be evaluated. In the following derivation, this integration is evaluated and its results are combined with the main expression, leading to the true closed form formula showed in Equation (4.1). The full derivation is included here for completeness.

both integrals are regrouped under a single integral from 0 to 1.

$$\begin{aligned} f_\Theta(\theta) &= \int_0^1 \left(f_{P,\Theta}(x,\theta) + \frac{f_{P,\Theta}\left(\frac{1}{x},\theta\right)}{x^2} \right) dx \\ &= \textstyle\int_0^1 u(\rho,\theta) dx. \end{aligned} \tag{4.5}$$

A series expansion of the integrand $u(\rho,\theta)$ of Equation (4.5) about the point $\rho_0 = 1$ is performed, resulting in

$$\begin{aligned} & u^*_(\rho,\theta) = \\ & \tfrac{2-\rho}{2}\mu^2\kappa^{1-\frac{\mu}{2}}(1+\kappa)^{1+\frac{\mu}{2}}|\sin 2\theta|^{\frac{\mu}{2}}|\sin 2\phi|^{1-\frac{\mu}{2}} \\ & \times \exp\left(-\mu(1+2\kappa) + 2\mu\sqrt{\kappa(1+\kappa)}\cos(\theta-\phi)\right) \\ & \times I_{\frac{\mu}{2}-1}\left(2\mu\sqrt{\kappa(1+\kappa)}|\cos\theta\cos\phi|\right) \\ & \times I_{\frac{\mu}{2}-1}\left(2\mu\sqrt{\kappa(1+\kappa)}|\sin\theta\sin\phi|\right) \\ & \times \operatorname{sech}\left(2\mu\sqrt{\kappa(1+\kappa)}\cos\theta\cos\phi\right) \\ & \times \operatorname{sech}\left(2\mu\sqrt{\kappa(1+\kappa)}\sin\theta\sin\phi\right) + O(\rho-1)^2. \end{aligned} \tag{4.6}$$

Now, the integral of $u(\rho,\theta)$ from $\rho = 0$ to $\rho = 1$ is found trivially,

$$\begin{aligned} & g_\Theta(\theta) = \\ & \tfrac{3}{2}\mu^2\kappa^{1-\frac{\mu}{2}}(1+\kappa)^{1+\frac{\mu}{2}}|\sin 2\theta|^{\frac{\mu}{2}}|\sin 2\phi|^{1-\frac{\mu}{2}} \\ & \times \exp\left(-\mu(1+2\kappa) + 2\mu\sqrt{\kappa(1+\kappa)}\cos(\theta-\phi)\right) \\ & \times I_{\frac{\mu}{2}-1}\left(2\mu\sqrt{\kappa(1+\kappa)}|\cos\theta\cos\phi|\right) \\ & \times I_{\frac{\mu}{2}-1}\left(2\mu\sqrt{\kappa(1+\kappa)}|\sin\theta\sin\phi|\right) \\ & \times \operatorname{sech}\left(2\mu\sqrt{\kappa(1+\kappa)}\cos\theta\cos\phi\right) \\ & \times \operatorname{sech}\left(2\mu\sqrt{\kappa(1+\kappa)}\sin\theta\sin\phi\right). \end{aligned} \tag{4.7}$$

Note that Equation (4.7) is the basis of Equation (4.1)), multiplied by a function of the parameters κ, μ and ϕ. Before integrating Equation (4.7) to find the area for normalization purposes, it is convenient to strip it of the multiplicative terms that are not function of θ or ϕ, resulting in

$$\begin{aligned} & g^*_\Theta(\theta) = |\sin 2\theta|^{\frac{\mu}{2}}|\sin 2\phi|^{1-\frac{\mu}{2}} \\ & \times \exp\left(2\mu\sqrt{\kappa(1+\kappa)}\cos(\theta-\phi)\right) \\ & \times I_{\frac{\mu}{2}-1}\left(2\mu\sqrt{\kappa(1+\kappa)}|\cos\theta\cos\phi|\right) \\ & \times I_{\frac{\mu}{2}-1}\left(2\mu\sqrt{\kappa(1+\kappa)}|\sin\theta\sin\phi|\right) \\ & \times \operatorname{sech}\left(2\mu\sqrt{\kappa(1+\kappa)}\cos\theta\cos\phi\right) \\ & \times \operatorname{sech}\left(2\mu\sqrt{\kappa(1+\kappa)}\sin\theta\sin\phi\right). \end{aligned} \tag{4.8}$$

Most interestingly, the integral of Equation (4.8) with respect to θ can be calculated with the aid of the following integral identity first found in [17, Eq. 17],

$$\begin{aligned} & I_{\mu-1}(x) = \\ & \tfrac{x}{8}|\sin(2\phi)|^{1-\frac{\mu}{2}}\int_0^{2\pi}|\sin 2\theta|^{\frac{\mu}{2}}\exp\left(x\cos(\theta-\phi)\right) \\ & \times I_{\frac{\mu}{2}-1}\left(x|\cos\theta\cos\phi|\right) I_{\frac{\mu}{2}-1}\left(x|\sin\theta\sin\phi|\right) \\ & \times \operatorname{sech}\left(x\cos\theta\cos\phi\right)\operatorname{sech}\left(x\sin\theta\sin\phi\right) d\theta. \end{aligned} \tag{4.9}$$

With this identity, the integration becomes straightforward, and after some algebraic manipulation we find the area to be

$$\int_0^{2\pi} g^*_\Theta(\theta)d\theta = \frac{4I_{\mu-1}\left(2\sqrt{\kappa(\kappa+1)}\mu\right)}{\sqrt{\kappa(\kappa+1)}\mu}. \tag{4.10}$$

Equation (4.1) is then found by dividing Equation (4.8) by Equation (4.10). Note that Equation (4.1)) is both non-negative and has unitary area, making it the description of the PDF of a new RV, denoted here by $\mathbb{O}$.

4.2.2 Special Cases

As already known, the κ-μ distribution encompasses several other distributions, including Nakagami-m and Rice. In this section, the behavior of the approximate expression for those two special cases is explored.

A) Rice Distribution

By setting $\mu = 1$ in Equation (4.1), the approximation can be evaluated for the Rician case. This is a straightforward substitution and results in a rather simple expression,

$$f_{\mathbb{O}}(\theta)_{Rice} = \frac{\exp\left(2\sqrt{\kappa(1+\kappa)}\cos(\theta-\phi)\right)}{2\pi I_0(2\sqrt{\kappa(1+\kappa)})}. \tag{4.11}$$

Strikingly, the expression in Equation (4.11) is the *exact* Von Mises (Tikhonov) distribution [57]. This result shows that the Von Mises (Tikhonov) distribution can be used to approximate the Rician phase distribution. Furthermore, since the parameters k and ϕ are described in terms of physical phenomena involved in wireless communications, it may give a physical interpretation to the Von Mises (Tikhonov) distribution as well.

B) Nakagami-m Distribution

The κ-μ channel becomes the Nakagami-m channel when $\kappa \to 0$. However, by making $\kappa \to 0$ in Equation (4.1) an indeterminacy is encountered. It can be shown [58] that

$$\lim_{x\to 0}\left(x^{\frac{1}{2}-\frac{\mu}{4}} I_{\frac{\mu}{2}-1}(ax^{1/2})\right) = \frac{(a/2)^{\frac{\mu}{2}-1}}{\Gamma\left(\frac{\mu}{2}\right)}. \tag{4.12}$$

With the aid of this limit, we obtain

$$f_{\mathbb{O}}(\theta)_{nak} = \frac{|\sin 2\theta|^{\mu-1}\Gamma(\mu)}{2^\mu \Gamma^2(\mu/2)}. \tag{4.13}$$

which, again strikingly, is exactly the Nakagami-m phase PDF as described in [13]. This is an interesting result that shows one particular case in which the proposed approximate phase PDF reduces to the exact function.

C) A New Phase/Angle Probability Density Function

It is noteworthy that the said tight approximate solution is indeed a totally new phase/angle PDF. It can be written more compactly as

$$\begin{aligned} &f_{\mathbb{O}}(\theta) = \\ &\tfrac{k\mu}{8I_{\mu-1}(k\mu)} |\sin 2\theta|^{\frac{\mu}{2}} |\sin 2\phi|^{1-\frac{\mu}{2}} \exp\left(k\mu\cos(\theta-\phi)\right) \\ &\times I_{\frac{\mu}{2}-1}\left(k\mu|\cos\theta\cos\phi|\right) I_{\frac{\mu}{2}-1}\left(k\mu|\sin\theta\sin\phi|\right) \\ &\times \operatorname{sech}\left(k\mu\cos\theta\cos\phi\right)\operatorname{sech}\left(k\mu\sin\theta\sin\phi\right), \end{aligned} \tag{4.14}$$

in which $k = 2\sqrt{\kappa(1+\kappa)}$.

Its special cases, as said, include Von Mises (Tikhonov) for $\mu = 1$, i.e.

$$f_{\mathbb{O}}\left(\theta\right) = \frac{\exp\left(k\cos\left(\theta-\phi\right)\right)}{2\pi\ I_0\left(k\right)} \tag{4.15}$$

and Nakagami-m for $\kappa \to 0$, i.e.

$$f_{\mathbb{O}}(\theta) = \frac{|\sin 2\theta|^{\mu-1}\Gamma(\mu)}{2^{\mu}\Gamma^2(\mu/2)} \tag{4.16}$$

4.3 Second Order Statistics - Exact Solution

The second order statistics, as explored here, concern the time derivative of the components of the signal. We start by calculating the joint distribution of X, Y, $\dot{X}$, and $\dot{Y}$, in which the dot signifies the time derivative of the variable. The variables X and Y denote respectively the in-phase and quadrature component of the κ-μ channel, defined in Equations (2.25) and (2.26) with the corresponding PDF given in Equation (2.35). We then proceed by making a transformation of variables to obtain the joint distribution of R, Θ, $\dot{R}$, and $\dot{\Theta}$.

4.3.1 PDF of $\dot{Z}$

As noted in Section 2.5, the in-phase and quadrature components of the κ-μ signal follow the same distribution, as defined in Equation (2.35), with their physical model given in Equation (2.27). By differentiating both sides of Equation (2.27) with respect to time and rearranging the terms, it is possible to write

$$\dot{Z} = \frac{\sum_{i=1}^{\mu}(Z_i+\lambda_i)\dot{Z}_i}{Z}. \tag{4.17}$$

Let $\dot{Z}|Z$ represent the variable $\dot{Z}$ conditioned on the value of all Z_i , $i = 1, ..., \mu$. For an isotropic environment, $\dot{Z}_i$ is a Gaussian random variable with zero mean and variance [12]

$$\dot{\sigma}^2 = 2\pi^2 f_d^2 \sigma^2, \tag{4.18}$$

in which f_d denotes the maximum Doppler shift [8]. The variance of each multipath cluster, σ^2, may be written in terms of the κ-μ parameters as [15]

$$\sigma^2 = \frac{\hat{r}^2}{2\mu(1+\kappa)}. \tag{4.19}$$

When Equation (4.17) is conditioned on Z_i, all Z_i, and hence Z, become known and thus they can be treated as constants. Because of this, Equation (4.17) becomes a sum of the μ Gaussian random variables $\dot{Z}_i$, which is itself a Gaussian random variable, and its PDF can be fully characterized by its first and second moments. The moments of each individual Gaussian component $\dot{Z}_i$ are (i) $E[\dot{Z}_i] = 0$, (ii) $E[\dot{Z}_i\dot{Z}_j] = \dot{\sigma}^2$, if $i = j$, and (iii) $E[\dot{Z}_i\dot{Z}_j] = 0$, if $i \neq j$. The mean value of $\dot{Z}|Z$ is

$$E[\dot{Z}|Z] = \frac{\sum_{i=1}^{\mu}(Z_i + \lambda_i)E[\dot{Z}_i]}{Z} = 0, \tag{4.20}$$

and its second moment is

$$E[\dot{Z}^2|Z] = \frac{\sum_{i=1}^{\mu}\sum_{j=1}^{\mu}(Z_i + \lambda_i)(Z_j + \lambda_j)E[\dot{Z}_i\dot{Z}_j]}{Z^2} = \dot{\sigma}^2. \tag{4.21}$$

The PDF $f_{\dot{Z}|Z}(\dot{z}|z)$ of $\dot{Z}|Z$ is then

$$f_{\dot{Z}|Z}(\dot{z}|z) = \frac{1}{\sqrt{2\pi\dot{\sigma}^2}}\exp\left(-\frac{\dot{z}^2}{2\dot{\sigma}^2}\right). \tag{4.22}$$

Because $f_{\dot{Z}|Z}(\dot{z}|z)$ is not a function of z, then $f_{\dot{Z}|Z}(\dot{z}, z) = f_{\dot{Z}}(\dot{z})$, which means that Z is independent of $\dot{Z}$, or, in other words, X is independent of $\dot{X}$ and Y is independent of $\dot{Y}$. Thus,

$$f_{\dot{Z}}(\dot{z}) = \frac{1}{\sqrt{2\pi\dot{\sigma}^2}}\exp\left(-\frac{\dot{z}^2}{2\dot{\sigma}^2}\right). \tag{4.23}$$

Again, by definition, because X and Y are independent processes, it follows that the variables $X, \dot{X}, Y, \dot{Y}$ are jointly independent.

4.3.2 Joint PDF of $X, \dot{X}, Y, \dot{Y}$:

Knowing that $X, \dot{X}, Y, \dot{Y}$ are jointly independent, then $f_{X,\dot{X},Y,\dot{Y}}(x, \dot{x}, y, \dot{y}) = f_X(x)f_{\dot{X}}(\dot{x})f_Y(y)f_{\dot{Y}}(\dot{y})$, in which the marginal PDFs are given by Equations (2.35) and (4.23), with the appropriate substitution of Z by X or Y and $\dot{Z}$ by $\dot{X}$ or $\dot{Y}$, as required. That is,

$$\begin{aligned} &f_{X,\dot{X},Y,\dot{Y}}(x, \dot{x}, y, \dot{y}) = \\ &\frac{|xy|^{\frac{\mu}{2}}}{8\pi\sigma^4\dot{\sigma}^2|pq|^{\frac{\mu}{2}-1}}\exp\left(-\frac{(x-p)^2+(y-q)^2}{2\sigma^2}\right)\exp\left(-\frac{\dot{x}^2+\dot{y}^2}{2\dot{\sigma}^2}\right) \\ &\times I_{\frac{\mu}{2}-1}\left(\frac{|px|}{\sigma^2}\right)I_{\frac{\mu}{2}-1}\left(\frac{|qy|}{\sigma^2}\right)\operatorname{sech}\left(\frac{px}{\sigma^2}\right)\operatorname{sech}\left(\frac{qy}{\sigma^2}\right). \end{aligned} \tag{4.24}$$

4.3.3 Joint PDF of $P, \dot{P}, \Theta, \dot{\Theta}$

Define P as the normalized envelope, as before, and $\dot{P}$ its time derivative. The joint PDF $f_{P,\dot{P},\Theta,\dot{\Theta}}(\rho, \dot{\rho}, \theta, \dot{\theta})$ of $P, \dot{P}, \Theta$,and $\dot{\Theta}$ is obtained through variable transformations, from the Cartesian coordinates (X, Y) to the polar coordinates $(\hat{r}P, \Theta)$. Then, $f_{P,\dot{P},\Theta,\dot{\Theta}}(\rho, \dot{\rho}, \theta, \dot{\theta}) = |J|f_{X,\dot{X},Y,\dot{Y}}(x, \dot{x}, y, \dot{y})$, in which J is the Jacobian of the transformation and $X/\hat{r} = P\cos\Theta$ and $Y/\hat{r} = P\sin\Theta$. Therefore $\dot{X}/\hat{r} = \dot{P}\cos\Theta - P\dot{\Theta}\sin\Theta$ and $\dot{Y}/\hat{r} = \dot{P}\sin\Theta + P\dot{\Theta}\cos\Theta$.

The Jacobian of this transformation is found to be $|J| = \hat{r}^2\rho^2$. Now, using the definitions for σ^2 and $\dot{\sigma}^2$ and carrying out the necessary algebraic manipulations, then

$$\begin{aligned}
&f_{P,\dot{P},\Theta,\dot{\Theta}}(\rho,\dot{\rho},\theta,\dot{\theta}) = \frac{\kappa^{1-\frac{\mu}{2}}(1+\kappa)^{2+\frac{\mu}{2}}\mu^3}{4\pi^3 f_d^2}\rho^{\mu+2} \\
&\times|\sin 2\theta|^{\frac{\mu}{2}}|\sin 2\phi|^{1-\frac{\mu}{2}}\exp\left(-\tfrac{\mu(1+\kappa)}{2\pi^2 f_d^2}(\dot{\rho}^2+\rho^2\dot{\theta}^2)\right) \\
&\times\exp\left(-\mu(1+\kappa)\rho^2-\kappa\mu\right) \\
&\times\exp\left(2\mu\sqrt{\kappa(1+\kappa)}\rho\cos(\theta-\phi)\right) \\
&\times I_{\frac{\mu}{2}-1}\left(2\mu\sqrt{\kappa(1+\kappa)}\rho|\cos\theta\cos\phi|\right) \\
&\times I_{\frac{\mu}{2}-1}\left(2\mu\sqrt{\kappa(1+\kappa)}\rho|\sin\theta\sin\phi|\right) \\
&\times\operatorname{sech}\left(2\mu\sqrt{\kappa(1+\kappa)}\rho\cos\theta\cos\phi\right) \\
&\times\operatorname{sech}\left(2\mu\sqrt{\kappa(1+\kappa)}\rho\sin\theta\sin\phi\right).
\end{aligned} \tag{4.25}$$

4.3.4 Joint PDF of $P, \dot{P}, \dot{\Theta}$

The joint PDF of $P, \dot{P}$ and $\dot{\Theta}$ is calculated by integrating Equation (4.25) with respect to Θ. This integration is achieved with the aid of the identity Equation (4.9), leading to

$$\begin{aligned}
&f_{P,\dot{P},\dot{\Theta}}(\rho,\dot{\rho},\dot{\theta}) = \pi^{-3}f_d^{-2}\kappa^{\frac{1-\mu}{2}}(1+\kappa)^{\frac{3+\mu}{2}}\mu^2 \\
&\times\rho^{\mu+1}I_{\mu-1}\left(2\mu\sqrt{\kappa(1+\kappa)}\rho\right)\exp\left(-\kappa\mu\right) \\
&\times\exp\left(-\tfrac{\mu(1+\kappa)}{2\pi^2 f_d^2}(\dot{\rho}^2+\rho^2\dot{\theta}^2)-\mu(1+\kappa)\rho^2\right).
\end{aligned} \tag{4.26}$$

4.3.5 Joint PDF of $P, \dot{P}, \Theta$

The joint PDF of $P, \dot{P}$ and Θ is calculated by integrating Equation (4.25) with respect to $\dot{\Theta}$, which results in the expression

$$\begin{aligned}
&f_{P,\dot{P},\Theta}(\rho,\dot{\rho},\theta) = \frac{\kappa^{1-\frac{\mu}{2}}(1+\kappa)^{\frac{3+\mu}{2}}\mu^{5/2}}{(2\pi)^{3/2}f_d}\rho^{\mu+1} \\
&\times|\sin 2\theta|^{\frac{\mu}{2}}|\sin 2\phi|^{1-\frac{\mu}{2}}\exp\left(-\tfrac{\mu(1+\kappa)}{2\pi^2 f_d^2}\dot{\rho}^2-\kappa\mu\right) \\
&\times\exp\left(2\mu\sqrt{\kappa(1+\kappa)}\rho\cos(\theta-\phi)-\mu(1+\kappa)\rho^2\right) \\
&\times I_{\frac{\mu}{2}-1}\left(2\mu\sqrt{\kappa(1+\kappa)}\rho|\cos\theta\cos\phi|\right) \\
&\times I_{\frac{\mu}{2}-1}\left(2\mu\sqrt{\kappa(1+\kappa)}\rho|\sin\theta\sin\phi|\right) \\
&\times\operatorname{sech}\left(2\mu\sqrt{\kappa(1+\kappa)}\rho\cos\theta\cos\phi\right) \\
&\times\operatorname{sech}\left(2\mu\sqrt{\kappa(1+\kappa)}\rho\sin\theta\sin\phi\right).
\end{aligned} \tag{4.27}$$

4.3.6 Joint PDF of $P, \Theta, \dot{\Theta}$

Similarly, the joint PDF of P, Θ and $\dot{\Theta}$ is calculated by integrating Equation (4.25) with respect to $\dot{P}$, which produces the function

$$
\begin{aligned}
f_{P,\Theta,\dot{\Theta}}(\rho,\theta,\dot{\theta}) &= \frac{\kappa^{1-\frac{\mu}{2}}(1+\kappa)^{\frac{3+\mu}{2}}\mu^{5/2}}{(2\pi)^{3/2} f_d}\rho^{\mu+2} \\
&\times |\sin 2\theta|^{\frac{\mu}{2}} |\sin 2\phi|^{1-\frac{\mu}{2}} \exp\left(-\tfrac{\mu(1+\kappa)}{2\pi^2 f_d^2}\rho^2\dot{\theta}^2 - \kappa\mu\right) \\
&\times \exp\left(2\mu\sqrt{\kappa(1+\kappa)}\rho\cos(\theta-\phi) - \mu(1+\kappa)\rho^2\right) \\
&\times I_{\frac{\mu}{2}-1}\left(2\mu\sqrt{\kappa(1+\kappa)}\rho|\cos\theta\cos\phi|\right) \\
&\times I_{\frac{\mu}{2}-1}\left(2\mu\sqrt{\kappa(1+\kappa)}\rho|\sin\theta\sin\phi|\right) \\
&\times \operatorname{sech}\left(2\mu\sqrt{\kappa(1+\kappa)}\rho\cos\theta\cos\phi\right) \\
&\times \operatorname{sech}\left(2\mu\sqrt{\kappa(1+\kappa)}\rho\sin\theta\sin\phi\right).
\end{aligned} \tag{4.28}
$$

4.3.7 Joint PDF of P, Θ

The joint PDF of P and Θ can be calculated from either Equation (4.27) or Equation (4.28) by integration, in the same fashion as before. This leads to

$$
\begin{aligned}
f_{P,\Theta}(\rho,\theta) &= \frac{1}{2}\kappa^{1-\frac{\mu}{2}}(1+\kappa)^{1+\frac{\mu}{2}}\mu^2\rho^{\mu+1} \\
&\times |\sin 2\theta|^{\frac{\mu}{2}} |\sin 2\phi|^{1-\frac{\mu}{2}} \exp\left(-\kappa\mu\right) \\
&\times \exp\left(2\mu\sqrt{\kappa(1+\kappa)}\rho\cos(\theta-\phi) - \mu(1+\kappa)\rho^2\right) \\
&\times I_{\frac{\mu}{2}-1}\left(2\mu\sqrt{\kappa(1+\kappa)}\rho|\cos\theta\cos\phi|\right) \\
&\times I_{\frac{\mu}{2}-1}\left(2\mu\sqrt{\kappa(1+\kappa)}\rho|\sin\theta\sin\phi|\right) \\
&\times \operatorname{sech}\left(2\mu\sqrt{\kappa(1+\kappa)}\rho\cos\theta\cos\phi\right) \\
&\times \operatorname{sech}\left(2\mu\sqrt{\kappa(1+\kappa)}\rho\sin\theta\sin\phi\right).
\end{aligned} \tag{4.29}
$$

Equation (4.29) is the non-normalized version of [17, Eq. (2)].

4.3.8 Joint PDF of $P, \dot{P}$

The joint PDF of P and $\dot{P}$ is calculated by integrating Equation (4.26) with respect to $\dot{\Theta}$, resulting in

$$
\begin{aligned}
f_{P,\dot{P}}(\rho,\dot{\rho}) &= \frac{\sqrt{2}}{\pi^{3/2} f_d}\mu^{3/2}\kappa^{\frac{1-\mu}{2}}(1+\kappa)^{1+\frac{\mu}{2}}\rho^{\mu} \\
&\times \exp\left(-\tfrac{\mu(1+\kappa)}{2\pi^2 f_d^2}\dot{\rho}^2 - \mu(1+\kappa)\rho^2 - \mu\kappa\right) \\
&\times I_{\mu-1}\left(2\mu\sqrt{\kappa(1+\kappa)}\rho\right).
\end{aligned} \tag{4.30}
$$

Equation (4.30) is exactly the same equation derived in [18] and is included in this chapter for completeness purposes.

4.3.9 Joint PDF of $P, \dot{\Theta}$

The joint PDF of P and $\dot{\Theta}$ is calculated by integrating Equation (4.26) with respect to $\dot{P}$, resulting in

$$
\begin{aligned}
f_{P,\dot{\Theta}}(\rho,\dot{\theta}) &= \frac{\sqrt{2}}{\pi^{3/2} f_d}\mu^{3/2}\kappa^{\frac{1-\mu}{2}}(1+\kappa)^{1+\frac{\mu}{2}}\rho^{\mu+1} \\
&\times \exp\left(-\tfrac{\mu(1+\kappa)}{2\pi^2 f_d^2}\rho^2\dot{\theta}^2 - \mu(1+\kappa)\rho^2 - \mu\kappa\right) \\
&\times I_{\mu-1}\left(2\mu\sqrt{\kappa(1+\kappa)}\rho\right).
\end{aligned} \tag{4.31}
$$

4.3.10 Joint PDF of $\dot{P}, \dot{\Theta}$

The joint PDF of $\dot{P}$ and $\dot{\Theta}$ is achieved by simply integrating Equation (4.26) with respect to P, which results in

$$\begin{aligned} f_{\dot{P},\dot{\Theta}}(\dot{\rho},\dot{\theta}) &= \frac{2^{\mu-1/2} f_d^{2\mu-1} \pi^{2\mu-2}}{\left(2\pi^2 f_d^2 + \dot{\theta}^2\right)^{\mu+\frac{1}{2}}} \frac{\Gamma\left(\mu+\frac{1}{2}\right)}{\Gamma(\mu)} \\ &\times \sqrt{\mu(1+\kappa)} \exp\left(-\tfrac{\mu(1+\kappa)\dot{\rho}^2}{2\pi^2 f_d^2} - \kappa\mu\right) \\ &\times {}_1F_1\left(\mu+\tfrac{1}{2}; \mu; \tfrac{2f_d^2\pi^2\kappa\mu}{2\pi^2 f_d^2+\dot{\theta}^2}\right). \end{aligned} \tag{4.32}$$

4.3.11 The Marginal PDFs of $\dot{P}$ and $\dot{\Theta}$

The marginal PDFs $f_{\dot{P}}(\dot{\rho})$ and $f_{\dot{\Theta}}(\dot{\theta})$ are found by integrating $f_{\dot{P},\dot{\Theta}}(\dot{\rho},\dot{\theta})$ appropriately. However, integration over $\dot{\theta}$ does not lead to a closed-form expression, whereas integration over $\dot{\rho}$ easily leads to

$$\begin{aligned} f_{\dot{\Theta}}(\dot{\theta}) &= \frac{\exp(-\kappa\mu)\Gamma\left(\mu+\frac{1}{2}\right)}{\sqrt{2}\pi^{3/2} f_d \Gamma(\mu) \left(1+\frac{\dot{\theta}^2}{2f_d^2\pi^2}\right)^{\mu+1/2}} \\ &\times {}_1F_1\left(\mu+\tfrac{1}{2}; \mu; \tfrac{\kappa\mu}{1+\frac{\dot{\theta}^2}{2f_d^2\pi^2}}\right). \end{aligned} \tag{4.33}$$

It is evident from Equation (4.33) that the density of $\dot{\Theta}$ has even symmetry, since all terms of $\dot{\theta}$ are squared. This means that the positive changes in phase occurs with the same frequency as negative ones. It is also independent of the phase parameter ϕ. Overall, the distribution has a single maximum centered at $\theta = 0$, declining as θ gets farther from the center.

We recognize that Equation (4.33) can be separated from the joint PDF in Equation (4.32). Dividing Equation (4.32) by Equation (4.33), we find the PDF of $\dot{P}$,

$$f_{\dot{P}}(\dot{\rho}) = \frac{\exp\left(-\frac{\dot{\rho}^2}{2\dot{\sigma}^2}\right)}{\sqrt{2\pi}\dot{\sigma}}, \tag{4.34}$$

in which $\dot{\sigma}^2$ is given by Equation (4.18) with $\hat{r} = 1$, since this statistics refers to the the normalized envelope. We note that Equation (4.34) was already described in [18] and is included here for completeness. An interesting conclusion that can be drawn from Equations (4.32) to (4.34)) is that $\dot{P}$ is independent of $\dot{\Theta}$, since their joint PDF is simply the multiplication of the marginal distributions.

We end this section by remarking that no closed-form expression was found for any joint PDF for a set of random variables that contains Θ but not P. Whereas the identity in Equation (4.9) is useful for removing Θ from the joint PDFs, no such artifice was found to remove P without removing Θ first.

4.3.12 A New Mathematical Identity

Earlier, we stated that the integration over the range of $\dot{\theta}$ in $f_{\dot{P},\dot{\Theta}}(\dot{\rho},\dot{\theta})$ was not possible. However, through alternative means, we have been able to obtain the corresponding marginal

PDFs. Now, because Equation (4.33) is a true PDF, its integration with respect to $\dot{\theta}$ over its range (from $-\infty$ to ∞) is equal to one. Knowing that this is an even function, we find the following identity of the confluent hypergeometric function of the first kind

$$\int_1^\infty \frac{{}_1F_1\left(a; a-\frac{1}{2}; \frac{b}{z}\right)}{z^a\sqrt{z-1}}dz = \frac{\sqrt{\pi}\Gamma\left(a-\frac{1}{2}\right)\exp(b)}{\Gamma(a)}. \tag{4.35}$$

To the best of the authors' knowledge, this is the first time this identity has been described in the literature.

4.4 Second Order Statistics - A Closed-Form Approximation

The integral needed to evaluate the phase PDF of the κ-μ model is very similar to the one needed to evaluate the PCR, as it can be recognized by comparing Equations (2.36) and (2.42). The two functions are composed by essentially the same building blocks, the difference between them being the power of ρ and the multiplicative constant that is only a function of κ, μ and ϕ. This suggests that a similar procedure can be used to find an approximation to the phase PDF. The same method used to attain Equation (4.7) is followed here by substituting $f_\Theta(\theta)$ and $f_{P,\Theta}(\rho,\theta)$ for $N_\Theta(\theta)$ and $N_\Theta(\rho,\theta)$, respectively. The detailed steps are avoided and the result is

$$\begin{aligned}
&h_\Theta(\theta) = \\
&\tfrac{3}{2} f_d \sqrt{\tfrac{\pi}{2}} (1+\kappa)^{\frac{1+\mu}{2}} \kappa^{1-\frac{\mu}{2}} \mu^{\frac{3}{2}} |\sin 2\theta|^{\frac{\mu}{2}} |\sin 2\phi|^{1-\frac{\mu}{2}} \\
&\times \exp\left(-\mu(1+2\kappa) + 2\mu\sqrt{\kappa(1+\kappa)}\cos(\theta-\phi)\right) \\
&\times I_{\frac{\mu}{2}-1}\left(2\mu\sqrt{\kappa(1+\kappa)}|\cos\theta\cos\phi|\right) \\
&\times I_{\frac{\mu}{2}-1}\left(2\mu\sqrt{\kappa(1+\kappa)}|\sin\theta\sin\phi|\right) \\
&\times \operatorname{sech}\left(2\mu\sqrt{\kappa(1+\kappa)}\cos\theta\cos\phi\right) \\
&\times \operatorname{sech}\left(2\mu\sqrt{\kappa(1+\kappa)}\sin\theta\sin\phi\right).
\end{aligned} \tag{4.36}$$

As before, Equation (4.36) is stripped of the terms that are not a function of θ, μ or ϕ, leading to

$$\begin{aligned}
&h^*_\Theta(\theta) = |\sin 2\theta|^{\frac{\mu}{2}} |\sin 2\phi|^{1-\frac{\mu}{2}} \\
&\times \exp\left(2\mu\sqrt{\kappa(1+\kappa)}\cos(\theta-\phi)\right) \\
&\times I_{\frac{\mu}{2}-1}\left(2\mu\sqrt{\kappa(1+\kappa)}|\cos\theta\cos\phi|\right) \\
&\times I_{\frac{\mu}{2}-1}\left(2\mu\sqrt{\kappa(1+\kappa)}|\sin\theta\sin\phi|\right) \\
&\times \operatorname{sech}\left(2\mu\sqrt{\kappa(1+\kappa)}\cos\theta\cos\phi\right) \\
&\times \operatorname{sech}\left(2\mu\sqrt{\kappa(1+\kappa)}\sin\theta\sin\phi\right).
\end{aligned} \tag{4.37}$$

Unsurprisingly, Equation (4.37) is exactly the same function as Equation (4.8). In order to obtain a satisfactory approximation, Equation (4.37) is normalized to match the same area of the exact PCR. This entails the integration of both Equations (2.41) and (4.37) from $\theta = 0$ to $\theta = 2\pi$. The former has already been performed and is given by Equation (4.10). The latter is calculated as follows. The desired area is

$$\int_0^{2\pi} N_\Theta d\theta = \int_0^{2\pi}\int_0^\infty N_\Theta(\rho,\theta)d\rho d\theta. \tag{4.38}$$

The order of integration is changed, leading to

$$\int_0^\infty \int_0^{2\pi} N_\Theta(\rho,\theta)d\theta d\rho = \int_0^\infty A(\rho)d\rho, \tag{4.39}$$

in which $A(\rho) = \int_0^{2\pi} N_\Theta(\rho,\theta)d\theta$. Using Equation (4.9) in Equation (4.39), $A(\rho)$ is found to be

$$\begin{aligned} A(\rho) &= \sqrt{2\pi} f \sqrt{\mu} \kappa^{\frac{1}{2}-\frac{\mu}{2}} (1+\kappa)^{\mu/2} \rho^{\mu-1} \exp\left(-\kappa\mu\right) \\ &\times \exp(-\mu(1+\kappa)\rho^2) I_{\mu-1}\left(2\mu\sqrt{\kappa(1+\kappa)}\rho\right). \end{aligned} \tag{4.40}$$

The integration of Equation (4.40) from $\rho = 0$ to $\rho = \infty$ yields the following closed-form formula for the area under the exact PCR,

$$\int_0^{2\pi} N_\Theta d\theta = f_d \sqrt{\frac{\pi}{2}} \frac{\Gamma\left(\mu - \frac{1}{2}\right)}{\Gamma(\mu)} {}_1F_1\left(\frac{1}{2}; \mu; -\kappa\mu\right). \tag{4.41}$$

The restriction $\mu > 1/2$ is needed for the integral to converge, whereas κ is always positive, by definition. Finally, the desired approximation $N_{\mathbb{O}}(\theta) \approx N_\Theta(\theta)$ is found by dividing Equation (4.41) by Equation (4.10) and multiplying the result by Equation (4.37),

$$\begin{aligned} N_{\mathbb{O}}(\theta) &= \frac{f_d \sqrt{\frac{\pi}{2}} \mu \sqrt{\kappa(1+\kappa)} \Gamma\left(\mu - \frac{1}{2}\right)}{4 I_{\mu-1}\left(2\mu\sqrt{\kappa(1+\kappa)}\right)\Gamma(\mu)} \\ &\times {}_1F_1\left(\tfrac{1}{2}; \mu; -\kappa\mu\right) |\sin(2\theta)|^{\mu/2} |\sin(2\phi)|^{1-\frac{\mu}{2}} \\ &\times \exp\left(2\mu\sqrt{\kappa(1+\kappa)}\cos(\theta-\phi)\right) \\ &\times I_{\frac{\mu}{2}-1}\left(2\mu\sqrt{\kappa(1+\kappa)}|\sin(\theta)\sin(\phi)|\right) \\ &\times I_{\frac{\mu}{2}-1}\left(2\mu\sqrt{\kappa(1+\kappa)}|\cos(\theta)\cos(\phi)|\right) \\ &\times \operatorname{sech}\left(2\mu\sqrt{\kappa(1+\kappa)}\cos(\theta)\cos(\phi)\right) \\ &\times \operatorname{sech}\left(2\mu\sqrt{\kappa(1+\kappa)}\sin(\theta)\sin(\phi)\right). \end{aligned} \tag{4.42}$$

When ϕ is a multiple integer of π and $\pi/2$, Equation (4.42) becomes

$$\begin{aligned} N_{\mathbb{O}}(\theta)_{\phi\to n\pi} &= \frac{f_d \sqrt{\frac{\pi}{2}} (\mu\sqrt{\kappa(1+\kappa)})^{\frac{\mu}{2}} \Gamma\left(\mu - \frac{1}{2}\right)}{2 I_{\mu-1}\left(2\mu\sqrt{\kappa(1+\kappa)}\right)\Gamma(\frac{\mu}{2})\Gamma(\mu)} \\ &\times {}_1F_1\left(\tfrac{1}{2}; \mu; -\kappa\mu\right) |\sin\theta|^{\mu-1} |\cos\theta|^{\frac{\mu}{2}} \\ &\times \exp\left(2\mu\sqrt{\kappa(1+\kappa)}\cos(\theta)\cos(\phi)\right) \\ &\times I_{\frac{\mu}{2}-1}\left(2\mu\sqrt{\kappa(1+\kappa)}|\cos\theta|\right) \\ &\times \operatorname{sech}\left(2\mu\sqrt{\kappa(1+\kappa)}\cos\theta\right) \end{aligned} \tag{4.43}$$

and

$$\begin{aligned} N_{\mathbb{O}}(\theta)_{\phi\to\frac{(2n+1)\pi}{2}} &= \frac{f_d \sqrt{\frac{\pi}{2}} (\mu\sqrt{\kappa(1+\kappa)})^{\frac{\mu}{2}} \Gamma\left(\mu - \frac{1}{2}\right)}{2 I_{\mu-1}\left(2\mu\sqrt{\kappa(1+\kappa)}\right)\Gamma(\frac{\mu}{2})\Gamma(\mu)} \\ &\times {}_1F_1\left(\tfrac{1}{2}; \mu; -\kappa\mu\right) |\cos\theta|^{\mu-1} |\sin\theta|^{\frac{\mu}{2}} \\ &\times \exp\left(2\mu\sqrt{\kappa(1+\kappa)}\sin(\theta)\sin(\phi)\right) \\ &\times I_{\frac{\mu}{2}-1}\left(2\mu\sqrt{\kappa(1+\kappa)}|\sin\theta|\right) \\ &\times \operatorname{sech}\left(2\mu\sqrt{\kappa(1+\kappa)}\sin\theta\right), \end{aligned} \tag{4.44}$$

where $n \in \mathbb{Z}$.

As its phase PDF counterpart, Equation (4.42) has the same features of the exact function and is substantially less complex to compute.

It is noteworthy that it is possible to arrive at Equation (4.42) by assuming that Θ and $\dot{\Theta}$ are independent RVs and by substituting Θ by $\mathbb{O}$. To find the PCR in this fashion, $f_{\Theta,\dot{\Theta}}(\theta,\dot{\theta})$ in Equation (2.1) is replaced by $f_{\mathbb{O}}(\theta)f_{\dot{\Theta}}(\dot{\theta})$, in which $f_{\mathbb{O}}(\theta)$ is given by Equation (4.1). Since $f_{\mathbb{O}}(\theta)$ is not a function of $\dot{\theta}$ it can be taken out of the integral, which now remains with the term $\dot{\theta}f_{\dot{\Theta}}(\dot{\theta})$. This integration produces a term which is a function of only κ and μ which, after being multiplied by $f_{\mathbb{O}}(\theta)$, results in Equation (4.42). In other words, this integration produces the scaling constant that transforms the approximate PDF into the approximate PCR. This means that, whilst the original RVs Θ and $\dot{\Theta}$ are not independent, the approximate PCR is compatible with a formulation in which Θ is substituted by the RV $\mathbb{O}$ with $\mathbb{O}$ and $\dot{\Theta}$ independent.

4.4.1 Special Cases

The study of the special cases are indeed very interesting and intriguing, since, in this case, we are dealing with approximate solutions.

A) Rice

By setting $\mu = 1$ in Equation (4.42), the approximation can be evaluated for the Rician case. This substitution is straightforward and leads to the compact formula

$$N_{\mathbb{O}}(\theta) = \frac{f_d I_0\left(\frac{\kappa}{2}\right)\exp\left(2\sqrt{\kappa(\kappa+1)}\cos(\theta-\phi)-\frac{\kappa}{2}\right)}{2\sqrt{2}I_0\left(2\sqrt{\kappa(\kappa+1)}\right)}. \tag{4.45}$$

Whereas this equation is not equal to the Rician PCR, it approximates it well, as shall be seen.

B) Nakagami-m

As with the Phase PDF, when $\kappa \to 0$, the approximate PCR of the Nakagami-m reduces to the *exact function*, obtained from Equation (2.17) by setting $p = 0$, which is rather intriguing. In other words, although the κ-μ PCR in Equation (4.42) is approximate, its special case for $\kappa \to 0$ is the *exact* Nakagami-m PCR.

4.5 Numerical Results

This section depicts three sets of plots, as follows: (i) one for the PDF of the time derivative of the phase, $f_{\dot{\Theta}}(\dot{\theta})$; (ii) another, comparing the exact and approximate phase PDFs, $f_{\Theta}(\theta)$ and $f_{\mathbb{O}}(\theta)$, respectively; (iii) and finally one comparing the exact and approximate PCRs, $N_{\Theta}(\theta)$ and $N_{\mathbb{O}}(\theta)$, respectively. In all figures, the parameters were chosen in a way to present the general behavior of the expressions over a wide range of scenarios.

Figures 4.1 to 4.3 show plots of the phase derivative PDF, respectively, for fixed μ and f_d, and varying κ, for fixed κ and f_d and varying μ and for fixed κ and μ and varying f_d.It

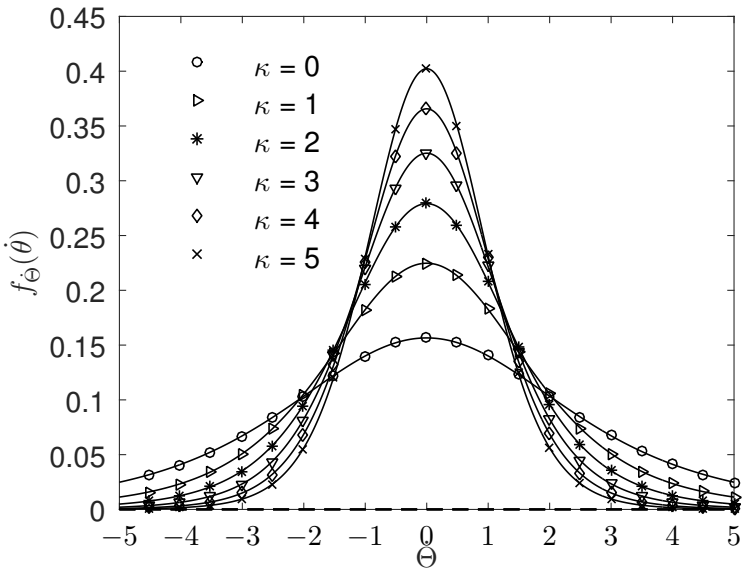

Figure 4.1: Phase derivative PDF for $\mu = 1.75$, $f_d = 1$ and varying κ.

is clear from the plots that the phase derivative becomes more impulsive as either κ or μ increases, or when f_d decreases. This means that for low values of κ and μ and high values of the Doppler shift f_d, large phase changes are expected. For high values of κ and μ and low Doppler shift f_d, there is less phase variation and it becomes more stable. In general, it can be seen that this PDF has an even symmetry and is independent of the phase parameter ϕ. The distribution is centered around zero and has a bell shape, but it is not Gaussian.

Figures 4.4 to 4.7 compare the exact and approximate phase PDFs, given by Equations (2.40) and (4.1), respectively. Note how close to each other the approximate and exact curves are. Of particular interest is Figure 4.7, which compares exact and approximate phase PDFs for $\mu = 1$. In such a case, the κ-μ phase PDF reduces to that of Rice, for the exact solution, and to Von Mises (Tikhonov), for the approximate solution. Note, here again, that both distributions are quite similar to each other, which is a rather interesting result. In all cases, the approximate solution is very close to the exact solution

Figures 4.8 to 4.11 show samples curves comparing exact and approximate PCR, given by Equations (2.41) and (4.42), respectively. It is observed that the PCR curves bear shapes very similar to those of the phase PDFs, as expected. Now comparing exact and approximate curves, it can be noticed that the approximations are very good in all cases. In general, the approximate curves are more impulsive, meaning that they slightly overestimate the phase crossings on the quadrant of the main lobe and underestimate the crossings on the other quadrants. The impulsive nature of the approximation is clearly seen in Figure 4.11, which compares the Rician exact PCR to the Rician approximate PCR. Note the bigger peaks and shorter tails of the approximation in relation to the exact function. In Figure 4.8 it can be seen that both the exact and approximate solutions coincide when $\kappa \to 0$, as predicted by the formulations.

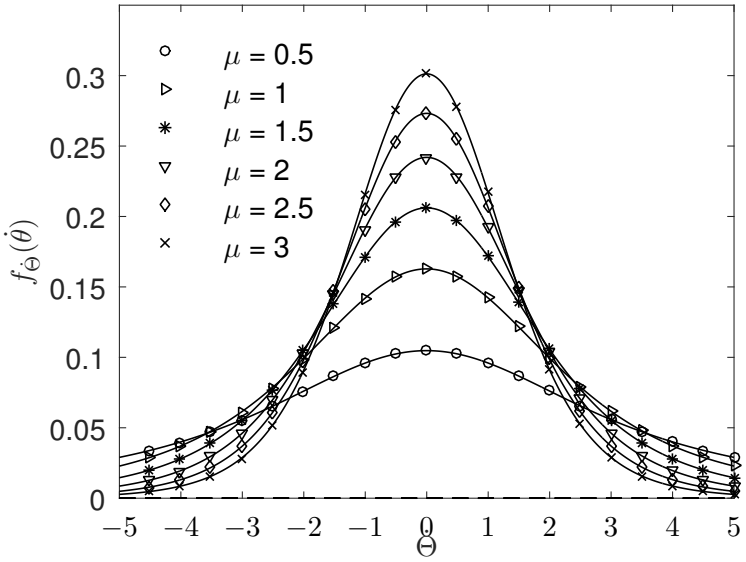

Figure 4.2: Phase derivative PDF for $\kappa = 1$, $f_d = 1$ and varying μ.

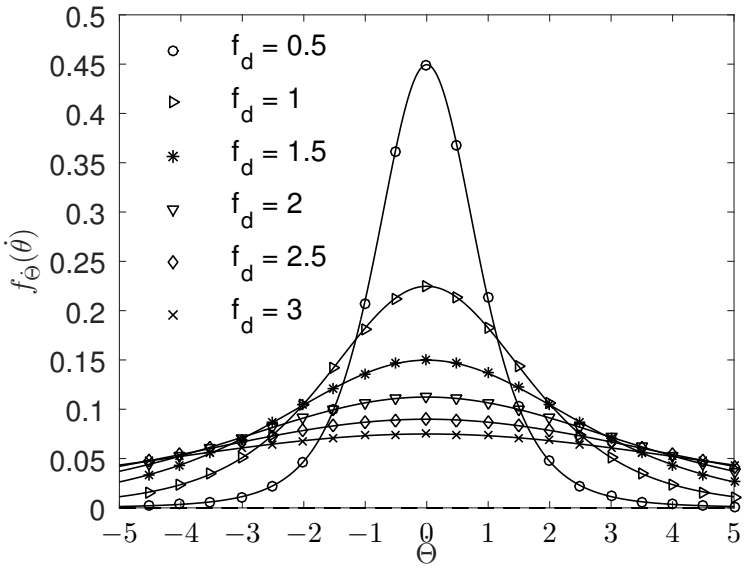

Figure 4.3: Phase derivative PDF for $\kappa = 1$, $\mu = 1.75$ and varying f_d.

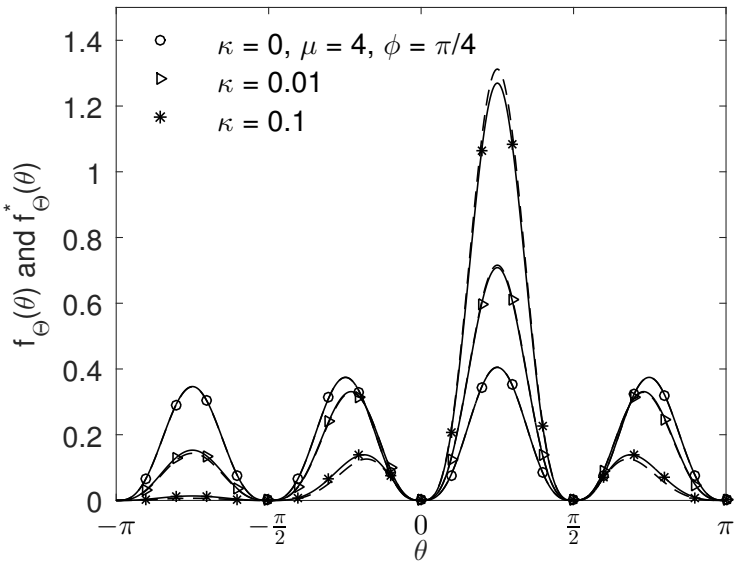

Figure 4.4: Comparison between exact (solid line) and approximate (dashed line) phase PDF for $\mu = 4$, $\phi = \pi/4$ and changing κ.

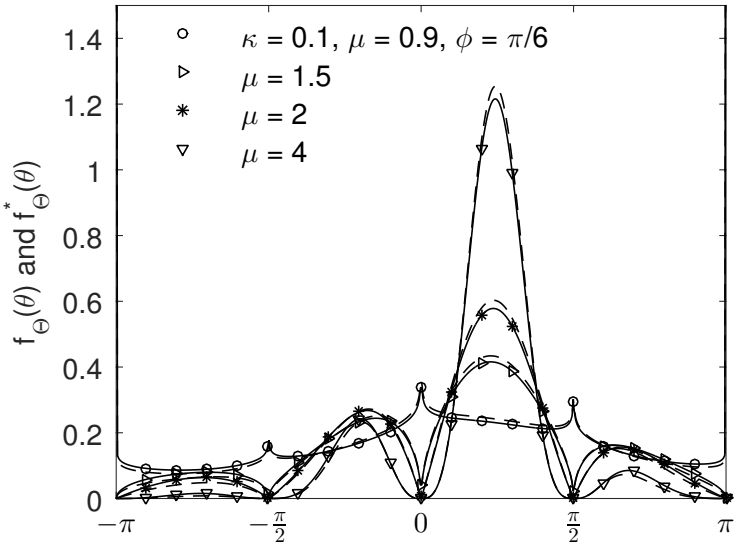

Figure 4.5: Comparison between exact (solid line) and approximate (dashed line) phase PDF for $\kappa = 0.1$, $\phi = \pi/6$ and changing μ.

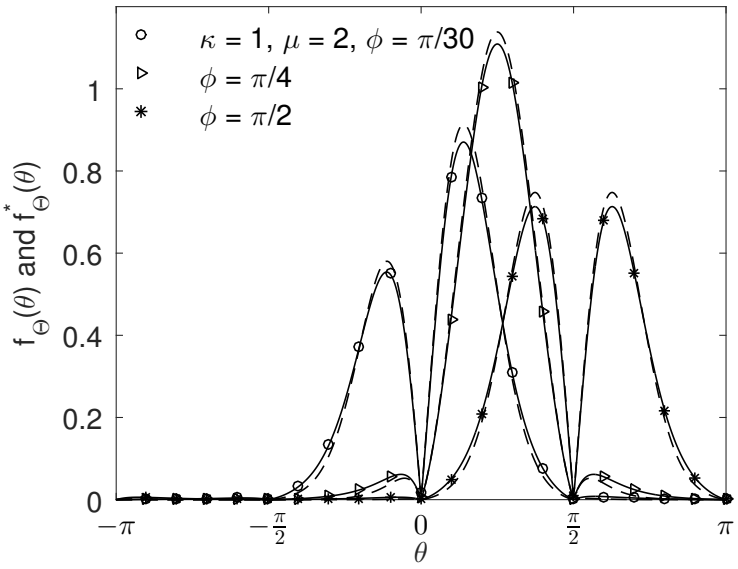

Figure 4.6: Comparison between exact (solid line) and approximate (dashed line) phase PDF for $\kappa = 1$, $\mu = 2$ and changing ϕ.

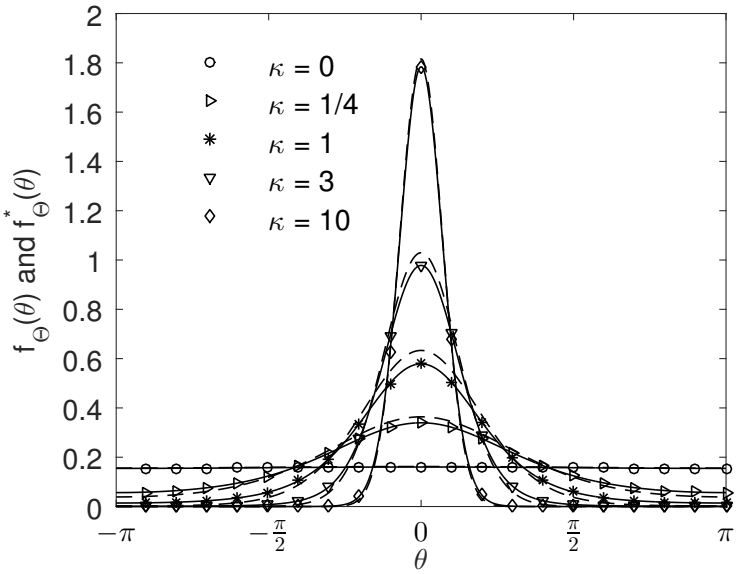

Figure 4.7: Comparison between exact (solid line) and approximate (dashed line) phase PDF of the Rician fading channel ($\mu = 1$, with $\phi = 0$). In this case, the approximate phase PDF follows a Von Mises distribution.

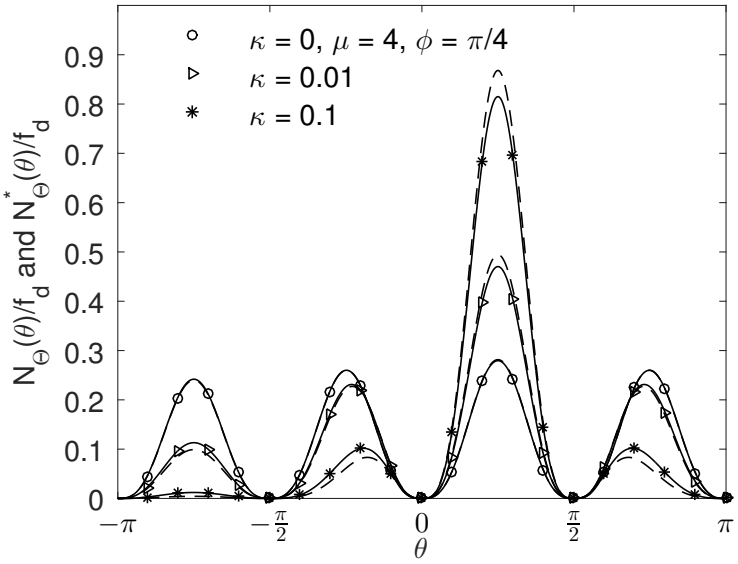

Figure 4.8: Comparison between exact (solid line) and approximate (dashed line) PCR for $\mu = 4$, $\phi = \pi/4$ and changing κ.

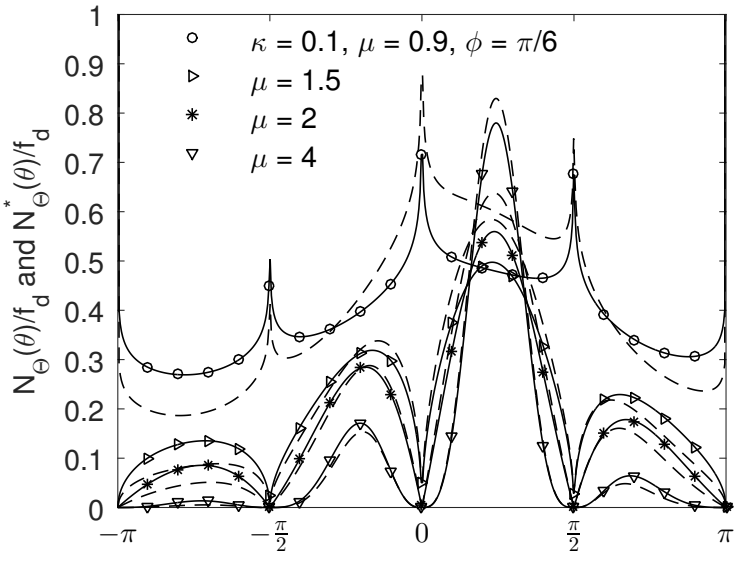

Figure 4.9: Comparison between exact (solid line) and approximate (dashed line) PCR for $\kappa = 0.1$, $\phi = \pi/6$ and changing μ.

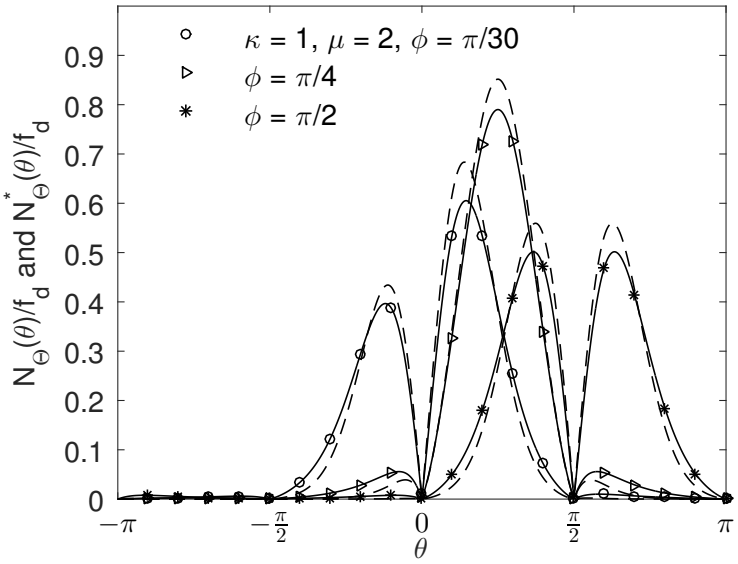

Figure 4.10: Comparison between exact (solid line) and approximate (dashed line) PCR for $\kappa = 1$, $\mu = 2$ and changing ϕ.

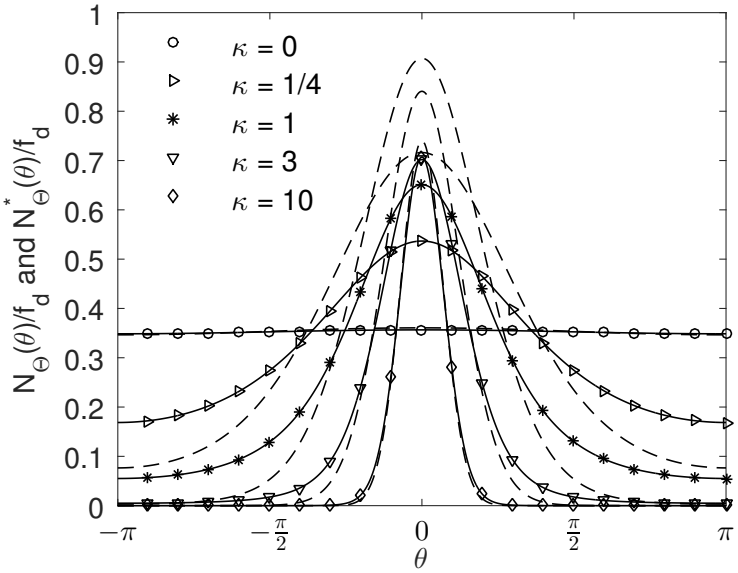

Figure 4.11: Comparison between exact (solid line) and approximate (dashed line) PCR of the Rician fading channel ($\mu = 1$, with $\phi = 0$).

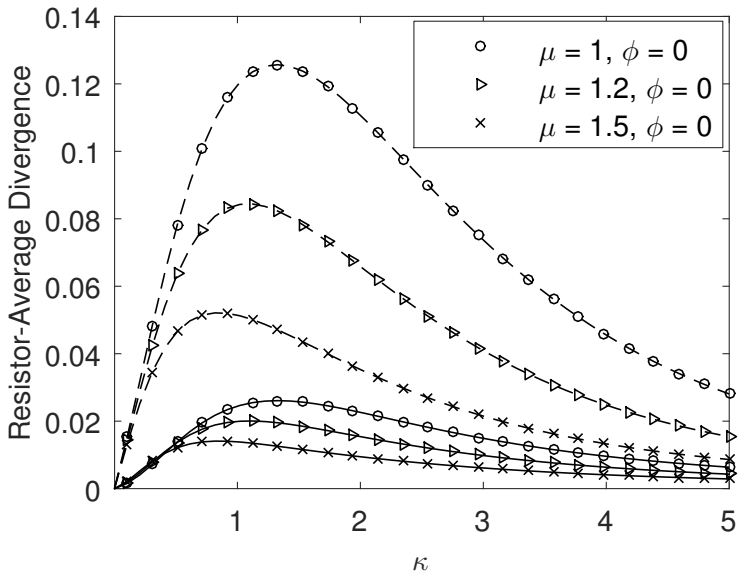

Figure 4.12: Resistor-Average Divergence between exact function and its respective approximation for the phase PDF (solid line) and normalized PCR (dashed line) for selected values of μ and ϕ and varying κ.

4.6 Information Loss Between Exact and Approximate Solutions

To assess the information loss associated with the approximation we used a metric called the Resistor-Average Divergence (RAD) [59], which is derived from the Kullback-Leibler Divergence (KLD)[2] [60]. The Resistor-Average Divergence satisfies the four conditions of distance metrics: i) it is non negative; ii) if $RAD(p_a, p_b) = 0 \rightarrow p_a = p_b$; iii) unlike the KLD, the RAD is symmetric, which means that $RAD(p_a, p_b) = RAD(p_b, p_a)$; and finally, it satisfies the triangle inequality, since $RAD(p_a, p_c) \leq RAD(p_a, p_b) + RAD(p_b, p_c)$.

The $\kappa - \mu$ phase PDF and its approximation can be compared directly using this metric, since both are true PDFs. The PCR and its approximation, however, are not PDFs and cannot be compared directly using this measurement. In order to be compared, they are first normalized to unitary area so that they become a PDF. Since both exact and approximate PCR have the same area by construction, their normalized version are scaled by a common factor and thus retain the same ratio as the original functions.

The divergence is synthesized in Figures 4.12 to 4.14. As expected, the divergence goes to zero as $\kappa \rightarrow 0$, since at that point the approximations reduce to the exact functions. As κ increases, the divergence reaches a maximum and then starts to recede, reducing monotonically as κ becomes larger. This monotonic decrease in the divergence is also observed when μ is increased, as it can be seen in Figure 4.13. With respect to ϕ, the divergence is periodic. It reaches its lowest values when ϕ is an integer multiple of $\pi/2$ and it is independent of ϕ when $\mu = 1$, at which point the parameter ϕ does not change the shape of the curve, only the phase shift. In all cases the PCR has a bigger divergence than the phase PDF, which means that the approximation fits the phase PDF better. This is in accordance to what was qualitatively observed in Section 4.5.

[2]The RAD is calculated as $RAD(p_0, p_1) = \frac{\mathbb{D}(p_0||p_1)\mathbb{D}(p_1||p_0)}{\mathbb{D}(p_0||p_1)+\mathbb{D}(p_1||p_0)}$, in which $\mathbb{D}(p_0||p_1)$ is the KLD from p_0 to p_1

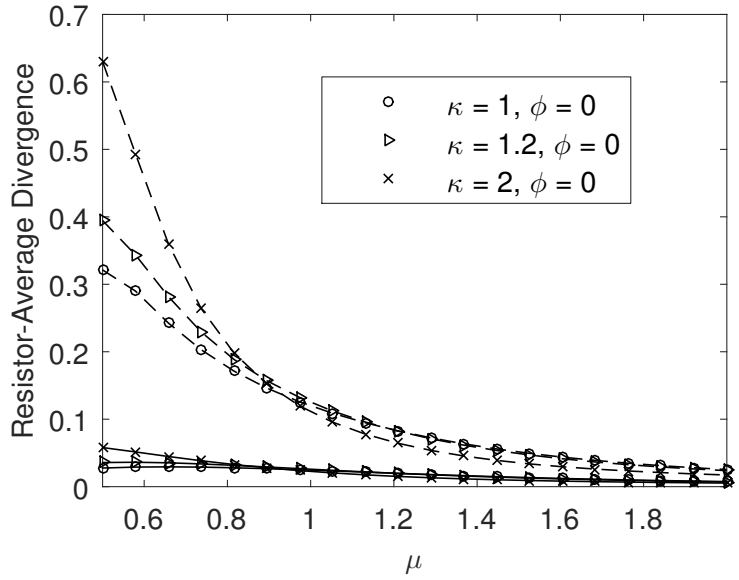

Figure 4.13: Resistor-Average Divergence between exact function and its respective approximation for the phase PDF (solid line) and normalized PCR (dashed line) for selected values of κ and ϕ and varying μ.

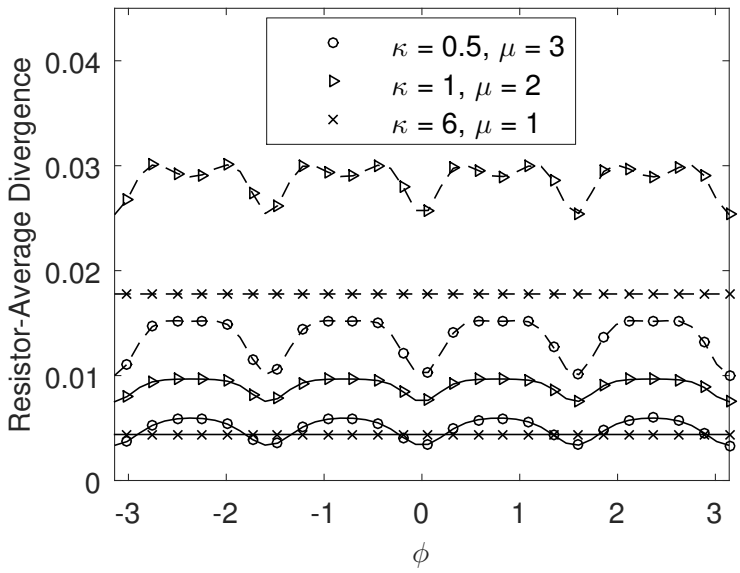

Figure 4.14: Resistor-Average Divergence between exact function and its respective approximation for the phase PDF (solid line) and normalized PCR (dashed line) for selected values of κ and μ and varying ϕ.

4.7 Conclusion

This chapter conducted a thorough investigation on the phase statistics of the κ-μ fading channel. It introduced several new statistics of the model: (i) tight approximate closed-form formula for the phase PDF; (ii) exact JPDF of combinations of phase, envelope, and their time derivatives; (iii) exact closed-form formula for the PDF of the time derivative of the phase; (iv) approximate closed-form formula for the PCR. As a result of the calculations carried out here, a new mathematical identity was also found.

A very interesting outcome of the approximation for the phase PDF is a new phase/angle random variable. Such a new RV has a closed-form expression for its PDF and can be computed very efficiently. It has been initially derived as a simpler approximate solution of the κ-μ phase PDF, but, strikingly, it turned out to be a generalization of both Von Mises (Tikhonov) and Nakagami-m phase distributions, both of them comprised in its PDF.

In general, it can be said that, as far as first-order statistics are concerned, the approximate phase PDF yields curves that are almost indistinguishable from those of the exact phase PDF. On the other hand, concerning the second-order statistics, exact and approximate PCR formulations indeed yield excellent fit to each other for the great majority of the cases, yielding slightly poorer results for intermediate values of κ (say, κ around 1) for low values of μ, as confirmed by the divergence plots provided.

A previous work [54] has already found that the κ-μ phase PDF has applicability in practice. Because the corresponding PCR yields shapes that are very similar to those of the phase PDF, it is expected that the formulations derived here will also find practical applications. Overall, this chapter has shown that κ-μ is a highly flexible and mathematically tractable fading model with a direct application in wireless scenarios. Furthermore, since its parameters carry physical meaning by construction, insight about real propagation conditions can be gained by fitting data to the model. Finally, the formulations presented here, be they in their exact or approximate forms, facilitate the usability of the model.

Chapter 5

On the Simulation of the κ-μ phase process

5.1 Introduction

The objective of this chapter is to propose a simulation technique for the phase of the κ-μ channel. The simulation of the κ-μ phase process cannot be done in the straightforward way discussed in Section 2.6 because the κ-μ model lacks a complete description of its complex envelope. Whereas the absolute value of both the in-phase and quadrature components of the κ-μ model can be easily inferred from Equations (2.25) and (2.26), the information about the sign of each component is lost in the exponentiation. The task of assigning a sign to each component thus becomes an important part of the simulation itself. Indeed, if those were known, it would be trivial to build a simulator for the phase of the κ-μ channel. How to estimate those signs in a way that the output sequence of the simulator maintains an overall compatibility with the statistics of the κ-μ channel becomes the central unknown that needs to be tackled by the simulation technique.

The final simulator proposed in this chapter addresses this problem by introducing a Markov-chain to estimate the instantaneous sign of each component, with transition probabilities driven by the instantaneous value of the component simulation. This dynamic probabilities are set so that the simulated phase has exactly the κ-μ phase statistics, as is proven in this chapter. An assortment of other simulation techniques are also discussed. In particular, two less sophisticated simulators that also relied on a Markov-chain to estimate the signs were developed and are explained in detail. Those simulators provide the basis for the construction of the final, dynamic simulator.

This chapter is structured in seven sections. Section 5.2 discusses some particularities of the κ-μ phase channel and presents two previous methods of estimating the components' signs. Section 5.3 presents a simulator that uses a Markov-chain to estimate the quadrant of a κ-μ sample, and from that determine its components' signs. Section 5.4 presents a Markov-chain sign estimator that goes in the opposite way, first choosing the signs of the individual components and from that establishing the quadrant. Section 5.5 provides the statistical characterization of the Markov simulators previously presented, deriving their phase PDF and proving that both sign selection approaches lead to the same statistics. Section 5.6 develops the final, dynamic Markov simulator, which is constructed in such a way to simulate the κ-μ phase statistics exactly. Finally, Section 5.7 concludes the chapter.

5.2 Considerations on the Phase of the κ-μ Processes

As briefly discussed in the introduction, the κ-μ phase process has a peculiarity that hinders its direct simulation. The absolute value of the X and Y components of the complex envelope $Z = X + jY$ of the signal are well defined, by Equations (2.25) and (2.26), but their signs are completely unknown. Without the sign information, it is not possible to assign each simulated sample to a specific quadrant.

The question that arises naturally is: how to create a phase simulation of a model that provides no information about the quadrant of the samples? It might come as a surprise that the phase PDF is known and that it has values in all four quadrants, despite the lack of an underlining physical model. Indeed, in [17] the authors used a clever mathematical observation to obtain the PDF. First the PDF of the absolute value of the in-phase and quadrature component was found, for which there is a well defined physical description. Then, they applied the boundary condition that, for $\mu = 1$, the distribution must revert to the Ricean distribution to maintain compatibility with this special case. From the PDF of X and Y the phase PDF is obtained through a Cartesian to polar coordinate change. Even though this method yields the expression of the PDF of the in-phase and quadrature components, as well as the PDF of the κ-μ phase, it does not provide any insight on the physical model that leads to that distributions. In the particular case of the Ricean distribution, the sum of squares disappears (since $\mu = 1$) and determining the sign becomes trivial, as seen in Equation (2.18).

5.2.1 Fixed Signs

The simplest sign estimation method is to simply arbitrarily assign a fixed positive or negative sign to all samples. For instance, the signs of X and Y can be fixed as positive, which would always generate samples bounded to the first quadrant. Evidently this is not well suited to simulate a phase model distributed over the four quadrants but even this simplistic method can yield a good simulator for certain parameter sets that naturally restrain the κ-μ PDF to a certain quadrant. Figure 5.1 illustrates this with two examples. The first set of parameters yields a curve that is mostly contained within the first quadrant. As a result, the naive simulation performs very well under this circumstance. In the same Figure is shown an example with a set of parameters that causes the κ-μ phase PDF to sprawl over the four quadrants. As expected, the naive simulator performs much worse, concentrating all the probability mass in the first quadrant and as a result overshooting the true PDF there, while remaining null over the rest of the phase domain.

By not allowing the simulation to change quadrants we have effectively created a new Random Variable. Let Ψ denote the RV obtained this way, and let $f_\Theta(\theta)$ denote the κ-μ phase PDF. The PDF of Ψ is found to be [44]

$$f_\Psi(\psi) = f_\Theta(\psi - \pi) + f_\Theta(-\psi) + f_\Theta(\psi) + f_\Theta(\pi - \psi), \qquad 0 < \psi < \pi/2. \tag{5.1}$$

Equation (5.1) describes how the naive simulator trasposes the samples to the first quadrant. Whenever Equation (5.1) is a good approximation to the κ-μ phase PDF, the simulator will perform well. In practice, this simulator gets better the closer the phase parameter ϕ is to $\pi/4$ and the greater κ and μ are, since this increases the impulsiveness of the phase PDF [44]. The naive simulator can also be used when ϕ is close to $-3\pi/4$, $-\pi/4$ and $\pi/4$,

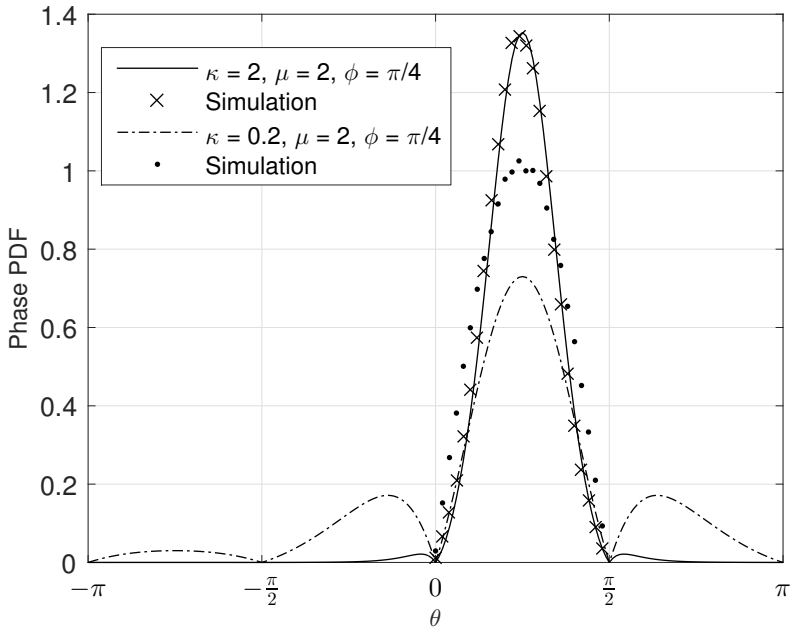

Figure 5.1: The κ-μ phase PDF and the naive simulation for two sets of parameters. The simulation never yields any sample outside the $[0, \pi/2)$ interval by construction and thus was suppressed outside this interval for greater visibility.

by toggling the sign from either or both the in-phase and quadrature components, to lock the simulator in the appropriate quadrant.

5.2.2 Sign Estimation Based in the Z_i Components

Another simulator discussed in [44] takes into account the instantaneous values of the Z_i components to estimate the sign of the sample. In this model, the sign is defined as

$$s_X[k] = \text{sign}\left(\sum_{i=1}^{\mu} X_i[k] + p_i\right) \qquad \text{and} \qquad s_Y[k] = \text{sign}\left(\sum_{i=1}^{\mu} Y_i[k] + q_i\right). \tag{5.2}$$

According to Equation (5.2), the sign is taken as the sign of the sum of all the μ independent individual samples that makes up the in-phase or quadrature component. The complex envelope of this simulator is then

$$R = s_X[k] \times \sum_{i=1}^{\mu}(X_i + p_i)^2 + j s_Y[k] \times \sum_{i=1}^{\mu}(Y_i + q_i)^2, \tag{5.3}$$

in which X_i and Y_i are the Gaussian simulations with auto-correlation described by Equation (2.8), and p_i and q_i are the mean values of the components, as defined in Equation (2.28).

Whereas Equation (5.3) does not perfectly yield the κ-μ statistics, it is an interesting approach that reduces back to the straightforward Rice simulator when $\mu = 1$. Furthermore, this simulation first and second order statistics fit very well the theoretical curves of the κ-μ channel in three types of scenarios: when all the four lobes are symmetric (Nakagami-m conditions); when the PDF is symmetric and the probability mass is concentrated in just two quadrants; and when almost all the probability mass is concentrated in one quadrant. The performance worsens when the phase PDF strays from these cases. Figures 5.2 to 5.4

show three examples of this simulator. The most probable quadrant is consistently under represented, which in turn leads to the lesser probable quadrants being over represented. Figure 5.2 shows two cases in which the simulation performs well: when $\kappa = 0$ the κ-μ distribution becomes Nakagami-m and the phase PDF becomes four symmetric lobes; and when $\kappa = 4$, in which case most probability mass is restricted to the first quadrant. Figure 5.4 shows another optimal case for this simulator, with the curve $\phi = 0$.

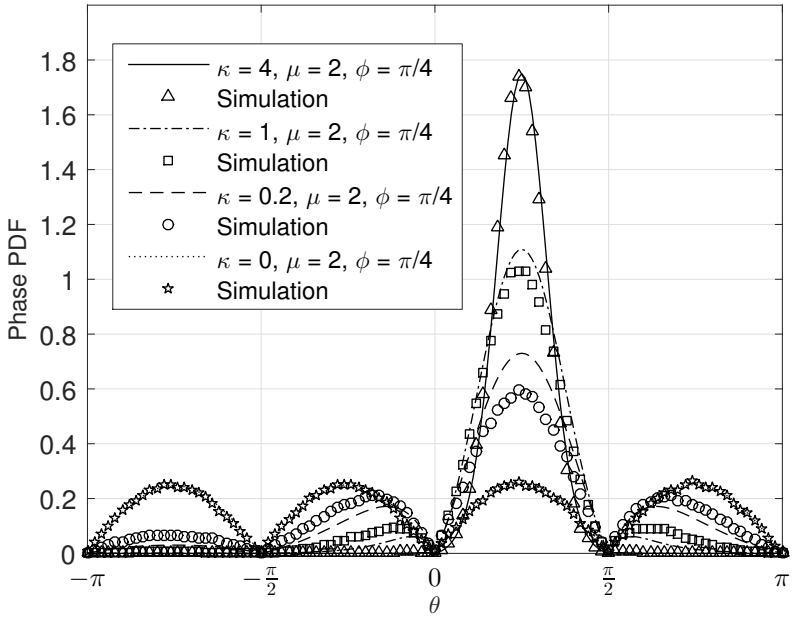

Figure 5.2: Four sets of the κ-μ phase PDF and the sign estimation simulation for three sets of parameters, illustrating how the simulation performs for different values of κ. The simulation gets better as $\kappa \to 0$.

A particularity of this simulation is that whenever $\mu \neq 1$ there are sudden phase jumps every time the quadrant changes, indicating that the sign changes when the envelope is non-zero. In fact, the probability that a sum of squared Gaussians is zero is null, as it would only happen if all the Gaussians simultaneously became zero, and the probability that a continuous RV will assume a certain value is null. There is never a chance to change quadrants without a phase jump, which implies that, to assure the change of quadrants, any practical simulation of the κ-μ channel will have to incorporate these jumps in one way or another. This gives insight on the kind of physical process underlying the κ-μ distribution: it must cross the quadrant boundary impulsively, suggesting that the in-phase and quadrature components are subjected to repeated brusque changes in signs.

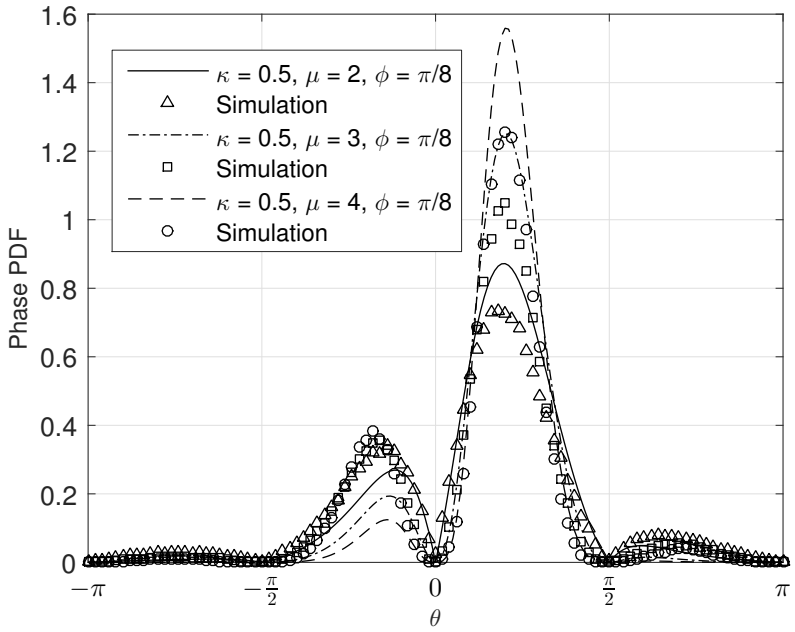

Figure 5.3: Three sets of the κ-μ phase PDF and the sign estimation simulation for three sets of parameters, illustrating how the simulation performs for different values of μ.

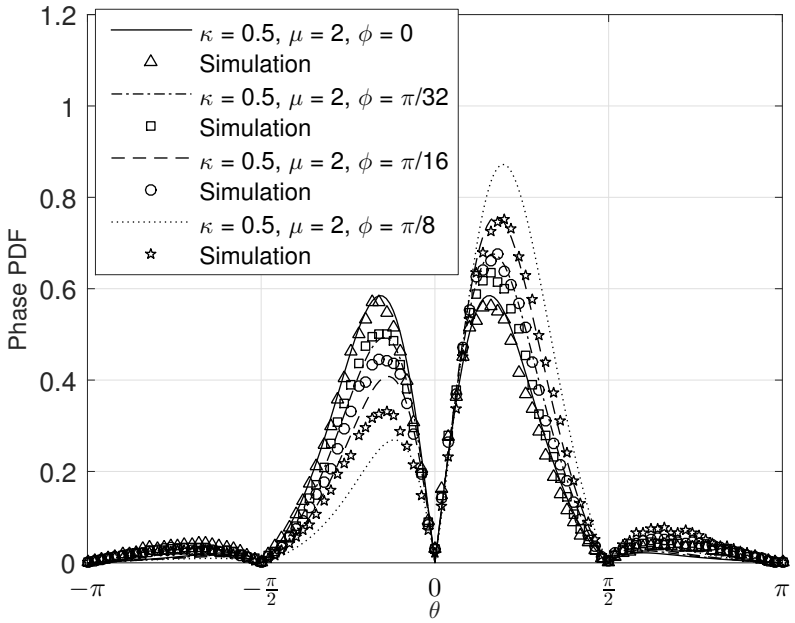

Figure 5.4: Four sets of the κ-μ phase PDF and the sign estimation simulation for three sets of parameters, illustrating how the simulation performs for different values of ϕ. The simulation gets better as ϕ approaches a quadrant boundary, in this case, 0.

5.3 Quadrant Sign Estimation

All the proposed simulation methods so far assigned the in-phase and quadrature signs independently to each other. A different approach would be to first choose the quadrant and then use that information to determine the sign of each component. By using a 4 state Markov-chain, with each state representing a quadrant, and carefully controlling the state transition probabilities, it is possible to build a simulator that keeps the quadrant probability the same as the theoretical model, performing better than all the previously described simulators. Figure 5.5 shows the proposed quadrant-estimating Markov-chain.

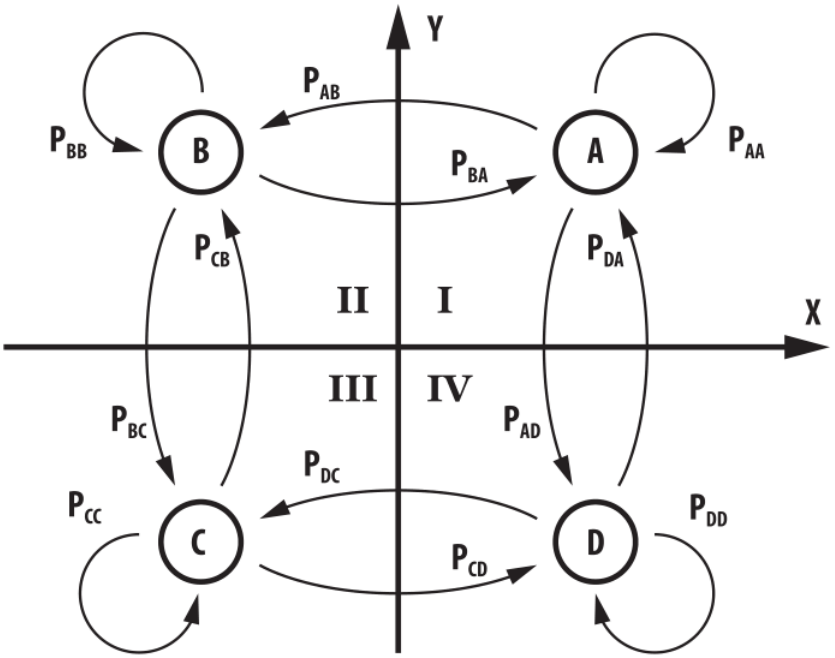

Figure 5.5: Markov-chain used to estimate the appropriate quadrant.

States A, B, C and D represent the quadrants I, II, III and IV, respectively. The process of sign assignment works as follows: first, two independent κ-μ sequences X and Y are generated using the method described in Section 2.6, with N samples per sequence. The first sample is randomly assigned to one of the quadrants and, from that sample on, the sign of the next sample is determined according to Figure 5.5. For instance, if the first sample is assigned to the first quadrant, the Markov-chain initiates at state A. The next sample has probability P_{AA} of staying in the first quadrant, probability P_{AB} of transitioning to the second quadrant and probability P_{AD} of transitioning to the fourth quadrant. In general terms, a sample in this simulation can stay in the quadrant of the former sample or it can transition to one of the adjacent quadrants, but can not transition directly to the opposite quadrant. In terms of the components, that means that it can either keep the same sign as the previous sample or change the sign of one of the components, but not both of them at the same step. This was a design choice and is not a requirement of the model. The elimination of the odd cases in which the signs of both the in-phase and quadrature flip at the same simulation step simplifies the stochastic matrix. This elimination does not change the statistics of the simulation, as will be shown in the next sections, which includes another simulator without this restriction.

The stochastic matrix P describes this chain,

$$P = \begin{bmatrix} P_{AA} & P_{AB} & 0 & P_{AD} \\ P_{BA} & P_{BB} & P_{BC} & 0 \\ 0 & P_{CB} & P_{CC} & P_{CD} \\ P_{DA} & 0 & P_{DC} & P_{DD} \end{bmatrix}. \tag{5.4}$$

In Equation (5.4) the sum of the elements of each line is unitary. At a first glance, this is a system of 4 equations and 12 unknowns, giving it 8 degrees of freedom. Therefore, there is a considerable autonomy for the selection of the transition probabilities. There is, however, one important consideration that adds more restrictions to this system. Let P_X be the probability that the Markov process is in state X, after a long number of iterations. We want P_X to be equal to the probability that the quadrant of a randomly chosen κ-μ phase sample is in quadrant X. Let θ_i and θ_f be the angles marking the boundaries of the quadrant X (for instance, if X is the first quadrant, $\theta_i = 0$ and $\theta_f = \pi/2$) and let $f_\Theta(\theta)$ denote the κ-μ phase PDF. We want P_X to be equal to

$$P_X = \int_{\theta_i}^{\theta_f} f_\Theta(\theta) d\theta. \tag{5.5}$$

The P_X probabilities can be directly calculated by the study of the steady-state condition of the Markov-chain. The chain is said to be in a steady-state when the probability of it being in a certain state does not change after a transition. Let P_A, P_B, P_C and P_D denote the steady-state probability of the chain being in states A to D respectively. The steady-state condition is mathematically written as

$$\begin{bmatrix} P_A & P_B & P_C & P_D \end{bmatrix} = \begin{bmatrix} P_A & P_B & P_C & P_D \end{bmatrix} \times \begin{bmatrix} P_{AA} & P_{AB} & 0 & P_{AD} \\ P_{BA} & P_{BB} & P_{BC} & 0 \\ 0 & P_{CB} & P_{CC} & P_{CD} \\ P_{DA} & 0 & P_{DC} & P_{DD} \end{bmatrix}. \tag{5.6}$$

The chain always converge to the steady-state in positive recurrent Markov-chains [61]. Positive recurrence means that every state of the chain has non null probability of being reached at any time in the future of the chain, which is always respected in Equation (5.4) when all transition probabilities are positive.

Equation (5.6) gives us 4 new Equations, but it is possible to demonstrate that only 3 of those are independent. By incorporating those new restrictions into the system, the number of degrees of freedom is decreased from 8 to 5, meaning that the solution space of the system of equations representing the transition probabilities with the steady-state restriction has 5 dimensions. There are, therefore, infinitely many different models that respect all the conditions imposed so far. How to further restrict the variables to obtain a definitive model is a choice of the designer.

After considering many different models, the following stochastic matrix was developed,

$$P = \begin{bmatrix} 1 - r(P_B + P_D) & rP_B & 0 & rP_D \\ rP_A & 1 - r(P_A + P_C) & rP_C & 0 \\ 0 & rP_B & 1 - r(P_B + P_D) & rP_D \\ rP_A & 0 & rP_C & 1 - r(P_A + P_C) \end{bmatrix}, \tag{5.7}$$

in which $0 \leq r \leq \min\{(P_B + P_D)^{-1}, (P_A + P_C)^{-1}\}$. The restrictions over r come from the fact that every element of the matrix must be at the same time greater than or equal to zero and smaller than or equal to one, since they represent probabilities. This model introduces a parameter r that controls the transition rate between states. The biggest r is, the biggest is the transition rate. When $r = 0$ there are no transitions; in this case, the Markov-chain remains locked to the state it was initialized in. When r is set to its maximum allowed value, the transition rate is maximized. In this case, the least probable states will have a transition probability of 1, meaning that even though those state are reachable, they are not stable. The choice of the parameter r is a sort of a Goldilocks problem. If r is set too high, the simulation will transition too often and the simulated signal will be increasingly discontinuous. If it is set too low, the simulation will take too long to leave a given state, taking a greater number of samples to converge. During simulations it was observed that the value $r = f_D/F_s$ is a good compromise for r, in which f_D is the maximum Doppler shift and F_s is the sample frequency of the simulation.

The main design driver of this model was to create a simulator in which the transition probability is proportional to the steady-state probability. For instance, if the chain is at state A, it will transition to state B with probability rP_B and to state D with probability rP_D, favoring the transition to the most probable state.

Figures 5.6 to 5.12 show some simulations obtained from this stochastic model, with the same sets of parameters used in Figures 5.2 to 5.4 for comparison. As can be seen, the simulator performs well in almost all scenarios, for both first and second order statistics. For most parameter choices, the simulator tends to concentrate more probability mass in the center of the quadrant when compared to the theoretical statistics. The biggest divergence is observed in the PCR when the simulator tries to generate Ricean samples, as shown in Figure 5.12. In this case, the forced transitions alters the second order statistics, by making the simulation cross the quadrant boundaries by jumping. This, in turn, causes the PCR to be zero at the quadrant boundaries and introduces artificial discontinuities to the Ricean PCR, altering significantly this statistics. However, as discussed in Chapter 2, the Ricean channel can be easily simulated by known methods and was included here for illustrative purposes of how the simulator performs in this extreme case.

From Equation (5.4) it is easy to compute the frequency of a quadrant jump. The probability that a jump occurs at any step is simply the sum over the conditional probabilities of a transition given that the chain is at state i. Mathematically,

$$P(\text{transition}) = \sum_{\text{all } i} P(\text{transition}|\text{state} = i)P(\text{state} = i), i \in \{A, B, C, D\}\,. \tag{5.8}$$

Applying Equation (5.8) to Equation (5.7), the transition probability is worked out to be

$$P(\text{transition}) = 2r(P_A + P_C)(P_B + P_D). \tag{5.9}$$

Equation (5.9) expresses the probability that a jump will occur at any step. In terms of simulation time, each step corresponds to a time period equal to the inverse of the sampling frequency F_s, so that there will be, in average, $P(T)$ transitions per time period of $1/F_s$.

Therefore, the simulated frequency of transitions, denoted by F_T, is equal to the transition probability times the sampling frequency,

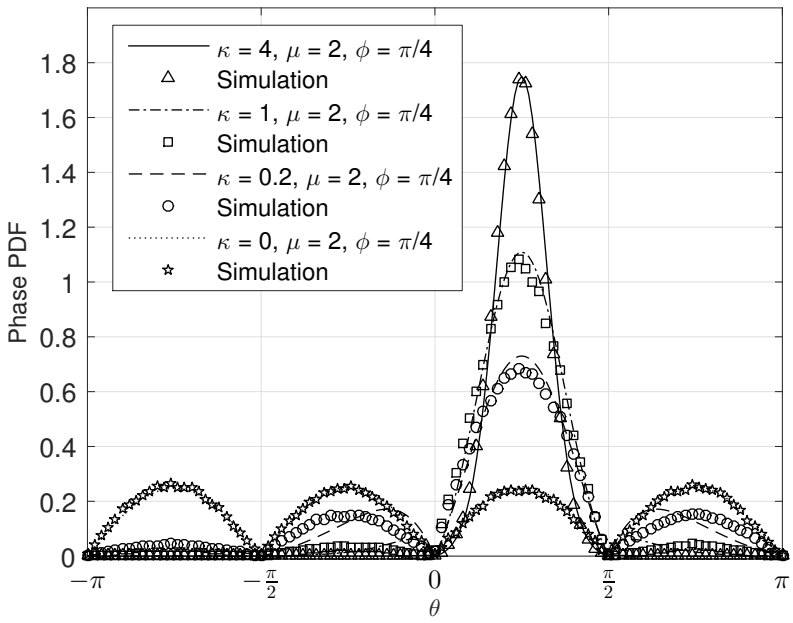

Figure 5.6: Four sets of the κ-μ phase PDF and the Markov-chain quadrant estimation simulation for three sets of parameters, illustrating how the simulation performs for different values of κ.

$$F_T = 2F_s r(P_A + P_C)(P_B + P_D). \tag{5.10}$$

Equation (5.10) can be used to find the appropriate r to obtain a desired transition frequency. The maximum achievable transition frequency is obtained when r is maximal. Since $0 \leq r \leq \min\{(P_B + P_D)^{-1}, (P_A + P_C)^{-1}\}$, the maximum transition frequency is

$$F_{T\max} = 2F_s \times \min\{(P_A + P_C), (P_B + P_D)\}. \tag{5.11}$$

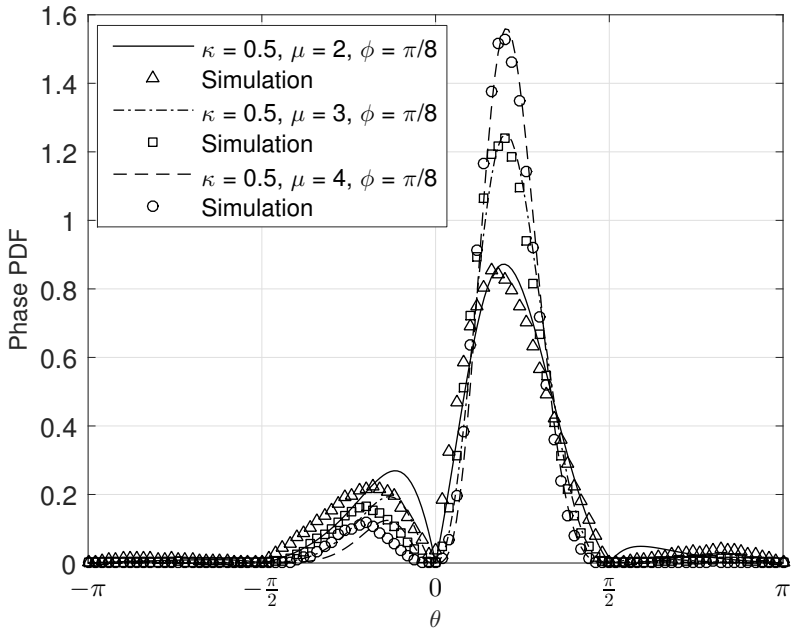

Figure 5.7: Three sets of the κ-μ phase PDF and the quadrant estimation simulation for three sets of parameters, illustrating how the simulation performs for different values of μ.

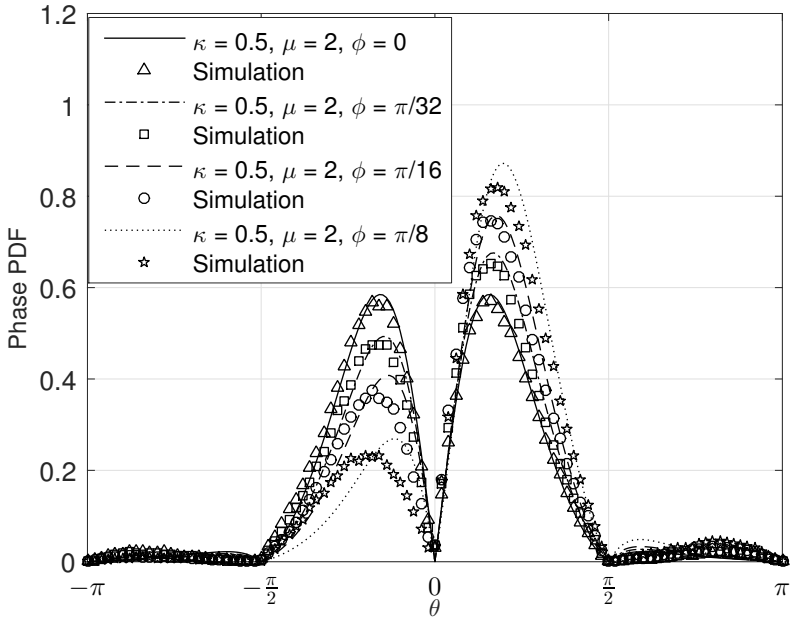

Figure 5.8: Four sets of the κ-μ phase PDF and the quadrant estimation simulation for three sets of parameters, illustrating how the simulation performs for different values of ϕ.

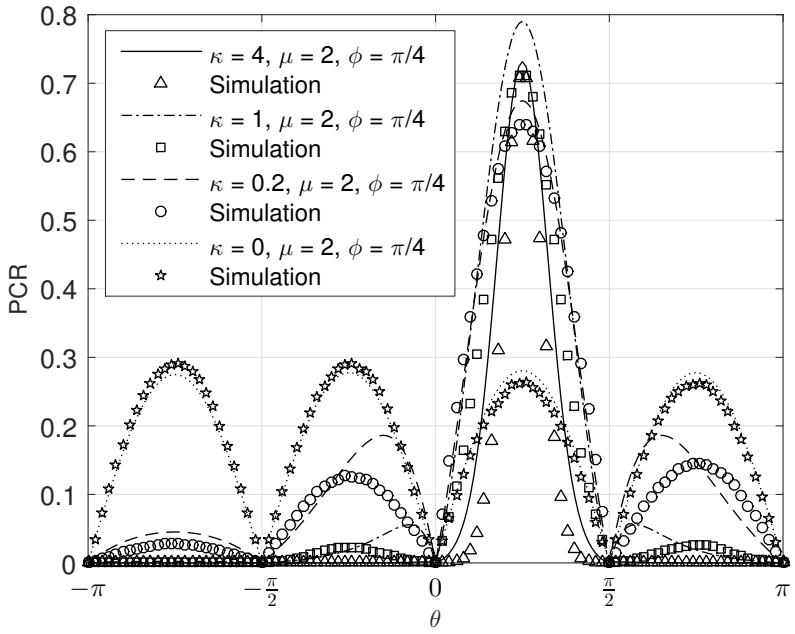

Figure 5.9: Four sets of the κ-μ PCR and the Markov-chain quadrant estimation simulation for three sets of parameters, illustrating how the simulation performs for different values of κ.

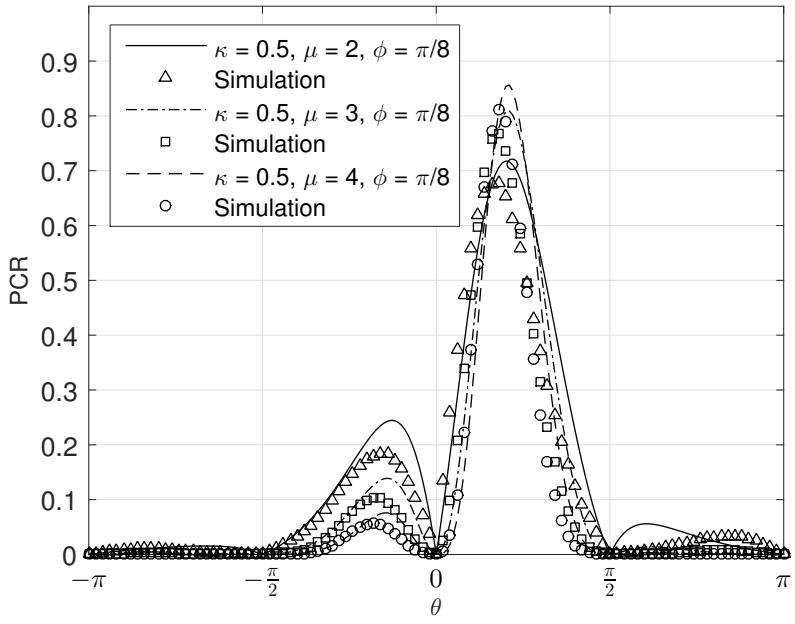

Figure 5.10: Three sets of the κ-μ PCR and the quadrant estimation simulation for three sets of parameters, illustrating how the simulation performs for different values of μ.

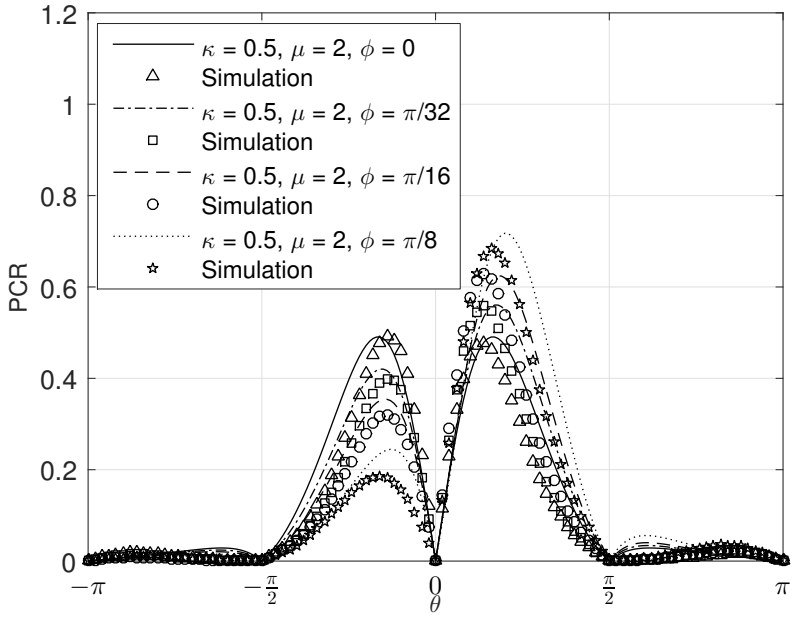

Figure 5.11: Four sets of the κ-μ PCR and the quadrant estimation simulation for three sets of parameters, illustrating how the simulation performs for different values of ϕ.

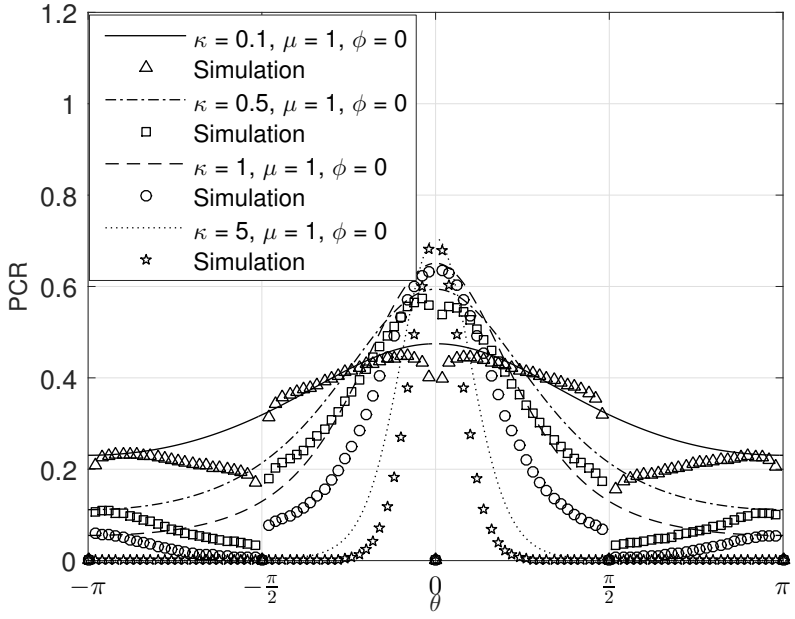

Figure 5.12: Four sets of the κ-μ PCR and the quadrant estimation simulation for $\mu = 1$, illustrating the Ricean case. The discontinuities in the simulation are caused by the constant quadrant flipping, which is not a feature of the Ricean model in particular. Note that the quadrant jumps cause the crossing rate to be zero at the quadrant boundaries.

5.4 Individual Component Sign Estimation

The previous section introduced a Markov-chain to first determine the quadrant of the sample and then select the appropriate signs of the components to assure it is in the given quadrant. An alternative approach can be used to build a simulator that works in the opposite way, one that determines the quadrant by first selecting the signs of the X and Y component independently. Instead of using a single 4-states Markov-chain, two 2-states Markov-chains are used, one to determine the sign of X and the other for the sign of Y. Let Z denote X or Y and let P_Z^+ and P_Z^- be the probabilities that Z is positive and negative, respectively. By following a similar method as before, the following transition matrix for Z was developed,

$$T = \begin{bmatrix} P_Z^{++} & P_Z^{+-} \\ P_Z^{-+} & P_Z^{--} \end{bmatrix} = \begin{bmatrix} 1 - r_Z P_Z^- & r_Z P_Z^- \\ r_Z P_Z^+ & 1 - r_Z P_Z^+ \end{bmatrix}, \tag{5.12}$$

$r_Z < \min\left\{1/P_Z^-, 1/P_Z^+\right\}$, in which the P_Z^{uv} represents the transition probability from state u to v. The associated Markov-chain is presented in Figure 5.13.

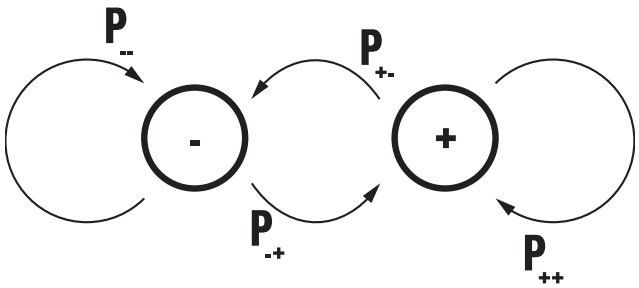

Figure 5.13: Markov-chain used to estimate the sign of each individual component.

Note that this simulation allows transitions from any quadrant to any other quadrant, since the components flip signs independently, as opposed to the quadrant sign estimator in the previous section.

The steady state probabilities P_X^+, P_X^-, P_Y^+ and P_Y^- can be written as functions of the steady state probabilities of the trigonometric quadrants P_A, P_B, P_C and P_D as

$$P_X^+ = P_A + P_D \tag{5.13a}$$

$$P_X^- = P_B + P_C \tag{5.13b}$$

$$P_Y^+ = P_A + P_B \tag{5.13c}$$

$$P_Y^- = P_C + P_D, \tag{5.13d}$$

or, conversely, the quadrant probabilities can be written as a function of the component's steady state probabilities,

$$P_A = P_X^+ P_Y^+ \tag{5.14a}$$

$$P_B = P_X^- P_Y^+ \tag{5.14b}$$

$$P_C = P_X^- P_Y^- \tag{5.14c}$$

$$P_D = P_X^+ P_Y^-, \tag{5.14d}$$

in which A, B, C and D represent the first, second, third and fourth quadrants, respectively.

The probability of a transition happening can be calculated, as before, by summing over all the conditional probabilities of a transition happening in a given state. The two chains are independent and the probability of a transition can be calculated by first calculating the probability that a transition occurs in each chain, summing them, and then subtracting the probability that a transition occurs at the same time in both chains, since that was counted twice in the sum. After the necessary algebraic manipulations, the transition probability is found as

$$P(\text{transition}) = 2r_X P_X^+ P_X^- + 2r_Y P_Y^+ P_Y^- - 4r_X r_Y P_X^+ P_X^- P_Y^+ P_Y^-. \tag{5.15}$$

The transition probability can be written in terms of the quadrant probabilities by substituting Equations (5.13) and (5.14) in Equation (5.15),

$$P(\text{transition}) = 2r_X(P_A + P_D)(P_B + P_C) + 2r_Y(P_A + P_B)(P_C + P_D) - 4r_X r_Y P_A P_C. \tag{5.16}$$

The transition frequency F_T is, as before, the transition probability times the sample frequency F_s,

$$F_T = 2F_s \left(r_X P_X^+ P_X^- + r_Y P_Y^+ P_Y^- - 2r_X r_Y P_X^+ P_X^- P_Y^+ P_Y^- \right). \tag{5.17}$$

The constants r_X and r_Y can take any value in the intervals $0 < r_X \leq \min\left\{1/P_X^-, 1/P_X^+\right\}$ and $0 < r_Y \leq \min\left\{1/P_Y^-, 1/P_Y^+\right\}$. If any of those are set to 0, the corresponding Markov-chain will be locked in its initial state; if any of those are set to its maximum value, the least probable state of the corresponding Markov-chain will have a transition probability of one and thus be unstable. The maximum possible quadrant transition frequency of this simulator is

$$F_T = 2F_s \left(\min\left\{P_X^+, P_X^-\right\} + \min\left\{P_Y^+, P_Y^-\right\} - 2\min\left\{P_X^+, P_X^-\right\} \min\left\{P_Y^+, P_Y^-\right\} \right). \tag{5.18}$$

Even though this simulator uses a different method to select the signs of the samples, both lead to the same statistics. This happens because both simulators choose the signs independently of the instantaneous value of the X and Y components. The main job of these simulators is to guarantee the correct proportion of positive and negative signs are distributed, so that the quadrant probabilities of the simulation are compatible with what was expected based on the theoretical probabilities. The secondary job is to moderate the dynamics of the sign distribution, controlling the rate of sign change to assure the resulting signal is not excessively discontinuous. In the next section, the statistics of these simulators will be derived in an exact manner.

5.5 Statistical Characterization of the Markov-Chain Simulators

In the previous sections, two sign generators based on a Markov-chain were proposed. The first used a 4-state Markov-chain to estimate the quadrant and the second used two 2-state Markov-chains to estimate the sign of each component directly. In both approaches, the sign generation is independent of the samples; the sign estimator does not take into account the instantaneous value of the channel to determine the sign. It was observed that this process does not produce the exact κ-μ theoretical channel. The PDF of the phase of the simulated samples is close to the theoretical phase PDF, but it is clearly distributed according to a different function. In this section we are interested in finding this function that describes the phase PDF of those simulators.

The two Markov-chain based simulators proposed are similar in nature, and can be summarized as follows: first, a sequence of N properly auto-correlated samples are generated for both the X and Y components. Each of these sequences will be distributed according to the PDF of $|Z|$ in Equation (2.34), with the same parameters σ and μ. The parameter λ is equal to p or q in Equations (2.32) and (2.33), depending on whether we are simulating X or Y. Then, each sample is assigned a positive sign with probability P_Z^+ and a negative sign with probability P_Z^-, in which Z means X or Y as required. Since the signs are independent of the values of the samples, the PDF of the simulated Z component can be written as

$$f_{simZ}(z) = P_Z^+ u(z) f_{|Z|}(z) + P_Z^- u(-z) f_{|Z|}(-z), \tag{5.19}$$

in which $u(\cdot)$ is the unit step function [47, Eq. (29.1.3)]. $u(z)$ is equal to 1 if $z > 0$, 0 if $z < 0$ and 1/2 if $z = 0$. Figures 5.14 and 5.15 show the simulations of the X and Y κ-μ components by a Markov-chain sign estimator. Notice that the simulation fits perfectly the theoretical PDF given by Equation (5.19), shown in solid line.

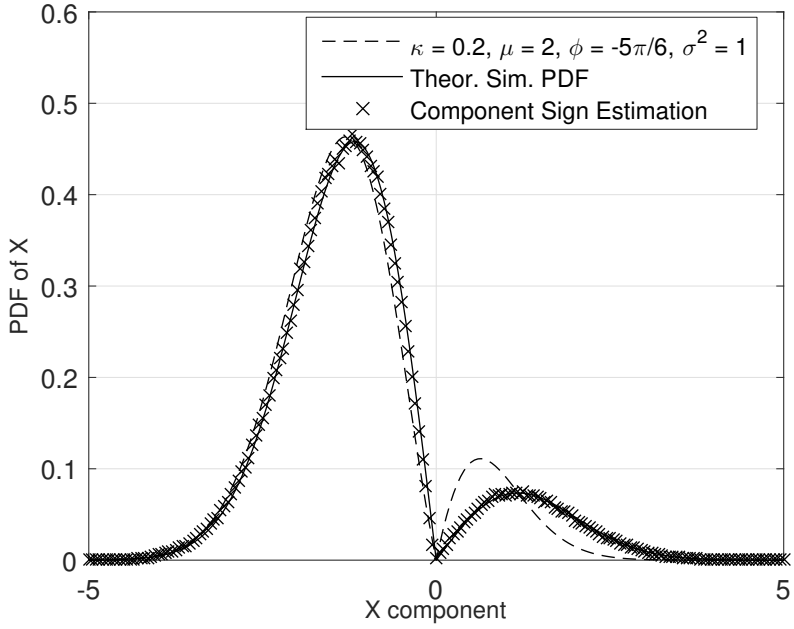

Figure 5.14: Comparison between the PDF of the theoretical κ-μ X component (dashed line) and the Markov-chain simulator (solid line. The crosses show the actual simulation.

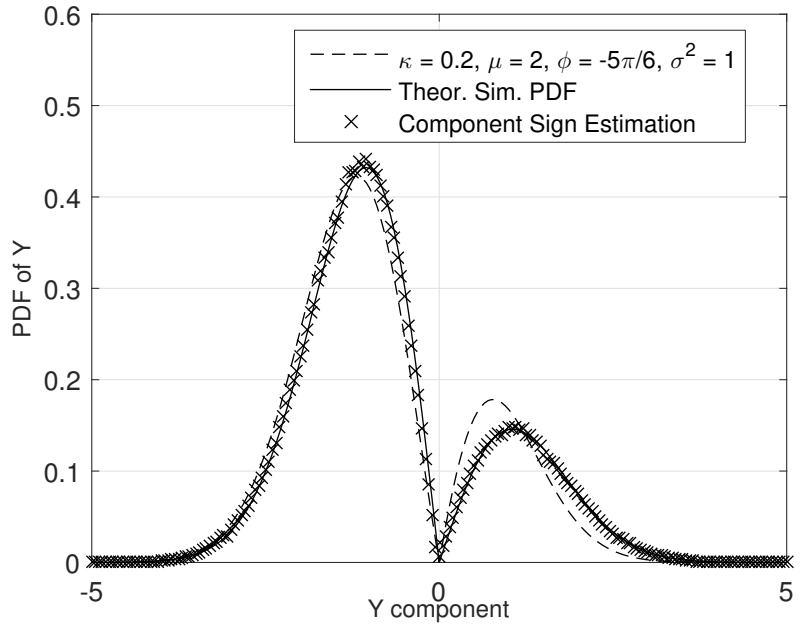

Figure 5.15: Comparison between the PDF of the theoretical κ-μ Y component (dashed line) and the Markov-chain simulator (solid line. The crosses show the actual simulation.

From the PDF of the components X and Y it is possible to find the PDF of the phase by first finding the joint PDF of X and Y, then performing a variable change to the polar variables R and Θ and finally calculating the marginal PDF of Θ. Since X and Y are independent, their joint PDF $f_{Xsim,Ysim}(x,y)$ can be found by multiplying their marginal PDFs,

$$\begin{aligned} f_{simX,Y}(x,y) = P_X^+ P_Y^+ u(x)u(y)f_{|X|}(x)f_{|Y|}(y) + P_X^+ P_Y^- u(x)u(-y)f_{|X|}(x)f_{|Y|}(-y) + \\ P_X^- P_Y^+ u(-x)u(y)f_{|X|}(-x)f_{|Y|}(y) + P_X^- P_Y^- u(-x)u(-y)f_{|X|}(-x)f_{|Y|}(-y). \end{aligned} \tag{5.20}$$

The phase-envelope joint distribution $f_{simR,\theta}(r,\theta)$ of the simulation can then be found by the following variable change,

$$X = R\cos\Theta \tag{5.21a}$$

$$Y = R\sin\Theta, \tag{5.21b}$$

and the expression for the joint PDF is calculated as

$$f_{simR,\theta}(r,\theta) = \left|\frac{\delta(x,y)}{\delta(r,\theta)}\right| f_{simX,Y}(x,y), \tag{5.22}$$

in which $|\delta(x,y)/\delta(r,\theta)|$ is the Jacobian of the transformation, which is easily found to be r. Let $g(x,y)$ be defined as

$$g(x,y) = f_{|X|}(x)f_{|Y|}(y), \tag{5.23}$$

for $x > 0$ and $y > 0$. $g(x,y)$ is the joint PDF of the absolute value of two κ-μ independent component random variables. The phase-envelope joint distribution $g_{P,\Theta}(\rho,\theta)$ is found after substituting Equations (5.20) and (5.21) in Equation (5.22),

$$\begin{aligned} g_{P,\Theta}(\rho,\theta) = 2\mu^2\kappa^{1-\frac{\mu}{2}}(1+\kappa)^{\frac{\mu}{2}+1}\rho^{\mu+1}|\sin 2\theta|^{\frac{\mu}{2}}|\sin 2\phi|^{1-\frac{\mu}{2}}\exp\left(-\mu(1+\kappa)\rho^2 - \kappa\mu\right) \\ \times I_{\frac{\mu}{2}-1}\left(2\rho\cos\theta|\cos\phi|\mu\sqrt{\kappa(1+\kappa)}\right) I_{\frac{\mu}{2}-1}\left(2\rho\sin\theta|\sin\phi|\mu\sqrt{\kappa(1+\kappa)}\right), \end{aligned} \tag{5.24}$$

in which $\rho = r/\hat{r}$ is the normalized envelope. After the required algebraic manipulations, the phase-envelope joint PDF of the simulator can be expressed as a function of $g_{P,\Theta}$ as

$$f_{simP,\Theta}(\rho,\theta) = g_{P,\Theta}(\rho,\theta) \times \Big(u(x)u(y)P_A - u(-x)u(y)P_B + u(-x)u(-y)P_C - u(x)u(-y)P_D\Big), \tag{5.25}$$

in which the terms P_A-P_D are the quadrant probabilities given in Equation (5.14). The terms inside the parentheses are mutually exclusive due to the step functions. For instance, if $0 \leq \theta < \pi/2$, the sample is in the first quadrant which implies that X and Y are positive; in turn, both $u(x)$ and $u(y)$ are equal to one. All the other terms inside the parentheses are null in this case, and the simulation PDF reduces to $f_{simP,\Theta}(\rho,\theta) = P_A \times g_{P,\Theta}(\rho,\theta)$. In order to obtain the marginal phase PDF of the simulator, Equation (5.25) is integrated over ρ from 0 to ∞. No closed form expression was found, however, but it is still possible to compute the phase PDF by numerical integration.

Each lobe of the simulator phase PDF is thus a scaled version of $g_{P,\Theta}(g,\theta)$, and the scaling factor is the corresponding quadrant probability. This behavior is expected, since the simulator draw from a pool of variates with the same PDF and selects a quadrant for them with the corresponding quadrant probability. Equation (5.25) encapsulates succinctly the mechanics behind this kind of simulators.

The only assumption needed to arrive at Equation (5.25) is that the choice of the components sign is independent of the sample values. This means that any simulator that chooses the signs based only on some fixed probabilities will have the same phase statistics. Figure 5.16 illustrates this property, by plotting in the same graph the phase statistics of both Markov-chain simulators. Notice that both follow perfectly the theoretical expression given by Equation (5.25). The true κ-μ phase PDF is also plotted, for comparison.

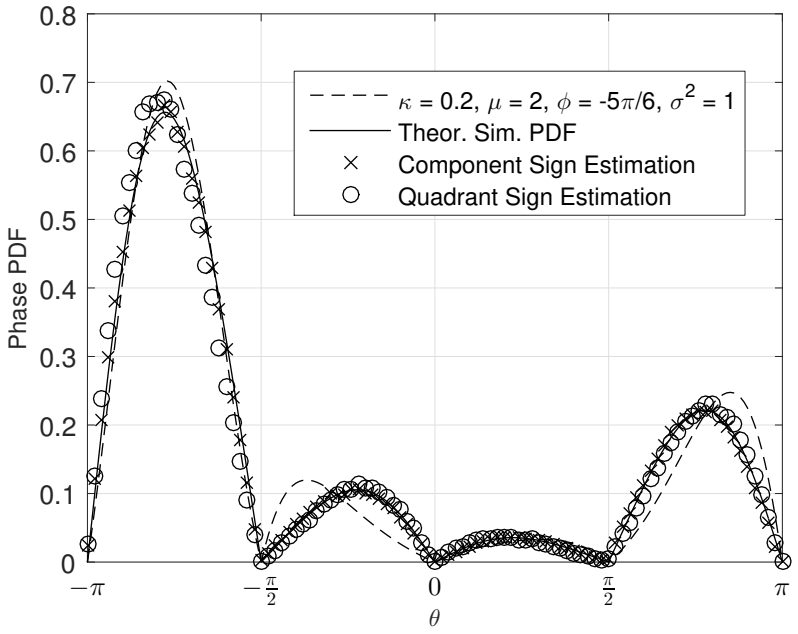

Figure 5.16: Comparison between the phase PDF of the theoretical κ-μ channel (dashed line) and the Markov-chain simulator (solid line. The crosses and circles show, respectively, the simulations by individual component and quadrant sign estimation.

5.6 Dynamic Markov-Chain Sign Estimation

The conclusion from last section is that any simulator that chooses the signs independently of the sample values based on fixed probabilities will have the same statistics, no matter how the signs are chosen. In order to improve on the simulator design, the sign selection has to take into account the instantaneous value of each component.

Consider the RV Z that represents a component of the κ-μ channel. The previous simulators create a new RV Z_S by taking samples from $|Z|$ and choosing a sign. The probability that Z_S is positive or negative is regulated by the probability that Z is positive or negative, and those probabilities are found by a numerical integration of the PDF $f_Z(z)$ described in Equation (2.35).

Now choose two positive real numbers z_a and z_b so that $0 \leq z_a < z_b$. Let p denote the probability that $f_Z(z)$ is positive if $z_a < z < z_b$. Define a simulator that chooses a positive sign for z_0 with probability p and a negative sign with probability $1-p$ if $z_a < z_0 < z_b$, and keeps a positive sign if z_0 is any number outside this interval. The statistics of this simulator will be the same as $|Z|$ for all points outside the interval $(z_a, z_b) \cup (-z_b, -z_a)$. Inside the interval, the simulator PDF will be

$$f_{simZ}(z) = u(z)pf_{|Z|}(z) + u(-z)(1-p)f_{|Z|}(-z), \tag{5.26}$$

in which p is computed as

$$p(z_a, z_b) = \frac{\int_{z_a}^{z_b} f_Z(t)dt}{\int_{z_a}^{z_b} f_Z(t)dt + \int_{-z_b}^{-z_a} f_Z(t)dt}. \tag{5.27}$$

The simulator takes probability mass from the interval (z_a, z_b) and redistribute it between the positive and negative parts of the domain. Note that the Markov-chain sign estimators from the previous sections are a particular case of this simulator when $z_a = 0$ and $z_b = \infty$. Let the length of the interval, $z_b - z_a$, become very small, so that $z_b = z_a + dz$, in which dz represents an infinitesimal length. The integral of a continuous and infinitely differentiable function $h(x)$ over an infinitesimal interval dz is simply $h(x)dx$, since $h(x) = h(x+dx)$ and the integral represents the area of the infinitesimal rectangle with sides $h(x)$ and dx. In this case, Equation (5.27) can be rewritten as

$$p(z_a) = \frac{\int_{z_a}^{z_a+dz} f_Z(t)dt}{\int_{z_a}^{z_a+dz} f_Z(t)dt + \int_{-z_a-dz}^{-z_a} f_Z(t)dz} = \frac{f_Z(z_a)dz}{f_Z(z_a)dz + f_Z(-z_a)dz} = \frac{f_Z(z_a)/f_Z(-z_a)}{f_Z(z_a)/f_Z(-z_a)+1}. \tag{5.28}$$

The terms dz in the numerator and denominator can be canceled out since, even though infinitesimal, they stand for the same distance. The PDF of the absolute value of a RV is related to the PDF of the RV by the following expression

$$f_{|Z|}(z) = f_Z(z) + f_Z(-z). \tag{5.29}$$

It is easy to see why Equation (5.29) holds. The absolute value operator takes any sample that was originally inside a negative interval $(-z_j, -z_i)$, such as $0 \leq z_i < z_j$, and moves it to the interval (z_i, z_j) keeping any sample that was originally within the interval (z_i, z_j) unchanged. The probability that a sample of $|Z|$ will be in the interval (z_i, z_j) is then

$$P(z_i < |Z| < z_j) = F_{|Z|}(z_j) - F_{|Z|}(z_i) = (F_Z(z_j) - F_Z(z_i)) + (F_Z(-z_i) - F_Z(-z_j)), \tag{5.30}$$

$\forall z_i, z_j \in \mathbb{R}^+ | z_i < z_j$, in which $F_Z(z)$ denotes the CDF of Z. Let $z_j = z_i + \Delta z$. Then,

$$\frac{F_{|Z|}(z_i + \Delta z) - F_{|Z|}(z_i)}{\Delta z} = \frac{F_Z(z_i + \Delta z) - F_Z(z_i)}{\Delta z} + \frac{F_Z(-z_i) - F_Z(-(z_i + \Delta z))}{\Delta z}. \quad (5.31)$$

By taking the limit $\Delta z \to 0$ of both sides of Equation (5.31), Equation (5.29) is obtained. Replacing Equations (5.28) and (5.29) in Equation (5.26) leads to

$$f_{simZ}(z = \pm z_a) = u(z_a) f_Z(z_a) + u(-z_a) f_Z(-z_a). \quad (5.32)$$

Equation (5.32) shows that, inside the infinitesimal interval $(-z_a - dz, -z_a) \cup (z_a, z_a + dz)$, this simulator has exactly the same statistics as the true κ-μ component. Thus, the final step to create a simulator that has exactly the same statistics as the κ-μ component everywhere is to allow the simulator to work on all positive z, from $z = 0$ to $z = \infty$. That is, create a rule that for every sample $|Z| = z$ it assigns a positive sign with probability

$$p(z) = \frac{f_Z(z)/f_Z(-z)}{f_Z(z)/f_Z(-z) + 1} = \frac{L(z)}{L(z) + 1}, \quad (5.33)$$

in which

$$L(z) = \frac{f_Z(z)}{f_Z(-z)} = \exp\left(\frac{2|z|\lambda}{\sigma^2}\right). \quad (5.34)$$

The function $L(z)$ in Equation (5.34) is found by simply substituting Equation (2.35) in Equation (5.33). The absolute value inside the exponential is added to augment the domain of Equation (5.33) to encompass the negative Reals as well, since $p(z)$ is defined as the probability of z being positive. As before, it doesn't matter how the signs are assigned, just that the probability in Equation (5.33) is respected. To control the rate of transitions, a parameter r can be added, in a dynamic Markov-chain that changes the transition probability according to the value of $|Z|$. The same Markov-chain of Figure 5.13 is used, with the steady state probabilities P_Z^+ and P_Z^- changed to

$$P_Z^+ = p(z) = \frac{L(z)}{L(z) + 1} \quad (5.35a)$$

$$P_Z^- = 1 - p(z) = \frac{1}{L(z) + 1}. \quad (5.35b)$$

The transition matrix for this simulator becomes

$$T = \begin{bmatrix} 1 - \dfrac{r(z)}{L(z)+1} & \dfrac{r(z)}{L(z)+1} \\ \dfrac{r(z)L(z)}{L(z)+1} & 1 - \dfrac{r(z)L(z)}{L(z)+1} \end{bmatrix}, \quad (5.36)$$

$r(z) \leq \min\{1 + 1/L(z), 1 + L(z)\}$. r is left as a function of z because it is not needed to be a fixed value, as by construction it does not alter the steady state probability of the matrix. The only restriction on $r(z)$ is that it must be an even function, such that $r(z) = r(-z)$, in order to maintain the desired steady state probabilities. If $\lambda > 0$, $\min\{1 + 1/L(z), 1 + L(z)\} = 1 + 1/L(z)$, and if $\lambda < 0$, $\min\{1 + 1/L(z), 1 + L(z)\} = 1 + L(z)$. The transition probability is computed as

$$\begin{aligned} P(\text{transition}) &= \int_{-\infty}^{\infty} P(\text{transition}|Z=z)P(Z=z)dz \\ &= \int_{-\infty}^{0} \frac{r(z)L(z)}{L(z)+1} f_Z(z)dz + \int_{0}^{\infty} \frac{r(z)}{L(z)+1} f_Z(z)dz \\ &= \int_{0}^{\infty} \frac{r(z)}{L(z)+1} \Big(L(z) f_Z(-z)\Big)dz + \int_{0}^{\infty} \frac{r(z)}{L(z)+1} f_Z(z)dz \\ &= 2\int_{0}^{\infty} \frac{r(z)}{L(z)+1} f_Z(z)dz. \end{aligned} \tag{5.37}$$

The maximum transition probability is obtained when $r(z) = \min\{1 + 1/L(z), 1 + L(z)\}$. If $\lambda > 0$, the maximum transition probability is

$$P_{\max}(\text{transition}|\lambda > 0) = 2\int_{-\infty}^{0} f_Z(z)dz, \tag{5.38}$$

and if $\lambda < 0$,

$$P_{\max}(\text{transition}|\lambda < 0) = 2\int_{0}^{\infty} f_Z(z)dz. \tag{5.39}$$

The maximum transition probability is equal to twice the probability of the least probable half of the real line. The simulated transition rate is, as discussed in the previous sections, the transition probability times the sampling frequency F_s,

$$F_T = 2F_s \int_{0}^{\infty} \frac{r(z)}{L(z)+1} f_Z(z)dz. \tag{5.40}$$

Figures 5.17 to 5.19 show the phase PDF of the final dynamic κ-μ sign estimation simulator. The simulator uses the technique developed in this section to simulate two κ-μ components X and Y, which are then combined to generate the phase samples. Note that, for every set of parameters, the simulator phase PDF is exactly the κ-μ phase PDF, as was expected.

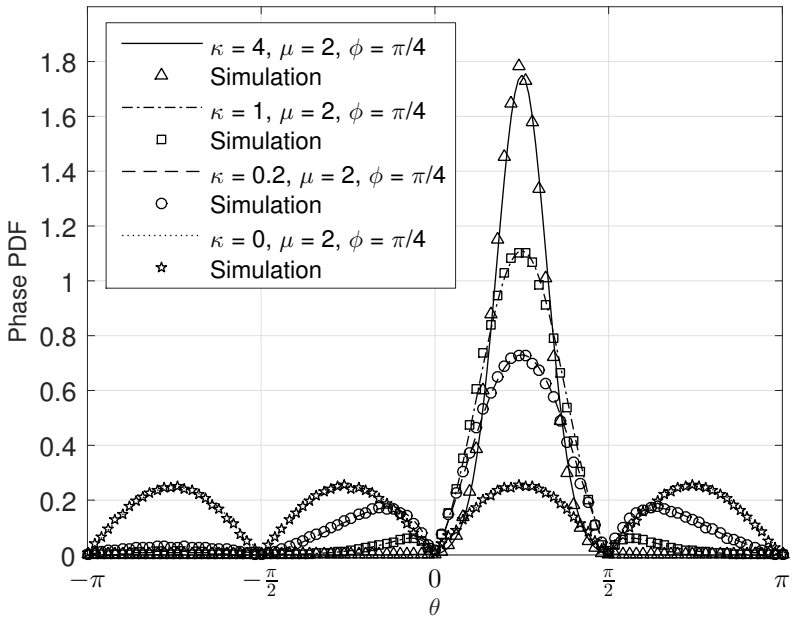

Figure 5.17: Four sets of the κ-μ phase PDF and the dynamic Markov-chain sign estimation simulation for three sets of parameters, illustrating how the simulation performs for different values of κ.

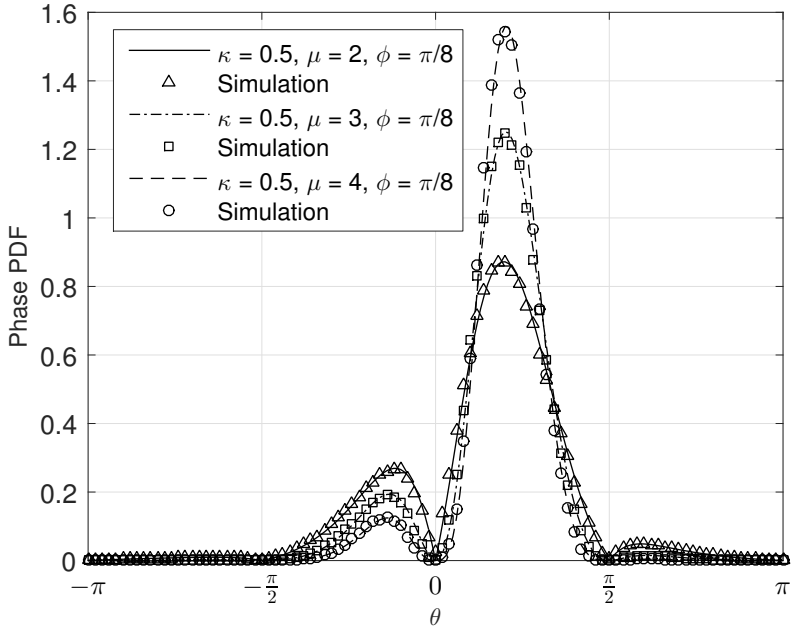

Figure 5.18: Three sets of the κ-μ phase PDF and the dynamic Markov-chain sign estimation simulation for three sets of parameters, illustrating how the simulation performs for different values of μ.

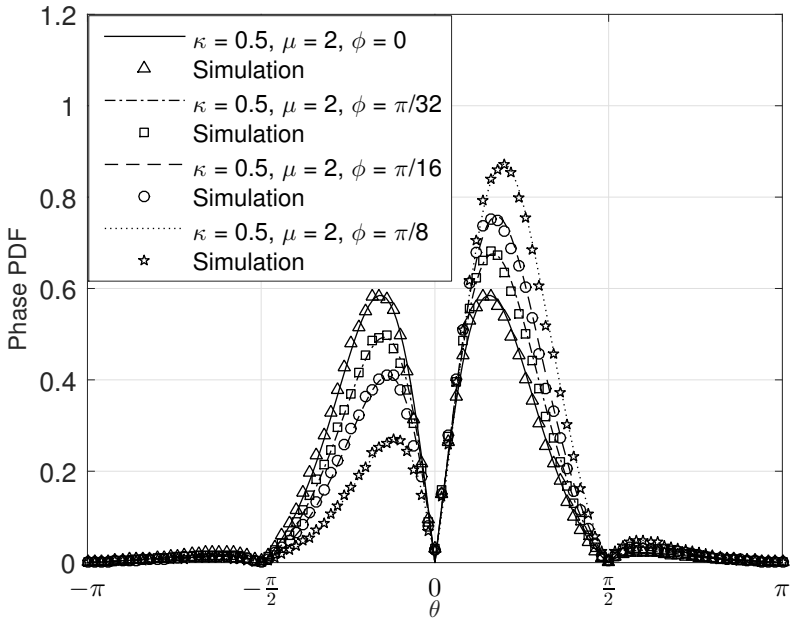

Figure 5.19: Four sets of the κ-μ phase PDF and the dynamic Markov-chain sign estimation simulation for three sets of parameters, illustrating how the simulation performs for different values of ϕ.

Figure 5.20 shows the simulated phase time series. In the leftmost graph, the transition $r(z)$ of the simulation of the components X and Y was set as its maximum instantaneous value of $r(z) = \min\{1 + 1/L(z), 1 + L(z)\}$, in order to maximize the number of transitions. The other two simulations used a constant value of r. As r increases, the simulation becomes increasingly discontinuous. The transition rate function $r(z)$ can be made as low as desired to make the simulation more continuous, although a very small $r(z)$ will require a large number of simulated samples to assure that at least some transitions will happen.

Figure 5.21 show the comparison between the PDF of the simulations in Figure 5.20. Even though the transition rate change, the PDF remains exactly the same as the κ-μ theoretical phase PDF, as was expected.

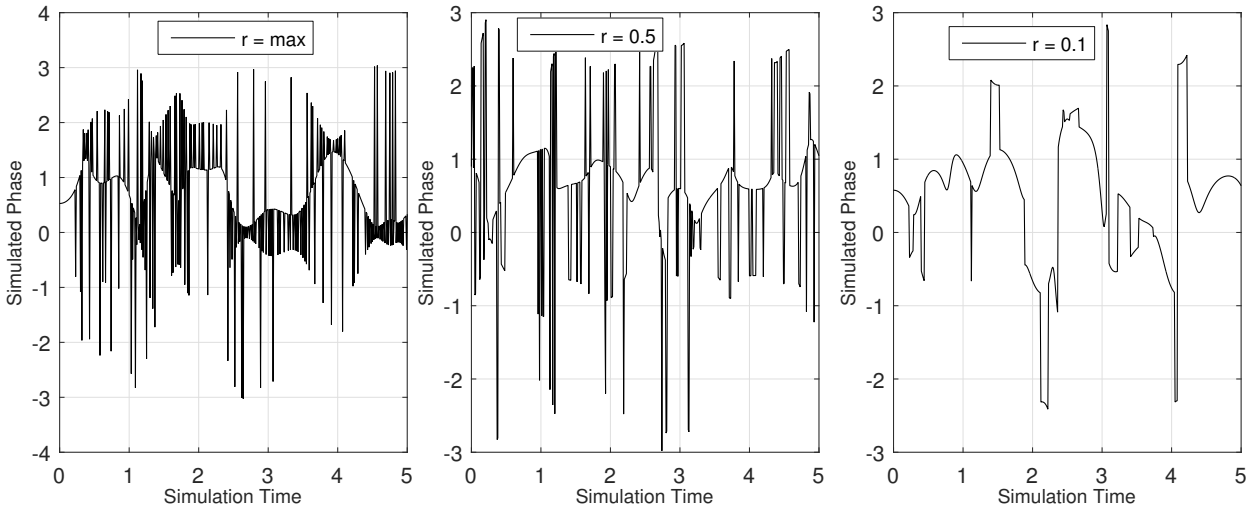

Figure 5.20: Comparison of the behavior of the simulated phase time series for different values of r, for $\kappa = 0.2$, $\mu = 2$ and $\phi = \pi/4$. The leftmost figure shows the behavior under the maximum achievable transition rate. Note that when r diminishes, the number of transitions diminishes as well, as expected.

The second order phase statistics of the simulator also approach the theoretical κ-μ statistics. Figures 5.22 to 5.24 show the PCR of the simulator compared to the κ-μ PCR. The transition rate used was $r = 0.5$. The PCR is also independent from r, although when r is too small it will take a greater number of samples for the PCR to converge in comparison to the phase PDF. To calculate the experimental PCR, only the continuous crossings are counted; when a discontinuity happen the signal is considered to have gone directly from one quadrant to the other, without passing through the phases in between.

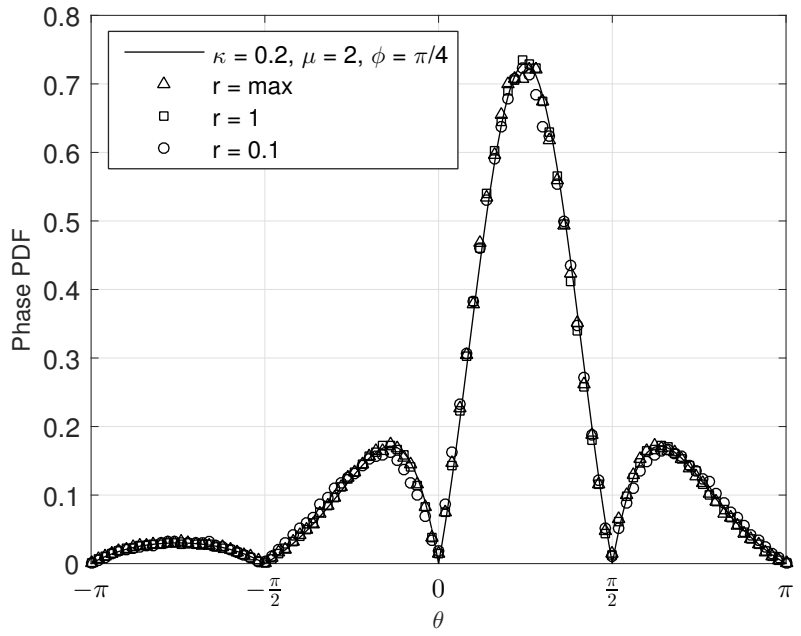

Figure 5.21: The κ-μ phase PDF along with the simulation PDF of the cases illustrated in Figure 5.20. This graph shows that the transition rate does not alter the phase PDF.

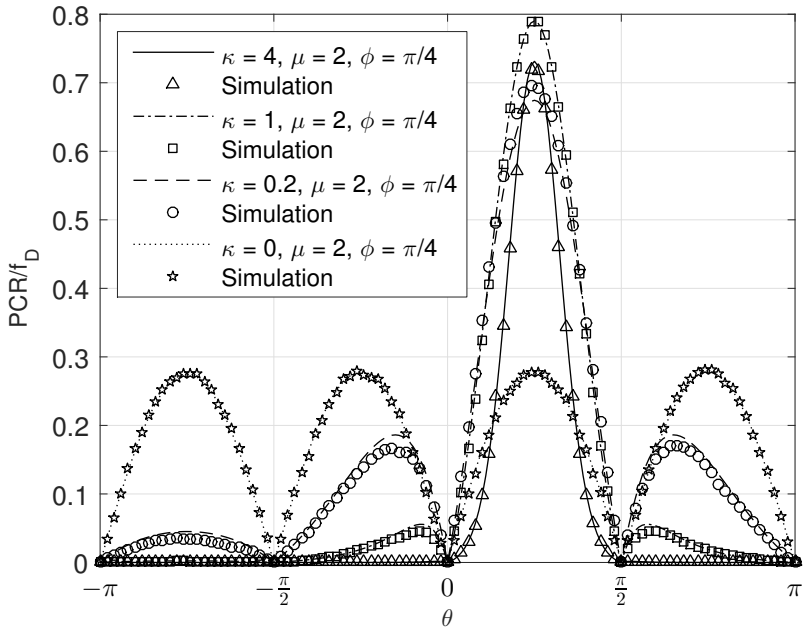

Figure 5.22: Four sets of the κ-μ PCR and the dynamic Markov-chain sign estimation simulation for three sets of parameters, illustrating how the simulation performs for different values of κ.

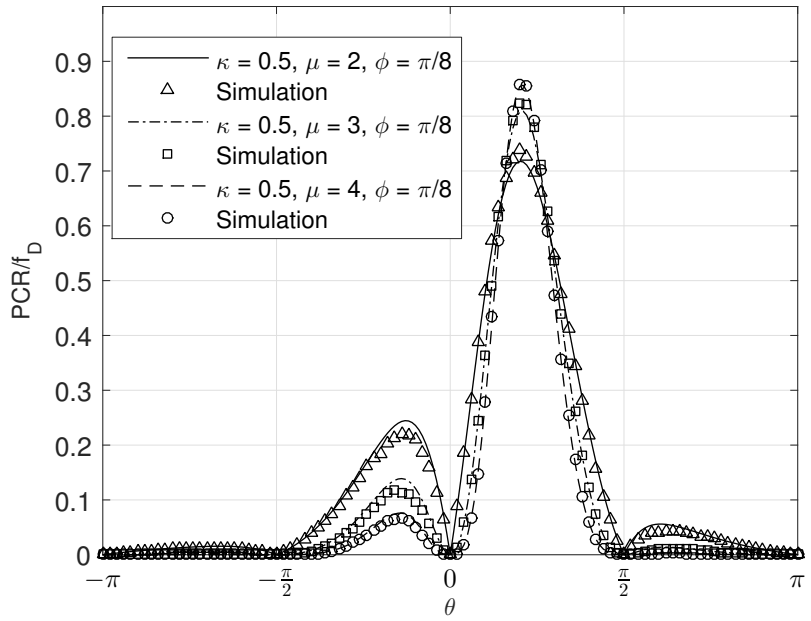

Figure 5.23: Three sets of the κ-μ PCR and the dynamic Markov-chain sign estimation simulation for three sets of parameters, illustrating how the simulation performs for different values of μ.

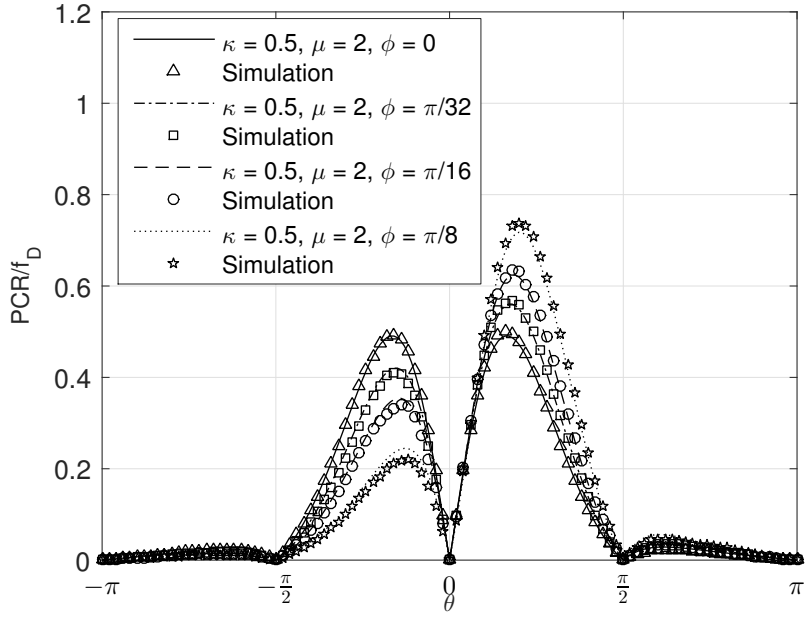

Figure 5.24: Four sets of the κ-μ PCR and the dynamic Markov-chain sign estimation simulation for three sets of parameters, illustrating how the simulation performs for different values of ϕ.

5.7 Conclusion

This chapter provided an in-depth exploration of the simulation of the κ-μ phase. It first established the inevitability of phase jumps, as being an inherent part of the κ-μ channel when $\mu \neq 1$. It also identified that the main challenge in making a working simulation of the κ-μ channel is the correct estimation of the signs of each component. The chapter proceeds to present various different ways to choose the signs, in order to generate a simulation that has the same phase statistics of the κ-μ channel.

A total of five different types of sign selection were presented: (i) - fixed signs; (ii) - Z_i component sign estimation; (iii) - quadrant selection by a fixed Markov-chain; (iv) - individual component sign selection by a fixed Markov-chain; and (v) - sign selection by a dynamic Markov-chain. The first simulator does not estimate the sign at all; it simply let the sign be fixed throughout the simulation. Still, it performs well in some cases, when the parameters lock the κ-μ phase to one quadrant. The second simulator used a technique that provided a perfect simulation when $\mu = 1$ and a good approximation in some other cases. Its performance decreases when the κ-μ phase is asymmetric. The third and fourth simulators use fixed Markov-chains to chose the sign of the components. They perform much better in asymmetric phase PDF conditions then the previous simulators, since the transition probabilities of the Markov-chains are set in a way to ensure that the simulator will have the same quadrant probabilities as the theoretical κ-μ phase PDF. It was later proved that both simulators have the same phase statistics, which expression was found in an exact way. Although close to the κ-μ phase PDF, the statistics are not identical.

Lastly, a final and definite simulator was created. This simulator uses a Markov-chain with transition probabilities that are dependent on the instantaneous value of the simulated signal components. The transition probabilities were tailored so that the simulator has the exact κ-μ phase statistics, as was demonstrated by the simulations provided. The transition probabilities can be efficiently computed, being dependent only on an exponential function, and the simulator does not require any numerical integration as did its predecessors. The simulator was also shown to be compatible with the κ-μ second order statistics, as the simulations included demonstrated. Finally, the chapter concluded with the characterization of the transitions, providing the formulas that govern the average frequency of transitions and showing how phase simulation is affected by the parameter that controls the rate of transitions.

Chapter 6

Conclusions and Further Work

This thesis is the culmination of the research conducted during my period as a PhD student. It presents many new improvements to the knowledge base of fading channels, providing new mathematical expressions, a statistical characterization of the κ-μ and Generalized Nakagami-m phase, and a new simulation method that generates correlated κ-μ with exact statistics. Although most of the work was focused on the κ-μ channel, the results are not restricted to it; for instance, the simulation method developed may be used to create simulators of other correlated Random Variables for which there is no quadrant information. Other possible contributions that may find use in other fields are the new Random Variable $\mathbb{O}$ and the mathematical identity presented in Chapter 4.

The first and second chapters of the thesis provide a summary of the current status of the research in the modeling of mobile radio channels, with emphasis on the phase processes. They can be used as both a bibliographical and quick reference guides for some widely used mobile channel fading models, namely the Rayleigh, Rice, Nakagami-m and κ-μ channels. The introduction provides a historical background of the research in this field, since its origin with the publication of the important paper by Rice in which he begins to investigate the statistical properties of signal fading. The many citations and descriptions of papers that punctuate the introduction help give an interested reader a basic map to guide further individual research. Chapter 2 presents, in a condensed way, information and relevant expressions about many common fading channels, along with the basics of the simulation technique. The chapter merges results from many different papers in the same place, for easy reference.

The third and fourth chapters contain the adapted versions of two papers published during the PhD studies: "Nakagami-m phase model: Further results and validation" [45] and "On the phase statistics of the κ-μ process" [46]. Chapter 3 provides the exact expressions of the Generalized Nakagami-m CDF and inverse CDF, along with field data fitted to that model. Chapter 4 presents many important results regarding the phase of the κ-μ process, in particular: (i) the analytic expression of a new phase Random Variable that is a tight approximation to the κ-μ phase PDF; (ii) the exact expressions of many joint distributions of the components of the κ-μ channel and its derivatives; (iii) the PDF of the derivative of the phase; (iv) a new integral identity of the confluent hypergeometric function of the first kind; and (v) a closed form approximation of the κ-μ phase crossing rate.

Finally, the fifth chapter explores the problems of the simulation of the phase of the κ-μ channel. From the initial observation that phase jumps are inherent to any general

κ-μ simulation, a series of different simulators are proposed, each providing incremental improvements over the preceding simulator, until a definitive simulator is found. This last simulator outputs correlated samples that have the exact first and second order statistics of the κ-μ fading channel. The creation of this simulator gives insight on the physical nature of the κ-μ fading. It also is a fundamental tool for the study of the effect of the κ-μ fading in transmission systems.

Further work will focus on improving the simulator, to allow the simulation of fractional values of μ. Other promising leads are applying the simulation technique developed to create simulators of other Random Variables and using the simulator to study the performance of communication schemes suffering κ-μ fading.

Appendices

Appendix A

MATLAB code

This appendix presents the MATLAB functions used to generate the data showed in the plots.

A.1 κ-μ functions

A.1.1 Exact Phase PDF

```
function [ y ] = km_ppdf( theta, parameters )
K = parameters(1);
M = parameters(2);
P = parameters(3);

theta = theta(:)';

st = numel(theta);
rho = linspace(0.005,1.0,200);
rho_inv = 1./rho;
rep_rho = repmat(rho, st,1)'; %[sr x st]
s = rho(2) - rho(1);
w1 = pdf_rt(rho,theta, K, M, P);
w2 = pdf_rt(rho_inv,theta, K, M, P)./(rep_rho.^2);
y = sum(w1+w2)*s;

t = isnan(y)|isinf(y);
y(t) = 0;
end
```

```
function [ f ] = pdf_rt(rho, theta, K, M ,P)
%PDF_RT returns the phase-enveloppe joint distribution f(rho, theta) for
%the kappa-mu model

%let size(theta) = [1 x st] and size(rho) = [1 x sr]
st = numel(theta);
sr = numel(rho);
b = exp(-K*M)*(1/(((2*K*M)^M)*8))/((abs(sin(2.*P))).^((M./2)-1)); %b is a multiplying constant
rep_theta = repmat(theta,sr,1); %size(f1) = [sr x st]
rep_rho = repmat(rho,st,1)';%size(f1) = [sr x st]
f1 = (abs(sin(2*rep_theta)).^(M./2)); % size(f1) = [sr x st];
f2 = (rep_rho.^(M+1)); %size(f2) = [sr x st]
f3 = exp(-(rep_rho.^2)/(4*K*M)+ rho'*cos(theta-P)); %size(f3) = [sr x st]
f4 = ...
    k_func((M/2)-1,rho'*abs(cos(theta)*cos(P))).*k_func((M/2)-1,rho'*abs(sin(theta)*sin(P))); ...
    %size(f4) = [sr x st]
f = b*f1.*f2.*f3.*f4;%size(f) = [sr x st]
end
```

```
function [ Y ] = k_func( nu, Z )
Y = besseli(nu,Z).*sech(Z);
end
```

A.1.2 Approximate Phase PDF ($\mathbb{O}$ Distribution)

```
function [ Y ] = km_apdf_closed( X, parameters )   %approximate PDF
K = parameters(1);
K = 2*sqrt(K*(1+K));
M = parameters(2);
P = parameters(3);
C1 = K*M*abs(sin(2*P))^(1-M/2);
C2 = 8 * besseli(M-1,K*M);
Y = ((abs(sin(2*X)).^(M/2)  ).*exp(K*M.*cos(X-P)).*k_func((M/2)-1,K*M*abs(cos(X).*cos(P)))...
.*k_func((M/2)-1,K*M*abs(sin(X).*sin(P))));
Y = Y*C1/C2;
end
```

A.1.3 PDF of the Z Components

```
function [ f ] = km_zpdf( z, mu, lambda, sigma2)
f = (abs(z).^(mu/2)).* exp(-((z-lambda).^2)/(2*sigma2)).*besseli(mu/2 - ...
    1,abs(lambda*z)/sigma2)...
    ./(2*sigma2*(abs(lambda).^(mu/2-1)).*cosh(lambda*z/sigma2));
nan_index = isnan(f);
f(nan_index) = 0;
end
```

A.1.4 Exact PCR

```
function [ y ] = km_pcr( theta, parameters )
%pcr for f_d = 1, in which f_d is the maximum Doppler shift in Hz
K = parameters(1);
M = parameters(2);
P = parameters(3);
y = zeros(size(theta));
rho = linspace(0.01,15,1000);
f = nrt(rho,theta,K,M,P);
y = sum(f,1)*(rho(2)-rho(1));
end
```

```
function [ f ] = nrt(rho, theta, kappa, mu ,phi)
%KM_NRT returns N(rho, theta), which if integrated from 0 to infinity in
%respect to rho yelds the PCR of the kappa-mu distribution.

rho = rho(:); % rho is a column vector
theta = theta(:)'; %theta is a row vector

f_const = (2*pi)*(1/sqrt(32*pi))*(mu^(3/2))*(kappa^(1-mu/2))*((1+kappa)^(1/2 + ...
    mu/2))*exp(-kappa*mu);
f_rho = (rho.^mu).*exp(-mu*(1+kappa)*rho.^2);
f_theta = ((abs(sin(2.*theta)).^(mu./2)).*(abs(sin(2.*phi))).^((mu./2)-1));
f_rho_theta =  exp(2*mu*sqrt(kappa*(1+kappa))*rho*cos(theta-phi)).*...
k_func((mu./2)-1,2.*mu.*sqrt(kappa.*(1+kappa)).*rho*abs(cos(theta).*cos(phi))).*...
k_func((mu./2)-1,2.*mu.*sqrt(kappa.*(1+kappa)).*rho*abs(sin(theta).*sin(phi)));
f = f_const*(f_rho*f_theta).*f_rho_theta; %[size_rho x size_theta]
end
```

A.1.5 Approximate PCR

```
function [ Y ] = km_apcr( X, parameters )
K = parameters(1);
M = parameters(2);
P = parameters(3);
```

```
Y = ((abs(sin(2*X)).^(M/2)).*exp(2*M*sqrt(K*(1+K)).*cos(X-P))...
.*k_func((M/2)-1,2*M*sqrt(K*(1+K))*abs(cos(X).*cos(P)))...
.*k_func((M/2)-1,2*M*sqrt(K*(1+K))*abs(sin(X).*sin(P))));
t = isnan(Y)|isinf(Y);
Y(t) = 0;
if M>=1
    [~,t] = max(Y);
else
    [~,t] = min(Y);
end
w = km_pcr(X(t),parameters)./Y(t);
Y = Y*w;
end
```

A.2 Generalized Nakagami-m functions

A.2.1 Exact Phase PDF

```
function [ f ] = nakmp_pdf( theta, m , p )
if p == 0
    f = (gamma(m)/((2^m)*gamma(m/2)*gamma(m/2)))*(abs(sin(2*theta)).^(m-1));
else
    f = (gamma(m)/((2^m)*gamma((1+p)*m/2)*gamma((1-p)*m/2)))*(abs(sin(2*theta)).^(m-1))...
    ./(abs(tan(theta)).^(p*m));
end
t = isnan(f)|isinf(f);
f(t) = 0;
end
```

A.2.2 Exact PCR

```
function [ f ] = nakmp_pcr( theta, m,p )
f = (sqrt(pi)*(abs(sin(2*theta)).^(m-1)).*(abs(tan(theta)).^(-p*m))...
.*gamma(m-1/2))/((2^(m+(1/2)))*gamma((1+p)*m/2)*gamma((1-p)*m/2));
end
```

A.3 Simulations

A.3.1 Rayleigh Simulator

```
function [g]=rayleigh_gen(Fd, Fs, N, sigma2)
%Fd is the maximum Doppler shift, Fs is the sampling frequency, N is the
%number of samples that will be generated, gi and gq are the time series of
%the in-phase and quadrature components, respectively

Tsim = N/Fs;
deltat  = Tsim/N;                               % Sampling period
deltaf  = 1/(N*deltat);                         % Espectral resolution


% ------------------------------ Doppler spectrum evaluation -------------------------
K    = ceil(Fd*N*deltat+1);              % Number of samples of the spectrum

fd   = (0:deltaf:Fd)';
H    = 1./sqrt(1-(fd(1:K-1)/Fd).^2);     % Doppler spectrum Samples

if K > 2
  %H=[H;(Fd-deltaf)*(pi/2-atan((Fd-2*deltaf)/sqrt(2*Fd-2*deltaf)))];  % Aprox. at f=Fd
  H=[H;2*H(K-1)-H(K-2)];                % this expression can be used too

else
   H=[H;1.5*H];

end
```

```
% ———————————————— White Gaussian noise Generation ————————————————
N_gauss = randn(K,1);

G = sqrt(H) .* N_gauss;

% ———————————————— evaluating Inverse Fast Fourier Transform ————————————————
g = real(ifft(G,N));            % Correlated in fase Gaussian vector

% ———————————————— Mean remmoval ————————————————————————————————————
g = g-mean(g);

% ———————————————— Normalizing the correlated gaussian vectors ————————————————
g = sqrt(sigma2)*g/sqrt(var(g));
g = g(:);
end
```

A.3.2 κ-μ Simulators - Markov-Chain Quadrant Sign Estimation

```
function [ km_channel ] = kmgen_quad_markov(N, Fd, Fs, r, parameters)
kappa = parameters(1);
mu = parameters(2);
phi = parameters(3);
sigma2 = 1;
p_i=sqrt(2*kappa*sigma2)*cos(phi);
q_i=sqrt(2*kappa*sigma2)*sin(phi);
M = N;
N = 2*N-1;

sign_i = zeros(N,1);
sign_q = zeros(N,1);
gi = zeros(N,1);
gq = zeros(N,1);


%get the quadrant probabilities
nquad = 50;
theta = linspace(0,2*pi,4*nquad);
f = km_ppdf(theta,parameters);
dtheta = theta(2)-theta(1);
[Pa, Pb, Pc, Pd] = quad_prob(parameters);
probabilities = [Pa, Pb, Pc, Pd];
quads = quad_markov(M,probabilities,r)';

for j = 1:mu
    [gi1,gq1]=rayleigh_gen(Fd, Fs, N, sigma2);
    gi = gi + (gi1 + p_i).^2;
    gq = gq + (gq1 + q_i).^2;
    sign_i = sign_i + p_i + gi1;
    sign_q = sign_q + q_i + gq1;
end

sign_i = (quads==1)+(quads==4)-1*((quads==2)+(quads==3));
sign_q = (quads==1)+(quads==2)-1*((quads==3)+(quads==4));
gi = gi(1:M);
gq = gq(1:M);
gi = sign_i.*sqrt(gi);
gq = sign_q.*sqrt(gq);


km_channel = gi + 1i*gq;
end



function [ Pa, Pb, Pc, Pd ] = quad_prob( parameters )

g = @(z) km_ppdf(z, parameters);
Pa = integral(g, 0, pi/2);
Pb = integral(g, pi/2, pi);
Pc = integral(g, -pi, -pi/2);
Pd = integral(g, -pi/2, 0);

end
```

```
function [quadrant] = quad_markov(N,probabilities,transition_ratio)
Pa = probabilities(1);
Pb = probabilities(2);
Pc = probabilities(3);
Pd = probabilities(4);
r = transition_ratio;
transition_matrix = ...
[[1-r*(Pb+Pd),r*Pb,0,r*Pd];...
[r*Pa,1-r*(Pa+Pc),r*Pc,0];...
[0,r*Pb,1-r*(Pb+Pd),r*Pd];...
[r*Pa,0,r*Pc,1-r*(Pa+Pc)]];
current_state = get_next_state(probabilities);
quadrant = zeros(1,N);
quadrant(1) = current_state;
for i=2:N
    current_state = get_next_state(transition_matrix(current_state,:));
    quadrant(i) = current_state;
end
return

function [next_state] = get_next_state(transition_prob_vector)
rd = rand();
if rd<= transition_prob_vector(1)
    next_state =1;
elseif rd<=transition_prob_vector(1)+transition_prob_vector(2)
    next_state = 2;
elseif rd<=transition_prob_vector(1)+transition_prob_vector(2)+transition_prob_vector(3)
    next_state = 3;
else
    next_state = 4;
end
return
```

A.3.3 κ-μ Simulators - Markov-Chain Individual Component Sign Estimation

```
function [ Zreal, Zimag ] = kmgen_bi_markov_rv(N, Fd, Fs, r,v, parameters, sigma2)
Zreal = Z_bi_markov(N, Fd, Fs, r, parameters, sigma2, 'x');
Zimag = Z_bi_markov(N, Fd, Fs, v, parameters, sigma2, 'y');
end
```

```
function [ Z ] = Z_bi_markov(N, Fd, Fs, r, parameters, sigma2, x_or_y)
%Simulates the kappa mu channel using a markov chain sign estimation
x_or_y = lower(x_or_y);
kappa = parameters(1);
mu = parameters(2);
phi = parameters(3);

if x_or_y == 'x'
    lambda = sqrt(2*mu*kappa*sigma2)*cos(phi);
elseif x_or_y == 'y'
    lambda = sqrt(2*mu*kappa*sigma2)*sin(phi);
else
    error('Specify a valid option for Z (X or Y)');
end
Z = Zgen(N, Fd, Fs, lambda, mu, sigma2);
%get the probabilities
p(1) = integral(@(x) Z_norm_pdf(x,parameters,x_or_y),0,100);
p(2) = 1-p(1);

signs = bi_markov(N,p,r)';

Z = signs.*Z;
end
```

```
function [ Y ] = Z_norm_pdf(chi, parameters, x_or_y)
kappa = parameters(1);
mu = parameters(2);
phi = parameters(3);
```

```
x_or_y = lower(x_or_y);

if x_or_y == 'x'
    Y = (abs(chi).^(mu/2)).*exp(-((chi - sqrt(2*mu*kappa)*cos(phi)).^2)/2)...
    .*besseli((mu/2)-1,abs(chi*sqrt(2*mu*kappa)*cos(phi)))...
    ./(2*(abs(sqrt(2*mu*kappa)*cos(phi))).^((mu/2)-1).*cosh(abs(chi*sqrt(2*mu*kappa)*cos(phi))));
elseif x_or_y == 'y'
    Y = (abs(chi).^(mu/2)).*exp(-((chi - sqrt(2*mu*kappa)*sin(phi)).^2)/2)...
    .*besseli((mu/2)-1,abs(chi*sqrt(2*mu*kappa)*sin(phi)))...
    ./(2*(abs(sqrt(2*mu*kappa)*sin(phi))).^((mu/2)-1).*cosh(abs(chi*sqrt(2*mu*kappa)*sin(phi))));
else
    error('Specify a valid option for Z (X or Y)');
end

end



function [states] = bi_markov(N,probs,transition_ratio)

r = transition_ratio;
transition_matrix = [[1-r*probs(1),r*probs(1)];[r*probs(2),1-r*probs(2)]]';


current_state = get_next_state(probs);
states = zeros(1,N);
states(1) = current_state;
for i=2:N
    current_state = get_next_state(transition_matrix(:,current_state));
    states(i) = current_state;
end
states(states==1) = -1;
states(states==2)=1;
return

function [next_state] = get_next_state(transition_prob_vector)
rd = rand();
if rd<= transition_prob_vector(1)
    next_state =1;
else
    next_state = 2;
end
return
```

A.3.4 κ-μ Simulators - Dynamic Markov-Chain Sign Estimation

```
function [ Zreal, Zimag] = kmgen_dyn_markov(N, Fd, Fs, r, parameters)
kappa = parameters(1);
mu = parameters(2);
phi = parameters(3);

sigma2 = 0.5;

p_i=sqrt(2*kappa*sigma2)*cos(phi);
q_i=sqrt(2*kappa*sigma2)*sin(phi);

p = p_i*sqrt(mu);
q = q_i*sqrt(mu);

Zreal = Zgen(N, Fd, Fs, p, mu, sigma2);
Zimag = Zgen(N, Fd, Fs, q, mu, sigma2);

sreal = dynamic_sign_r(Zreal, r, p, sigma2);
simag = dynamic_sign_r(Zimag, r, q, sigma2);

Zreal = Zreal.*sreal;
Zimag = Zimag.*simag;
end



function [ Z ] = Zgen(N, Fd, Fs, lambda, mu, sigma2 )
%ZGEN Simulates the absolute value of the in-phase or quadrature component of the kappa-mu
```

```
%channel

lambda_i = lambda/sqrt(mu);
M = N;
N = 2*N-1;
Z = zeros(N,1);

for j = 1:mu
    g = rayleigh_gen(Fd, Fs, N, sigma2);
    Z = Z + (g + lambda_i).^2;
end
Z = sqrt(Z);
Z = Z(1:M);
end



function [ signs ] = dynamic_sign_r( Z, r, lambda, sigma2)
%DYNAMIC_SIGN returns the appropriate signs for the given Z vector
%if r == -1, the maximum possible transition rate is set

random_vector = rand(size(Z));

if r == -1
    if lambda>0
        r = 1 + 1./z_lh(Z,lambda,sigma2);
    else
        r = 1 + z_lh(Z,lambda,sigma2);
    end
end

Tab = r.*T(Z, lambda, sigma2);
Tba = r.*T(-Z, lambda, sigma2);


pos_transitions = random_vector<Tab;
neg_transitions = random_vector<Tba;
signs = ones(size(Z));
current_sign = 1;
for i = 1:length(Z)
    if current_sign == 1
        if pos_transitions(i) == 1
            current_sign = -1;
        end
    else
        if neg_transitions(i) == 1
            current_sign = 1;
        end
    end
    signs(i) = signs(i)*current_sign;
end

end



function [ L ] = z_lh(z, lambda, sigma2)
%Z_LH function that measures the likelihood that Z is positive over Z is
%negative
L = exp(2*z*lambda/sigma2);
end



function [ t ] = T(z, lambda, sigma2)
%Non-normalized positive to negative transition probability given z
t = 1./(z_lh(z,lambda,sigma2)+1);
end
```

References

[1] M. D. Yacoub, *Foundations of Mobile Radio Engineering*, 1st ed. Boca Raton, FL, USA: CRC Press, Inc., 1993.

[2] T. Rappaport, *Wireless Communications: Principles and Practice*, 2nd ed. Upper Saddle River, NJ, USA: Prentice Hall PTR, 2001.

[3] Proakis, *Digital Communications 5th Edition*. McGraw Hill, 2007.

[4] D. Cox, R. Murray, and A. Norris, "800-MHz attenuation measured in and around suburban houses," *AT T Bell Laboratories Technical Journal*, vol. 63, no. 6, pp. 921–954, July 1984.

[5] R. Bernhardt, "Macroscopic diversity in frequency reuse radio systems," *IEEE Journal on Selected Areas in Communications*, vol. 5, no. 5, pp. 862–870, Jun 1987.

[6] S. O. Rice, "Statistical properties of sine wave plus random noise," *Bell System Technical Journal*, vol. 27, pp. 109 – 157, Jan. 1948.

[7] J. F. Ossanna, "A model for mobile radio fading due to building reflections: Theoretical and experimental fading waveform power spectra," *Bell System Technical Journal*, vol. 43, no. 6, pp. 2935–2971, Nov 1964.

[8] R. H. Clarke, "A statistical theory of mobile-radio reception," *Bell Systems Technical Journal*, vol. 47, pp. 957–1000, 1968.

[9] J. Young, W.R., "Comparison of mobile radio transmission at 150, 450, 900, and 3700 mc," *Transactions of the IRE Professional Group on Vehicular Communications*, vol. 3, no. 1, pp. 71–84, Jun 1953.

[10] W. C. Jakes, *Microwave Mobile Communications*. John Wiley & Sons Inc, 1975.

[11] M. Nakagami, "The m-distribution, a general formula of intensity of rapid fading," in *Statistical Methods in Radio Wave Propagation: Proceedings of a Symposium held June 18-20, 1958*, W. C. Hoffman, Ed. Pergamon Press, june 1960, pp. 3–36.

[12] M. D. Yacoub, J. E. V. Bautista, and L. Guerra de Rezende Guedes, "On higher order statistics of the Nakagami-m distribution," *IEEE Transactions on Vehicular Technology*, vol. 48, no. 3, pp. 790–794, May 1999.

[13] M. Yacoub, G. Fraidenraich, and J. Santos Filho, "Nakagami-m phase-envelope joint distribution," *Electronics Letters*, vol. 41, no. 5, pp. 259 – 261, march 2005.

[14] M. Yacoub, "The α- μ distribution: A physical fading model for the Stacy distribution," *IEEE Transactions on Vehicular Technology*, vol. 56, no. 1, pp. 27–34, Jan 2007.

[15] ——, "The κ-μ distribution and the η-μ distribution," *IEEE Antennas and Propagation Magazine*, vol. 49, no. 1, pp. 68 –81, feb. 2007.

[16] U. Dias, M. Yacoub, and D. da Costa, "The κ-μ phase-envelope joint distribution," in *Proc. IEEE 19th International Symposium on Personal, Indoor and Mobile Radio Communications, 2008. PIMRC 2008.*, sept. 2008, pp. 1 –5.

[17] U. Dias and M. Yacoub, "The κ-μ phase-envelope joint distribution," *IEEE Transactions on Communications*, vol. 58, no. 1, pp. 40 –45, january 2010.

[18] S. Cotton and W. Scanlon, "Higher-order statistics for κ-μ distribution," *Electronics Letters*, vol. 43, no. 22, 25 2007.

[19] P. Sofotasios, E. Rebeiz, L. Zhang, T. Tsiftsis, D. Cabric, and S. Freear, "Energy detection based spectrum sensing over κ-μ and κ-μ extreme fading channels," *IEEE Transactions on Vehicular Technology*, vol. 62, no. 3, pp. 1031–1040, March 2013.

[20] G. Chandrasekaran and S. Kalyani, "Performance analysis of cooperative spectrum sensing over κ-μ shadowed fading," *IEEE Wireless Communications Letters*, vol. PP, no. 99, pp. 1–1, 2015.

[21] K. Peppas, G. Alexandropoulos, and P. Mathiopoulos, "Performance analysis of dual-hop AF relaying systems over mixed η-μ and κ-μ fading channels," *IEEE Transactions on Vehicular Technology*, vol. 62, no. 7, pp. 3149–3163, Sept 2013.

[22] B. Kumbhani and R. S. Kshetrimayum, "Error performance of two-hop decode and forward relaying systems with source and relay transmit antenna selection," *Electronics Letters*, vol. 51, no. 6, pp. 530–532, 2015.

[23] M. Milisic, M. Hamza, and M. Hadzialic, "Outage performance of L-branch maximal-ratio combiner for generalized κ- μ fading," in *Proc. IEEE Vehicular Technology Conference.*, May 2008, pp. 325–329.

[24] X. Wang and N. Beaulieu, "Switching rates of two-branch selection diversity in κ-μ and α-μ distributed fadings," *IEEE Transactions on Wireless Communications*, vol. 8, no. 4, pp. 1667–1671, April 2009.

[25] R. Subadar, T. Reddy, and P. Sahu, "Performance of an L-SC receiver over κ -μ and η -μ fading channels," in *Proc. IEEE International Conference on Communications (ICC)*, May 2010, pp. 1–5.

[26] P. Kumar and P. Sahu, "Analysis of M-PSK with MRC receiver over κ -μ fading channels with outdated CSI," *IEEE Wireless Communications Letters*, vol. 3, no. 6, pp. 557–560, Dec 2014.

[27] M. Arezoomandan and A. Shahzadi, "SER expression for M-ary dual ring star QAM over κ-μ fading channels," in *Proc. 7th International Symposium on Telecommunications (IST)*, Sept 2014, pp. 379–382.

[28] S. Kumar, G. Chandrasekaran, and S. Kalyani, "Analysis of outage probability and capacity for κ - μ/η - μ faded channel," *IEEE Communications Letters*, vol. 19, no. 2, pp. 211–214, Feb 2015.

[29] A. M. Oliveira Ribeiro and E. Conforti, "Asymptotically efficient moment-based estimator of the κ parameter for the κ -μ distribution," *IEEE Antennas and Wireless Propagation Letters*, vol. 14, pp. 598–601, 2015.

[30] S. L. Cotton, "Human body shadowing in cellular device-to-device communications: Channel modeling using the shadowed κ -μ fading model," *IEEE Journal on Selected Areas in Communications*, vol. 33, no. 1, pp. 111–119, Jan 2015.

[31] S. Khatalin, "Performance analysis of switch and stay combining diversity system over κ-μ fading channels," *AEU - International Journal of Electronics and Communications*, vol. 69, no. 2, pp. 475 – 486, 2015. [Online]. Available: http://www.sciencedirect.com/science/article/pii/S1434841114002830

[32] P. C. Sofotasios, T. A. Tsiftsis, Y. A. Brychkov, S. Freear, M. Valkama, and G. K. Karagiannidis, "Analytic expressions and bounds for special functions and applications in communication theory," *IEEE Transactions on Information Theory*, vol. 60, no. 12, pp. 7798–7823, Dec 2014.

[33] A. Annamalai and E. Adebola, "Asymptotic analysis of digital modulations in κ-μ, η-μ and α-μ fading channels," *IET Communications*, vol. 8, no. 17, pp. 3081–3094, Nov 2014.

[34] E. Adebola and A. Annamalai, "Unified analysis of energy detectors with diversity reception in generalised fading channels," *IET Communications*, vol. 8, no. 17, pp. 3095–3104, Nov 2014.

[35] E. Adebola, A. Olaluwe, and A. Annamalai, "Partial area under the receiver operating characteristics curves of diversity-enabled energy detectors in generalised fading channels," *IET Communications*, vol. 8, no. 9, pp. 1637–1647, Jun 2014.

[36] S. L. Cotton, "A statistical model for shadowed body-centric communications channels: Theory and validation," *IEEE Transactions on Antennas and Propagation*, vol. 62, no. 3, pp. 1416–1424, March 2014.

[37] J. F. Paris, "Statistical characterization of κ - μ shadowed fading," *IEEE Transactions on Vehicular Technology*, vol. 63, no. 2, pp. 518–526, Feb 2014.

[38] D. Hess, "Cycle slipping in a first-order phase-locked loop," *IEEE Transactions on Communication Technology*, vol. 16, no. 2, pp. 255 –260, april 1968.

[39] J. G. Proakis and D. K. Manolakis, *Digital Signal Processing (4th Edition)*. Upper Saddle River, NJ, USA: Prentice-Hall, Inc., 2006.

[40] K. Hamdi, "Analysis of OFDM over Nakagami-m fading with nonuniform phase distributions," *IEEE Transactions on Wireless Communications*, vol. 11, no. 2, pp. 488–492, February 2012.

[41] C. Zhong, S. Jin, T. Ratnarajah, and K.-K. Wong, "On the capacity of non-uniform phase MIMO Nakagami-m fading channels," *IEEE Communications Letters*, vol. 14, no. 6, pp. 536–538, June 2010.

[42] M. Vu and A. Paulraj, "Optimum space-time transmission for a high K factor wireless channel with partial channel knowledge," *Wiley Journal on Wireless Communications and Mobile Computing*, vol. 4, pp. 807–816, 2004.

[43] R. Vaughan, "Signals in mobile communications: A review," *IEEE Transactions on Vehicular Technology*, vol. 35, no. 4, pp. 133–145, Nov 1986.

[44] I. B. G. Porto, "Approximation and higher order statistics for the κ-μ phase fading model," Master's thesis, UNICAMP, Campinas - SP - Brasil, 2013. [Online]. Available: http://repositorio.unicamp.br/jspui/handle/REPOSIP/259664

[45] I. Porto, M. Yacoub, J. Santos Filho, S. Cotton, and W. Scanlon, "Nakagami-m phase model: Further results and validation," *IEEE Wireless Communications Letters*, vol. 2, no. 5, pp. 523–526, October 2013.

[46] I. B. G. Pôrto and M. D. Yacoub, "On the phase statistics of the κ-μ process," *IEEE Transactions on Wireless Communications*, vol. 15, no. 7, pp. 4732–4744, July 2016.

[47] M. Abramowitz and I. A. Stegun, *Handbook of Mathematical Functions*, 10th ed. Washington: National Bureau of standards, 1972.

[48] M. Yacoub, "Nakagami-m phase-envelope joint distribution: A new model," *IEEE Transactions on Vehicular Technology*, vol. 59, no. 3, pp. 1552 –1557, march 2010.

[49] D. da Costa, M. Yacoub, J. Filho, G. Fraidenraich, and J. Mendes, "Generalized nakagami-m phase crossing rate," *IEEE Communications Letters*, vol. 10, no. 1, pp. 13 – 15, jan 2006.

[50] Y. Li, J. Chen, Y. Song, and R. Lin, "On the study of the crossing statistics of phase processes in rice mobile fading channels," in *Proc. IET Conference on Wireless, Mobile and Sensor Networks, 2007. (CCWMSN07).*, dec. 2007, pp. 158 –161.

[51] J. I. Smith, "A computer generated multipath fading simulation for mobile radio," *IEEE Transactions on Vehicular Technology*, vol. 24, no. 3, pp. 39–40, Aug 1975.

[52] D. J. Young and N. C. Beaulieu, "On the generation of correlated Rayleigh random variates by inverse discrete Fourier transform," in *Proceedings of ICUPC - 5th International Conference on Universal Personal Communications*, vol. 1, Sep 1996, pp. 231–235 vol.1.

[53] D. Young and N. Beaulieu, "The generation of correlated Rayleigh random variates by inverse discrete Fourier transform," *IEEE Transactions on Communications*, vol. 48, no. 7, pp. 1114 –1127, jul 2000.

[54] S. Cotton, U. Dias, W. Scanlon, and M. Yacoub, "On the distribution of signal phase in body area networks," *IEEE Communications Letters*, vol. 14, no. 8, pp. 728 –730, august 2010.

[55] G. Conway and W. Scanlon, "Antennas for over-body-surface communication at 2.45 GHz," *IEEE Transactions on Antennas and Propagation*, vol. 57, no. 4, pp. 844–855, Apr. 2009.

[56] R. Mallik, "A new statistical model of the complex Nakagami-m fading gain," *IEEE Transactions on Communications*, vol. 58, no. 9, pp. 2611–2620, 2010.

[57] M. Evans, N. Hastings, and B. Peacock, *Statistical Distributions*. Wiley-Interscience, 2000.

[58] Wolfram Research, Inc., *Mathematica Edition: Version 8.0.1*. Champaign, Illinois: Wolfram Research, Inc., 2011.

[59] D. H. Johnson and S. Sinanovic, "Symmetrizing the Kullback-Leibler distance," IEEE Transactions on Information Theory, Tech. Rep., 2000. [Online]. Available: http://www.ece.rice.edu/ dhj/resistor.pdf

[60] S. Kullback and R. A. Leibler, "On information and sufficiency," *The Annals of Mathematical Statistics*, vol. 22, no. 1, pp. 79–86, 03 1951. [Online]. Available: http://dx.doi.org/10.1214/aoms/1177729694

[61] R. Serfozo, *Basics of Applied Stochastic Processes (Probability and Its Applications)*. Springer, 2009.